ENERGY DISTRIBUTIONS of ELECTRONS in RADIATION INDUCED-HELIUM PLASMAS

by

RONNIE HUNG-KIE LO

NUCLEAR ENGINEERING PROGRAM

UNIVERSITY of ILLINOIS at URBANA-CHAMPAIGN

URBANA , 1972

ENERGY DISTRIBUTIONS OF ELECTRONS IN RADIATION INDUCED-HELIUM PLASMAS

BY

RONNIE HUNG-KIE LO

B.S., University of Wisconsin, 1966
M.S., University of Wisconsin, 1968

THESIS

Submitted in partial fulfillment of the requirements
for the degree of Doctor of Philosophy in Nuclear Engineering
in the Graduate College of the
University of Illinois at Urbana-Champaign, 1972

Urbana, Illinois

ENERGY DISTRIBUTIONS OF ELECTRONS IN RADIATION-INDUCED HELIUM PLASMAS

Ronnie H. Lo, Ph.D.
Nuclear Engineering Program
University of Illinois, Urbana, Illinois, 1972

Electron energy distributions resulting from a continuous primary source at high energies in helium have been calculated. Contributions from both the primary electrons and subsequent secondaries are included. In the cases analyzed, the primary electrons are taken to be produced via the ionization of helium by heavy-charged particles from the nuclear reaction ${}_0n^1 + {}_5B^{10} \rightarrow {}_3Li^7 + {}_2He^4$ which represents an important means of using the neutron flux from a nuclear reactor to produce a plasma. The calculation covers an energy range from zero to about 1 KeV, the highest energy of the primary electrons associated with such a source. Electron-neutral collisions are assumed to be the dominate collision process. While this limits the fractional ionization to 10^{-5}, this region is of interest for application in areas such as radiation-pumped lasers and the buffer-gas region of the gaseous core nuclear reactor.

Balance equations for a finite system are developed for the slowing-down region, and the appropriate collision kernels are evaluated. These equations are solved numerically for the electron-flux distributions for primary source energies from 100 eV to 1 KeV, gas pressures from 0.1 to 10 Torr and also various plasma dimensions up to and including an infinite medium. Calculations of the W-value from these distributions for electrons in helium are found to be within 10% of experimental measurements. The results are also generally consistent with previous Monte Carlo calculations.

A Boltzmann equation with appropriate source and sink terms is considered for the low-energy range for cases both with and without a superimposed electric field ($0 \leq E/p \leq 10$ V -cm^{-1} - Torr^{-1}). Without the field, major deviations from a Maxwellian distribution are only observed for low gas pressures ($\lesssim$ 0.4 torr), small systems (tube radius $\lesssim$ 1 cm) and moderately high neutron flux values ($\gtrsim$ 5 x 10^{13} cm^{-2} -sec^{-1}). For the cases with an electric field, deviations from a Druyvestyen-type distribution are observed when the neutron flux density is high ($\gtrsim$ 5 x 10^{14} cm^{-2} -sec^{-2}) while the electric field is small ($E/p \lesssim$ 4 V -cm^{-1} Torr^{-1}). In general, the shifts of the distribution due to leakage and recombination depreciate the density in the low-energy region. This is attributed to the leakage of electrons during the slowing process.

It is suggested that the methods developed here can be used to aid Monte Carlo calculations through the development of a combined analytic-Monte Carlo approach. The methods described can also be extended to applications involving different gases or gas mixtures, although the derivation of new collision kernels is required.

ACKNOWLEDGMENT

The author wishes to thank and express sincere gratitude to Professor George H. Miley, his advisor, without whose guidance and invaluable suggestions the present work would not have been possible.

The author also wishes to thank Professor M. E. Wyman, head of the Nuclear Engineering Program and Professor J. T. Veradeyen for their encouragement and advice. Many of the discussions the author shared with his colleagues, Dr. J. C. Guyot, Dr. B. H. Wang and others in the Laser project proved to be enlightening and helpful. This work was supported in part by the Physics Branch of the AEC Research Division under Grant No. AT (11-1) - 2007 and by the NASA-AEC Space Power Office under Grant No. NGR 14-31-005-183.

The author thanks Mrs. Ruth Mann and Mrs. Eva Kingston for their excellent typing of the thesis manuscript.

The author wants to express appreciation for his parents! continuous encouragement and support. The author also wishes to express deepest gratitude to his wife, Josephine, for her love, understanding and patience; to his children, Yodia and Raoulie, for providing the much needed comic relief throughout the course of this work.

TABLE OF CONTENTS

CHAPTER I

DISCUSSION OF THE PROBLEM

A. Introduction

1. The Problem and Objectives

The present study is concerned with energy distribution of high energy electrons as they slow down and thermalize in a gaseous medium. The energy distribution in the entire energy range from source energies down is studied analytically. In particular, attention is given to a helium medium in which primary electrons are created by the passage of heavy-charged particles from nuclear reactions. As discussed later, a radiation-induced plasma of this sort is of interest in a variety of applications such as radiation pumped lasers and gaseous core nuclear reactors.

A continuous source of high-energy electrons will establish a quasi-steady-state in the energy distribution of the entire electron population. The problem is complicated by the fact that this population not only includes the primary electrons but also secondaries created by ionization collisions during slowing down. This situation has been analysed not only for an isolated system but also for the important case where an external electric field is imposed upon the medium.

2. Previous Work Related to the Problem

Electron energy distributions in the absence of high-energy sources have been extensively analyzed[1],[2], [3]. These studies all consider the situation where the distribution is sustained by an electric field, such as in the case of a gaseous discharge tube. On the other hand, the problem of electrons born at a high energy has only been studied in the case of β-irradiations or for electrons created by gamma irradiation[4] [5].

However, in these cases the energy range considered has been restricted to quite high energies --- from MeV to the low keV region --- since the interest has been mainly from the point of view of shielding calculations.

Lacking complete electron energy distributions, previous workers interested in applications of radiation-induced plasmas have generally estimated electron ionization and excitation rates assuming a thermalized electron swarm with a characteristic temperature[6],[7]. While it is true that the slowing down time of electrons is frequently short so that a bulk of the electron population approaches a Maxwellian shape (no electric field), the tail of the distribution determines these reaction rates, and the assumption of a Maxwellian "tail" can lead to erroneous results. Stated another way, we note that electrons born at high energies suffer inelastic collisions during the slowing process, and the resulting ionization and excitation rates are not adequately described by the Maxwellian tail associated with the thermalized electrons.

B. Physical Applications

Plasmas resulting from electrons slowing down after creation at high energies are of interest in many recent applications. In a laser system which utilizes nuclear energy input, the primary electrons are created in the lasing gas through the passage of heavy-charged particles through the gas[8]. In the nuclear light-bulb reactor concept[9], the primary electrons enter as β-radiation or from the ionizations due to fission fragments passing through the fuel region and through a buffer gas region. In the electron-beam fluorescence technique[10] which is used to study basic parameters in gas dynamics, primary electrons are introduced into the system in the form of a beam from an electron accelerator or "gun".

The slowing down processes in these situations differ. In the laser, electron-neutral gas atom processes generally dominate. For the nuclear light-bulb reactor, the thermal temperature is high and the uranium is thermally ionized. This leads to a high degree of ionization and electron interactions with uranium ions play an important role. In the electron beam fluorescence technique, the spatial geometry and the space charge of the beam become important. However, in all of these systems the problem of high energy electron slowing down and the resultant total electron energy distribution is of common concern.

The present study calculates the time and space independent electron energy spectrum for electrons slowing down in Helium. In particular, references are made to a system in which electrons are created by the passage and slowing of nuclear radiation as in a nuclear excited laser system. However, with some modifications, the present study can be applied to other situations. One situation of interest now at the University of Illinois is the electron-energy distribution in the region close to the fuel boundary and the buffer gas region of a nuclear light-bulb reactor.

C. The Model

A variety of schemes have been suggested to use nuclear energy in achieving laser excitation[8]. One method employed by the University of Illinois group is to utilize the neutron flux from a reactor for the nuclear reaction $n + \beta^{10} \rightarrow \alpha + Li$[11],[12]. Thus a laser tube is coated with Boron-10 and inserted into a nuclear reactor. The resultant heavy-charged particles traverse the laser gas and deposit their energy which may enhance laser excitation. Over half of the energy deposited is in the form of ionized δ-electrons. The resultant energy distribution of electrons studied here is therefore important to this concept.

A continuous δ-electron source is assumed. Many of the actual experiments at Illinois have employed a reactor pulse. However, the full-width at half-maximum of the reactor pulse is of the order of ten milli-seconds whereas the collision time of electrons in helium at one torr is the order of micro-seconds or less. Thus the electron energy distribution at any time during the pulse can be viewed as a quasi steady-state distribution.

While the present study primarily deals with the electron energy spectrum in helium, other gases or gas mixtures can be studied by the same method. Helium was chosen here because it is a main ingredient in many laser gas mixtures. Also it is representative of the noble gases such as neon that have been considered for use in the fuel and the buffer gas regions of the nuclear light-bulb reactor. Another reason for studying helium in this first analysis is that an abundance of cross section data available for it. This allows us to concentrate on the analytic technique, although even for helium great care is required in the development and selection of appropriate cross sections.

Many of the physical parameters employed in the present study such as tube dimensions, the boron-coating thickness, and the neutron flux magnitudes were selected to be consistent with radiation-induced plasma experiments performed by J. C. Guyot et al.[12],[13] Other assumptions involved include uniform physical properties in the system and the approximation of the cylindrical geometry by a slab geometry when energy deposition rates are computed (Figure G-1 of Appendix G).

A Monte Carlo calculation has been performed using the same model[14, 15] Both the present study and the Monte Carlo simulation serve to illustrate methods to obtain the solutions that can be applied to other situations of interest in the future. These methods compliment each other and depending on

the particular feature of a given problem, it may be that one of these methods is better from the point of view of efficiency and accuracy. For instance, in the high energy interval, the present analytical approach appears to be more efficient. This suggests that one future application of the present analytic method might be to combine it with the Monte Carlo code such that the high-energy region is treated analytically and this serves as a source to the low-energy Monte Carlo simulation.

CHAPTER II

THE ELECTRON FLUX DISTRIBUTION AT ENERGIES ABOVE THE FIRST EXCITATION POTENTIAL OF HELIUM

A. The Slowing-Down Flux Conservation Equations

After creation via heavy charged-particle ionization or via direct introduction as a high energy electron beam in a gaseous medium, electrons lose their energy traversing the medium. The resulting distribution is described by the electron distribution function $f_e(\vec{r},\vec{v},t)\, d\vec{r}d\vec{v}dt$, defined as the number of electrons in the phase space element, $d\vec{r}\, d\vec{v}\, dt$, at position $\vec{r}$ with velocity $\vec{v}$ and at time t. This function is governed by the Boltzmann Equation:

$$\frac{\partial}{\partial t} f_e(\vec{r},\vec{v},t) + \vec{v}\cdot\nabla_r f_e(\vec{r},\vec{v},t) + \frac{\vec{F}}{m_e}\cdot\nabla_v f(\vec{r},\vec{v},t) = \left(\frac{\partial}{\partial t} f(\vec{r},\vec{v},t)\right)_{coll.} \qquad (II\text{-}1)$$

where $\vec{F}$ is the externally imposed force. The collision term on the right hand side describes the sources and sinks of new particles into the phase space due to collisions. These collisions include processes such as elastic scattering, excitation, ionization and recombination.

To begin the problem at hand, we shall first consider a time and space independent case with no external force field imposed. In this limit, the energy distribution of electrons while slowing down is simply described by the collision term of the Boltzmann equation. The electrons are born at δ-ray energies and suffer large energy losses through a series of inelastic collisions. These include ionization collisions which produce secondary electrons that in turn slow down. Both primary and secondary electrons eventually thermalize, but we will first concentrate on the slowing down problem and therefore, we restrict the lowest energy to the first excitation potential of the gas. In this range, the electrons are at a much

"Page missing from available version"

included in the total flux calculation. Thus, instead of the approximation of equation (II-2), we consider the exact balance equation for collisions into and out of an energy interval dE at E due to the slowing down of electrons originating from a delta function source at E_o. This is:

$$\Sigma_{tot}(E)\Phi(E)dE = S_p\delta(E-E_o)dE + \sum_j \Sigma_j(E'\rightarrow E)\Phi(E')dE'dE + S(E)dE \qquad \text{(II-3)}$$

where, $\Sigma_{tot}(E)$ = total collisional cross-section at energy E

$\Sigma_j(E'\rightarrow E)dE$= differential cross-section for the scattering of electrons with energy E' into energy dE at E through the j^{th} type of collision.

$S(E)dE$ = source of secondary electrons introduced in the energy band dE at E.

In practice it is most convenient to use an integral form of equation (II-3). This eliminates the delta function and in effect smooths the cross-sections leading to less fluctuations in numerical integrations.

From appendix (B), the integral form of equation (II-3) takes the form:

$$\sum_j \int_E^{E_o} \Phi(E_o,E')K_j(E',E)\,dE' = S_p + \int_E^{E_o} \Phi(E_o,E'')K_s(E'',E)dE'' \qquad \text{(II-4)}$$

where j denotes various excitation and ionization processes.

$K_j(E',E)$ = probability per track length that an electron suffers a j^{th} type collision and slows down past energy E from E'.

$K_s(E'',E)$ = probability per track length that a secondary electron is born with energy larger than E due to a collision by a primary electron with original energy E''.

The equivalence of this equation and equation (II-3) is demonstrated in appendix (B).

Equation (II-4) states that the number of electrons slowing down past energy E must be equal to the introduction of electrons with energies larger than E. Spencer and Fano and other authors[16,17] have worked with the same type of balance equation for high energy β-radiations (MeV slowing to keV). They used the Möller[18] relativistic collision cross-sections and included Bremsstrahlung energy losses. In the present case, Bremsstrahlung can be neglected but energy losses from excitation collisions must be included. Also Vrien's Binary Collision Model cross-section[19,20], which is more appropriate for the lower energy range, is employed.

As shown below, elastic scatterings between neutral gas atoms and electrons give only a small contribution to the slowing down of electrons. [This effect, however, plays a role in the diffusion leakage of electrons out of a finite system, and will be considered later.] This elastic collision cross-section, as approximated by the Lenz relation[21], is:

$$\frac{Q_{in}}{Q_{el}} \approx \frac{4}{z} \log \frac{h v_e z^{1/3}}{\pi E_o a_o} \qquad \text{(II-5)}$$

where, Q_{in} = total inelastic collision cross-section,

Q_{el} = total elastic collision cross-section,

h = Plank's constant,

E_o = ionization potential of gas atom,

a_o = first Bohr radius,

and V_e = velocity of impinging electron.

For an electron with energy above tens of eV in helium, Q_{in} and Q_{el} are of roughly the same order of magnitude. Since the mass ratio between electrons and the neutral atom is about 1/7300, the energy loss due to elastic collisions can be neglected. This fact has been further verified in Appendix (C),

where the average fractional energy loss per track length due to elastic collisions with neutral atoms is shown to be small compared to that for inelastic collisions with atomic electrons. This comparison is done for the energy range above the excitation potential such that the Born approximation is applicable for elastic collisions and the Möller cross-section is valid for electron-electron inelastic collisions.

B. The Slowing-Down Kernels

The binary encounter collision theory employed here follows the classical theory of atomic collisions developed by M. Gryzinski[22,23] with later corrections and discussions by various authors[24,25,26]. This type of cross-section was selected in preference to purely quantum mechanical cross-sections because their relatively simple form permits analytic integration. Another reason is their apparent good agreement with experimental measurements, especially in the lower energy range.

In contrast to the Thomson cross-section, the Gryzinski cross-section accounts for the motion of atomic electrons in the target atom. The original Gryzinski model, however, is asymmetrical for the two interacting electrons. Thus, if both the incident electron and the atomic electron are at a distance r from the nucleus, one would have zero and the other would have $-e^2/r$ potential energy. To correct this, Burgess[27] and Vriens[29] introduced a binary encounter model with symmetrical treatment of the two interacting electrons. Thus, the incident electron gains a kinetic energy W and at the same time loses the same amount of potential energy as it interacts with the atomic electron. The atomic electron is assumed to be bounded with the same potential energy, W; thus the two electrons are symmetrical and indistinguishable upon interchange.

In a later refinement, Vriens[20] developed a quantum mechanical formulae for transfer of momentum and energy between a pair of free colliding electrons. He then applied these formulae to the electron-atom binary encounter theory to obtain differential and total cross-sections. The symmetrical collision model was also incorporated and the influence of the nucleus was included. The resultant differential cross-section contains the direct, exchange, and interference contributions, and it is given by Appendix (D). The differential cross-section for a loss of energy ΔE is given as:

$$\sigma_{\Delta E} = \frac{1}{4}\sigma^{+}_{\Delta E} + \frac{3}{4}\sigma^{-}_{\Delta E} \tag{II-6}$$

and

$$\sigma^{\pm}_{\Delta E}\, d\Delta E = \frac{\pi e^4}{E_3}\left[\frac{1}{\Delta E^2} + \frac{4}{3}\frac{E_2}{\Delta E^3} + \frac{1}{(E_3-E_2-\Delta E)^2} + \frac{4}{3}\frac{E_2}{(E_3-E_2-\Delta E)^3} \pm \frac{2\Phi'}{\Delta E(E_3-E_2-\Delta E)}\right] d\Delta E; \quad E'_3 \geq E_2 \tag{II-7}$$

$$\sigma^{\pm}_{\Delta E}\, d\Delta E = \frac{\pi e^4}{E_3}\left[\frac{1}{\Delta E^2} + \frac{4}{3}\frac{E'_3}{\Delta E^3} - \frac{1}{(E_3-E_2-\Delta E)^2} + \frac{4}{3}\frac{E'_3}{(E_3-E_2-\Delta E)^3} \pm \frac{2\Phi'}{|E_3-E_2-\Delta E|\Delta E}\right]\left(\frac{E'_3}{E_2}\right)^{1/2} d\Delta E; \quad E'_3 \leq E_2 \tag{II-8}$$

where E_1 = energy of incident electron

E_2 = average kinetic energy of atomic electron

$E_3 = E_1 + E_2 + U$

U = ionization potential energy

$E'_3 = E_3 - \Delta E$

and $\Phi' = \cos \frac{R}{E_3-E_2}^{1/2} \ln \frac{E}{E_3-E_2-E}$

R = Ryberg's constant.

The total ionization cross-section derived from this differential cross section has been compared with experimental results, and good agreement is observed at low to moderate energies. However, in the present work, we are more interested in a direct check of the differential cross sections [Equations (II-7) and (II-8)] since they lead to the slowing down kernels. Since direct measurements of the cross sections are not available, it was decided to compare calculated and measured energy distributions for secondary electrons produced by a primary beam of electrons of energy E on a suitable thin target. Figures (1 to 5) compare the calculated probabilities using binary models with experimental measurements by C. B. Opal et.al.[28]. The experiments were performed at a pressure of 2×10^{-5} torr or less and multiple scatterings would be expected to be negligible. Quite good agreement is observed, lending confidence to our use of these cross-sections.

Appendix D gives the calculation of slowing-past kernels by integrating the differential energy loss cross-sections over the appropriate limits. The probability per unit track length that an electron will emerge with energy less than E from energy E' due to an ionization collision, $K_I(E',E)$, is given by:

for $(E' + U)/2 \leq E'-E$; $\quad K_I(E',E) = 0$ (II-9)

for $(E' + U)/2 \geq E'-E > U$;

$$K_I(E',E) = \frac{N_e \pi e^4}{E_3}\left\{\frac{1}{E'-E} - \frac{1}{E_3-E_2} - \frac{2}{3}E_2\left[\frac{1}{(E'-E_2)^2} + \frac{1}{(E_3-E_2)^2}\right]\frac{\Phi''}{(E'+U)}\ln\left(\frac{E+U}{E'-E}\right)\right\} \quad \text{(II-10)}$$

and for $(E'-E) \leq U$:

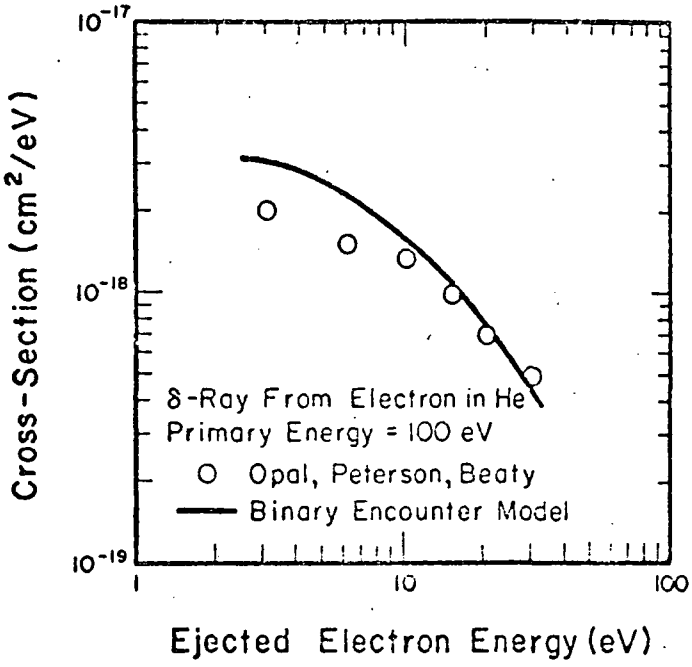

Figure 1.

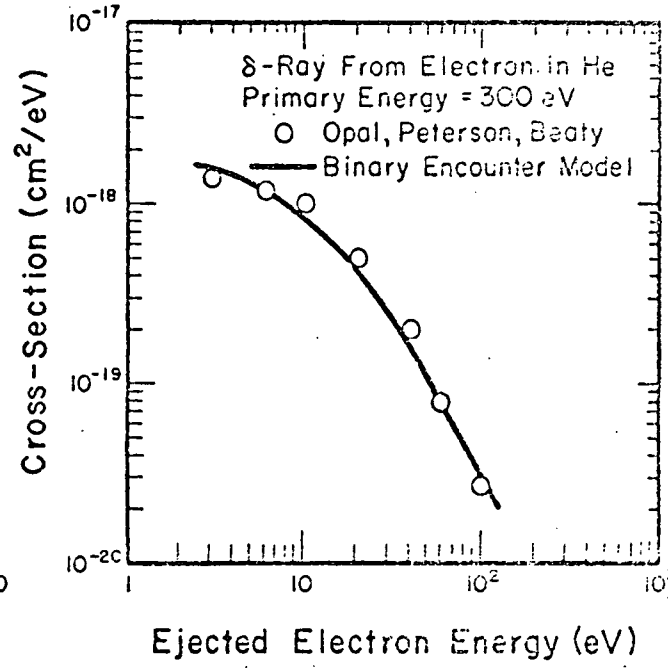

Figure 2.

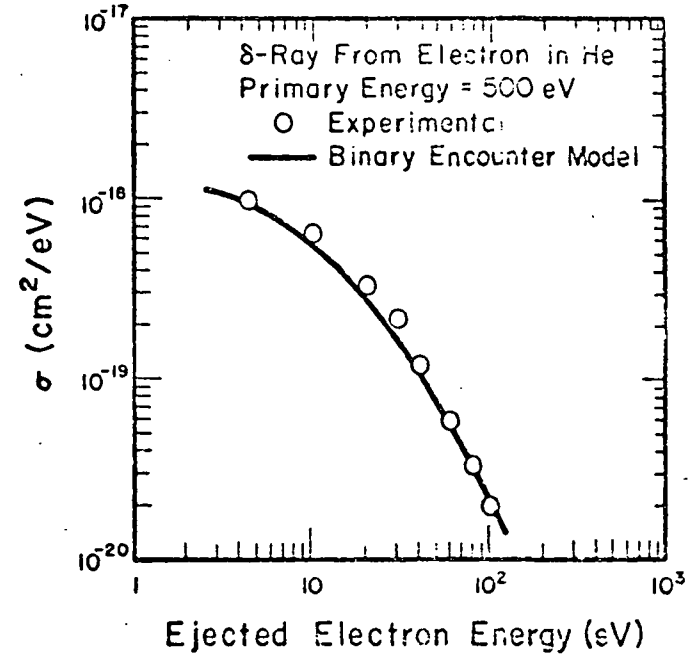

Figure 3.

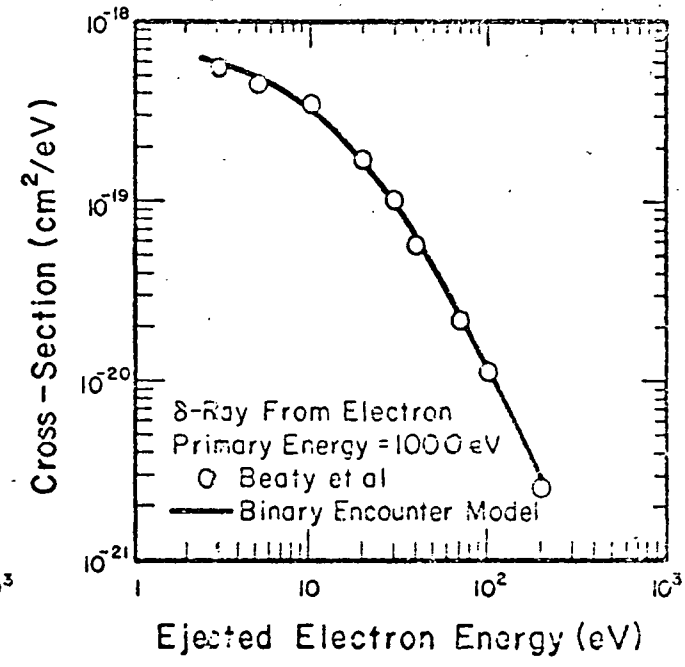

Figure 4.

Figures 1. to 4. Comparison of Calculated and Measured Secondary-Electron Distributions for Primary Energies of 100, 300, 500 and 1000 eV

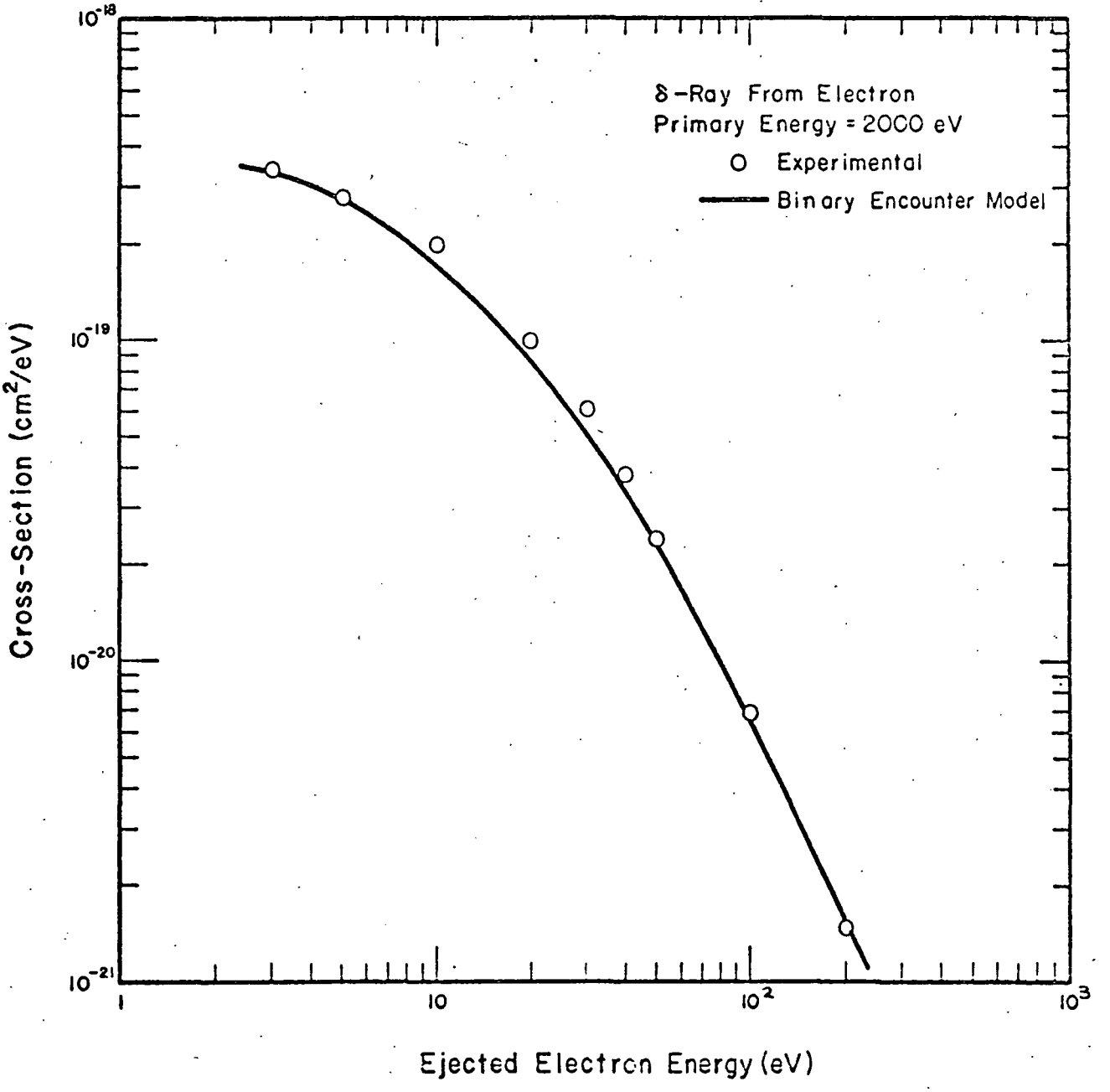

Figure 5. Comparison of Calculated and Measured Secondary-Electron Distributions for Primary Energy of 2000 eV

$$K_I(E',E) = \frac{N_e \pi e^4}{E_3} \left\{ \frac{1}{U} - \frac{1}{E'} + \frac{2}{3} E_2 \left[\frac{1}{U^2} - \frac{1}{E'^2} \right] \right.$$

$$\left. - \frac{\Phi''}{(E'+U)} \ln \left(\frac{E'}{U} \right) \right\} , \qquad \text{(II-11)}$$

where we have used the same notations as in equations (II-7) and (II-8) with the addition that N_e is the total number of valance atomic electrons per cm^3. In the case of helium, $N_e = 2N$ where N is the density of helium atoms, and one does not have to sum over the electrons in different atomic shells as in the case of more complex atoms discussed in Appendix D. Also Φ'' is defined in Appendix D.

The probability per unit track length that an electron will emerge with energy less than E from energy E' due to an excitation collision is $K_{ex}(E',E)$. Within the one excitation level model discussed in Appendix D, the incident electron loses an amount of energy τ which is larger than the first excitation energy but less than the ionization energy of the atom. The atomic electron does not gain sufficient energy to be ionized, an excitation is considered to have occurred, and the excitation slowing-past kernel is given by:

for $E'-E \geq U$; $\quad K_{ex}(E',E) = 0 \qquad \text{(II-12)}$

for $U \geq E'-E \geq U_1$;

$$K_{ex}(E',E) = \frac{N_e \pi e^4}{E_3} \left\{ \frac{1}{E'-E} - \frac{1}{U} + \frac{1}{E'} - \frac{1}{E+U} + \frac{2}{3} E_2 \left[\frac{1}{(E'-E)^2} \right.\right.$$

$$\left.\left. - \frac{1}{U^2} - \frac{1}{E'^2} - \frac{1}{(E+U)^2} \right] - \frac{\Phi'''}{(E'+U)} \ln \left[\frac{U(E+U)}{E'(E'-E)} \right] \right\} \qquad \text{(II-13)}$$

and for $U_1 \geq E'-E$;

$$K_{ex}(E',E) = \frac{N_e \pi e^4}{E_3} \left\{ \left(\frac{1}{U_1} - \frac{1}{U} \right) - \left(\frac{1}{E'} - \frac{1}{E'+U-U_1} \right) + \frac{2}{3} E_2 \left[\frac{1}{U_1^2} - \frac{1}{U^2} - \frac{1}{E'^2} - \right.\right.$$

$$\left.\left. \frac{1}{(E'+U-U_1)^2} \right\} - \frac{\Phi'''}{E'+U} \ln \left[\frac{U(E'+U-U_1)}{E' U_1} \right] \right\} \qquad \text{(II-14)}$$

where U_1 is the first excitation level energy and Φ''' is defined in Appendix D.

The secondary production kernel is defined as the probability per unit track length that an electron with energy E' will produce, through an ionization collision, two electrons with energies both larger than E. This is given by Appendix D as:

for $$E' \leq 2E + U \quad ; \quad K_s(E', E) = 0 \tag{II-15}$$

for

$$E' \geq 2E + U$$

$$K_s(E', E) = \frac{N_e \pi e^4}{E_3} \left\{ \frac{1}{E+U} - \frac{1}{E'-E} + \frac{2E_2}{3} \left[\frac{1}{(E+U)^2} - \frac{1}{(E'-E)^2} \right] - \frac{\Phi''}{E'+U} \ln \left[\frac{E'-E}{E+U} \right] \right\} \tag{II-16}$$

When equation (II-4) is rewritten with the three slowing down past kernels considered above, we obtain:

$$\int_{E+U}^{E+\Delta} K_I(E', E)\, \Phi(E')\, dE' + \int_{E+U_1}^{E+\Delta} K_{ex}(E', E)\, \Phi(E')\, dE' = S_p + \int_{2E+U}^{E_0} K_s(E', E)\, \Phi(E')\, dE' \tag{II-17}$$

where $\Delta = E + U$ for $2E + U \leq E_0$ and $\Delta = E_0 - E$ if $2E + U \geq E_0$

The form of $K_{ex}(E', E)$ can stand some improvement. When experimental excitation cross-sections are available $K_{ex}(E', E)$ can be expressed exactly according to the experimental results. We shall let $K_{ex}^{\lambda}(E', E)$ be the probability that an electron will slow down past E from E' per unit track length due to an excitation collision which leaves the atomic electron

in the j^{th} excited state. Then the relation between $K_{ex}^{j}(E',E)$ and $N_e \sigma^j(E')$, the total excitation cross-section at energy E' for the j^{th} excitation level, is:

$$K_{ex}^{j}(E',E) = 0 \qquad \text{for} \quad E' \leq U_j \tag{II-18}$$

$$K_{ex}^{j}(E',E) = N_e \sigma^j(E') \qquad \text{for} \quad (E'-E) \leq U_j \,, \; E' \geq U_j \tag{II-19}$$

$$K_{ex}^{j}(E',E) = 0 \qquad \text{for} \quad (E'-E) \geq U_j \tag{II-20}$$

where U_j = j^{th} level excitation energy.

We are able to define $K_{ex}^{j}(E',E)$ in this simple manner because a definite amount of energy is lost in an excitation collision. No such relation exists, however, for ionization collisions so the experimental total ionization cross-section cannot be utilized in this manner. With the notation of $K_{ex}^{j}(E',E)$, equation (II-17) takes the form:

$$\int_{E}^{E+\Delta} K_I(E',E)\Phi(E')dE' + \sum_j \int_{E}^{E+\Delta} K_{ex}^{j}(E',E)\Phi(E')dE' =$$

$$S_p + \int_{2E+U}^{E_0} K_s(E',E)\Phi(E')dE' \tag{II-21}$$

For the case of helium, we shall include the excitation levels with the largest cross-sections in our calculations. Although the experimental observations are incomplete, especially for n = 2, we shall approximate them with analytic expressions. We shall demonstrate that this is superior to the one-level Gryzinski-type excitation model.

C. W-Value and Leakage

The production of secondary electrons and the excitation of atoms occur at an energy above the first excitation potential in neutral ground state noble gases. Thus the energy flux spectrum obtained through equation (II-4)

or equation (II-21) can be used to calculate the primary input energy necessary to produce one ion-pair. This is best done through $q(E = U_1)$, the slowing down past density (total # slowing down past energy E/time volume), which is as shown in Appendix E:

$$q(E = U_1) = \int_{U_1}^{E} \Phi(E'') K_{IN}(E'', U_1)\, dE'' \qquad \text{(II-23)}$$

where $K_{IN}(E'', U_1)$ is defined as the number of electrons that appear with energy below U_1 per unit track length at energy E''. With this, the energy necessary to produce an ion-pair, W, can be calculated as:

$$W = S_p E_o / q(E = U_1) \qquad \text{(II-24)}$$

The W-value found in this manner provides a convenient check with experimental data since a number of such measurements have been reported.

Another aspect of the present problem is that leakage must be considered if the system is finite, i.e. especially when the system is small and/or pressure low. The inclusion of leakage losses with a spatially dependent source is a complex problem. We shall assume cylindrical geometry with uniform electron production throughout the gas volume. Then if leakage is approximated by the first fundamental mode as postulated by J. C. Guyot[12,13] in his atomic metastable density calculations, the spatial flux $\Phi(r, z)$ is given by:

$$\Phi(r, z) \doteq A J_o\left(\frac{2.405\, r}{R}\right) \cos\left(\frac{\pi z}{L}\right) \qquad \text{(II-25)}$$

where R and L are the radius and length of tube and the origin of the co-ordinate system is at the center of the tube, and A is an normalization which depends on the source strength.

The diffusion approximation of the particle transport equation (Appendix F) gives a diffusion coefficient in terms of collision cross-sections. For the high energies involved in slowing down, this diffusion coefficient

should be used instead of the ambipolar diffusion coefficient. Then the leakage term is approximated by:

$$-D(E)\nabla^2\Phi(E_o,E) = \frac{D(E)}{\Lambda^2}\Phi(E_o,E) \qquad \text{(II-26)}$$

where Λ is a characteristic length of the system. For a cylindrical tube, within the fundamental mode approximation, Λ^2 is given by:

$$\Lambda^2 = \left(\frac{2.405}{R}\right)^2 + \left(\frac{\pi}{L}\right)^2 \qquad \text{(II-27)}$$

With this leakage term included, equation (II-21) becomes:

$$\int_E^{E_o} \frac{D(E')}{\Lambda^2}\Phi(E_o,E')\,dE' + \int_E^{E+\Delta} K_I(E',E)\Phi(E_o,E') + \sum_j \int_E^{E+\Delta} K_{ex}^j(E',E)\Phi(E_o,E)dE'$$

$$= S_p + \int_{2E+U}^{E_o} K_s(E',E)\Phi(E_o,E')\,dE' \qquad \text{(II-28)}$$

where the first term on the L.H.S. accounts for rate of leakage out of the system by electrons with energy larger than E.

D. Computation and Results

1. Infinite Medium

The case when leakage can be neglected is considered first. Following Fano and Spencer[16], equation (II-17) was solved numerically. The integrals are expanded by summations and equation (II-17) becomes:

$$\sum_j \sum_{i=n}^{k'} K_j(E_i,E_n)\Phi(E_k,E_i)W_i\Delta E_i = S_p + \sum_{\ell=2n+I}^{k} K_s(E_\ell,E_n)\Phi(E_k,E_\ell)W_\ell\Delta E_\ell \qquad \text{(II-29)}$$

where W_i, W_ℓ are weights of numerical integration, $I = U/\Delta E$ gives the number of intervals in the ionization potential, and the index j denotes the j^{th} type of slowing down process. The quantity k' is equal to $2n+I$ if $2n+I \leq k$, or equal to k if $2n+I \geq k$, E_o being the maximum δ-ray

energy. For $2n+1 \geq k$ the last term on the right hand side of equation (II-29) vanishes. Equation (II-29) is solved step-wise on a computer from n = k down. For a general n , $\Phi(E_k, E_n)$ is given by:

$$\Phi(E_k,E_n) = \frac{\left[1 + \sum_{\ell=2n+1}^{k} K_s(E_\ell,E_n)\Phi(E_k,E_\ell)W_\ell \Delta E_\ell - \sum_j \sum_{i=n-1}^{k'} K_j(E_i,E_n)\Phi(E_k,E_\ell)W_i \Delta E_i \right]}{\sum_j K_j(E_n,E_n)W_n \Delta E_n} \qquad \text{(II-30)}$$

The flux density distribution of equation (II-30) has been solved using several different models of cross-sections in helium. These cross sections are illustrated in the following figures and table. Figure [6] compares the total ionization cross-section obtained through the integration of Vrien's differential cross-section (binary collision theory) with experimental observation. A semi-empirical "modified" Vriens cross-section is also shown which uses multiplicative fitting parameters to match the experimental results.

For excitation losses, since we can utilize the total experimental cross-sections, empirical formulas are used to fit the experimental data. Table (II-1) and Figures (7-10) illustrate some of the excitation cross-sectional values we used. We have only included the six largest excitation cross-sections as the others will give comparatively little contribution. When experimental measurements are not available, we have resorted to a Bethe-Born type approximation [30,31].

Figure (II-11) compares the electron flux density spectrum for a unit primary electron source at 500 eV obtained by using a one excitation level model with that obtained using the excitation cross-sections of Table (II-1). The general shape of distribution is similar to those obtained by Miller [17] for β-radiation in water, and it is also in general agreement with Monte-

"Page missing from available version"

Table II-1. Fitted Excitation Cross-Section for Helium

Excited State	Cross-section $(A^o)^2$	Energy Range(eV)	Reference for Data Used in Fit
2^3S	$\frac{0.0306(E-19.8)}{0.25+(E-19.8)^2} + 0.0086$	Above 19.7	[34],[35]
2^1S	$\frac{3.5}{E/R}\left[0.0455 - \frac{0.0317}{E/R}\right]$	Above 20.6	[30],[31]
2^3P	$\frac{0.0114(E-20.8)}{0.25+(E-20.8)^2} + 0.0032$	Above 21.2	[36]
2^1P	$\frac{3.5}{E/R} - 0.085+0.177\ \ell n\ \frac{E}{R} + \frac{0.0376}{E/R}$	Above 21.5	[30],[31]
3^3S	$[9.6E - 224] \times 10^{-4}$	22.6-35	[33]
	$[-4.66E + 273] \times 10^{-4}$	35 - 65	
	$[2 \times 10^{-4}]$	Above 65	
3^1S	$[3.4E - 78] \times 10^{-4}$	22.8 - 37	[33]
	$[-0.45E + 64.8] \times 10^{-4}$	37 - 70	
	$[-0.112E + 40.8] \times 10^{-4}$	70 - 207	
	$[-0.0208E + 22.17] \times 10^{-4}$	207 - 1000	
3^1P	$[6E - 100] \times 10^{-4}$	23.3 - 65	[33]
	$[1.1E + 200] \times 10^{-4}$	65 - 100	
	$[-0.433E + 373.3] \times 10^{-4}$	Above 100	

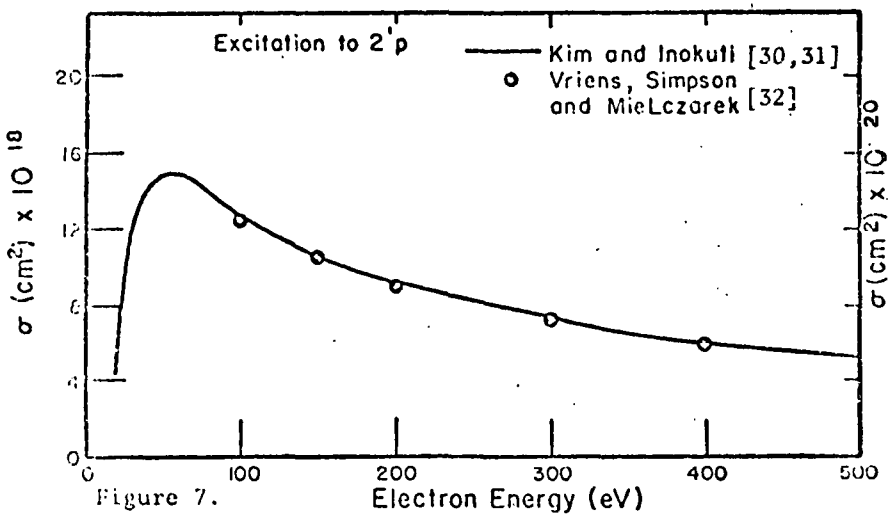

Figure 7.

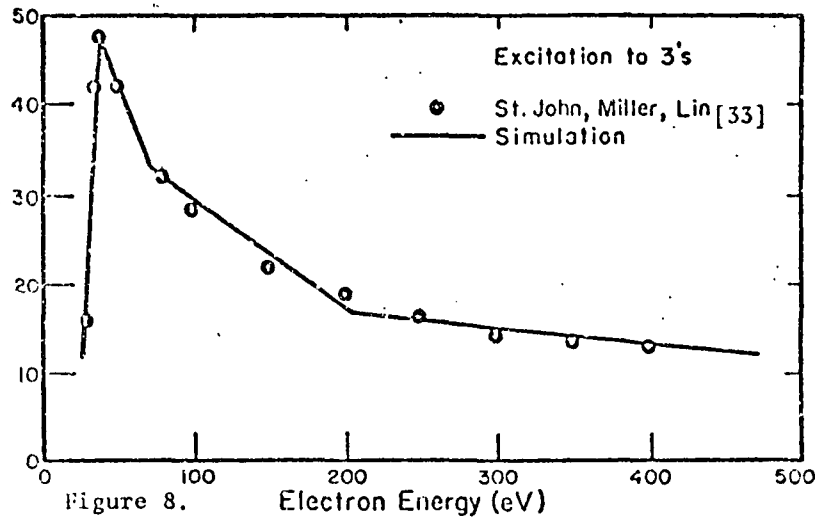

Figure 8.

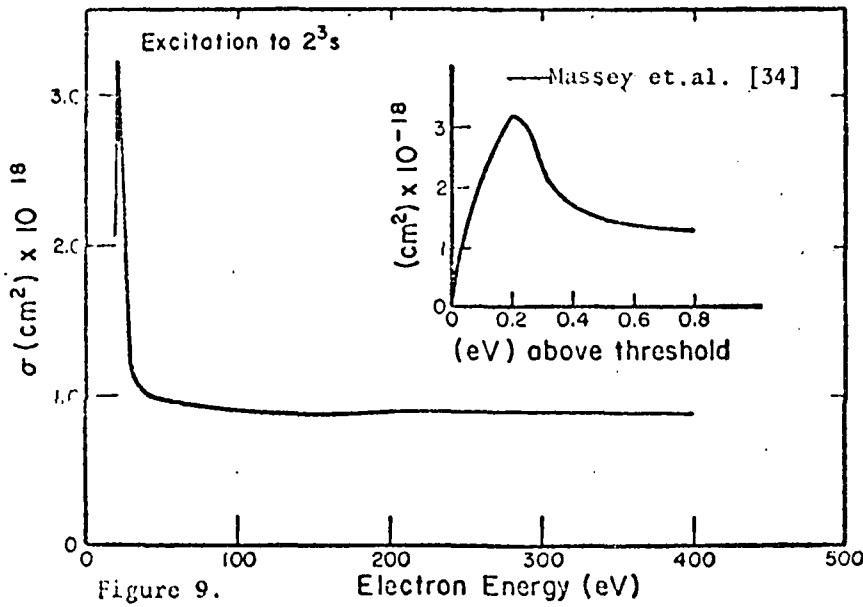

Figure 9.

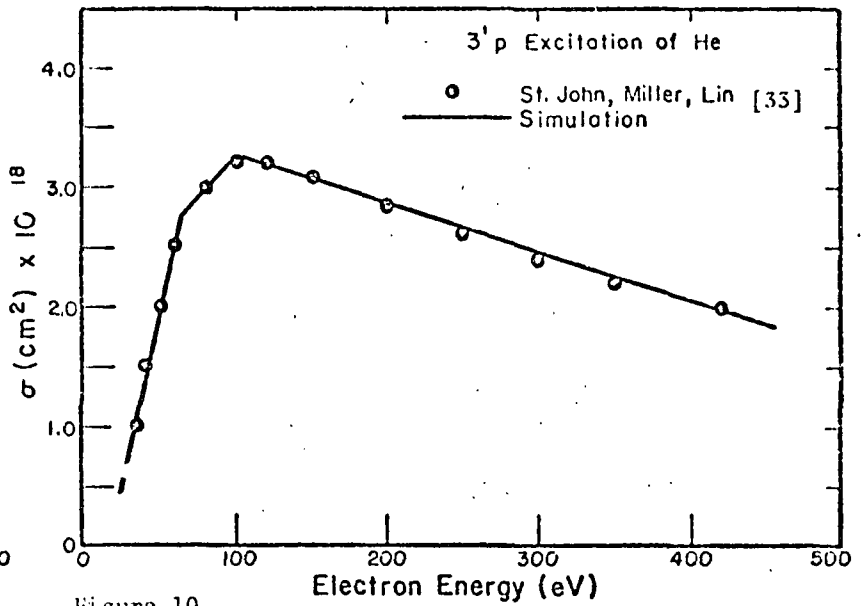

Figure 10.

Figures 7. to 10. Comparison of Simulated and Measured Excitation Cross Sections of Helium

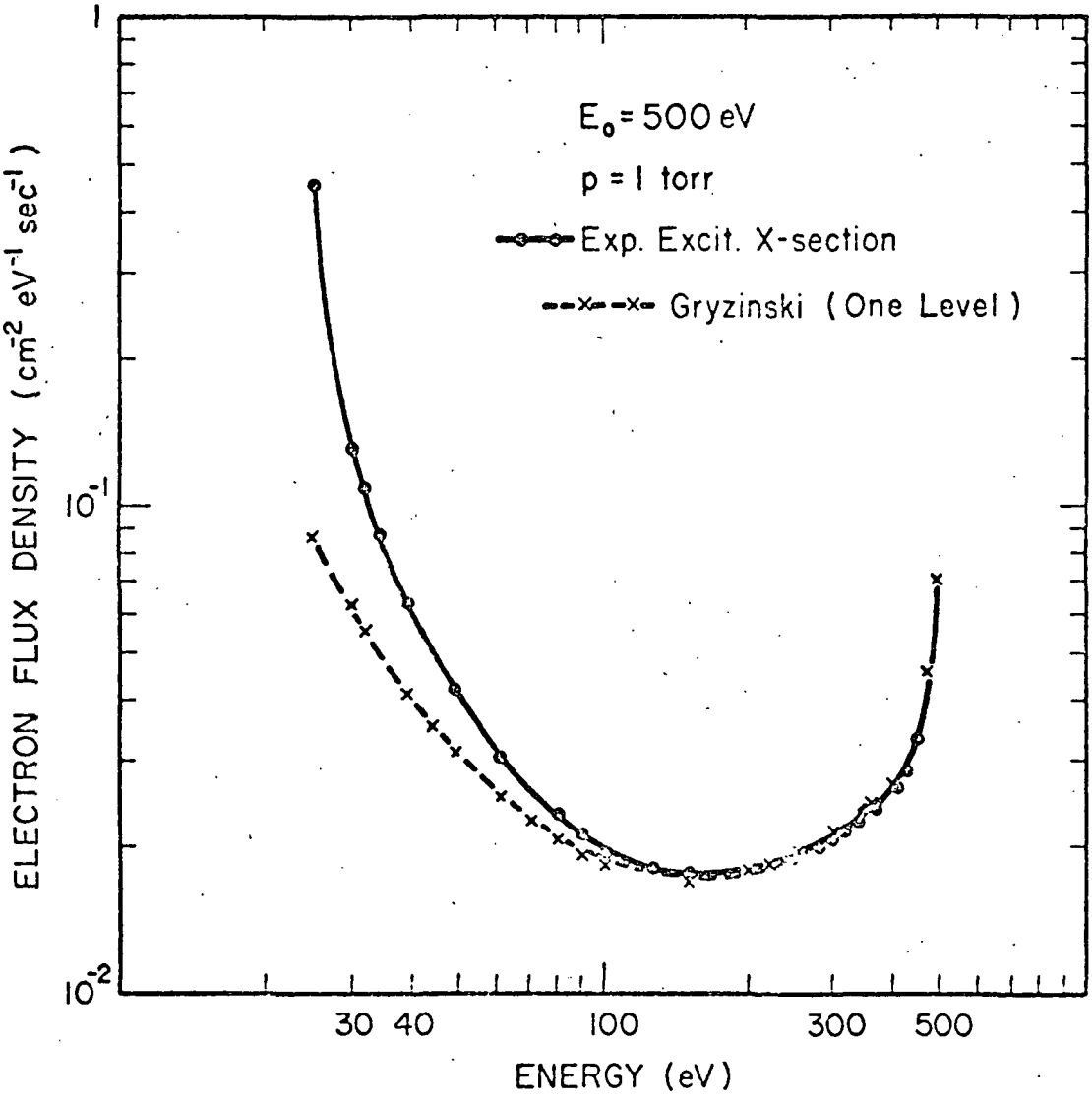

Figure 11. Electron Flux Distributions for 500-eV Primary Source Calculated by a One-Level Excitation Model and by Experimental Excitation Cross Sections

Carlo calculation by B. Wang[15]. The rise of the flux density after about 150 eV is entirely due to the creation and slowing down of the secondary electrons. W-values have been calculated from these distributions using the slowing-past kernel $K_{iN}(E,U_i)$ developed in Appendix E. The W-value obtained from the distribution from the experimental excitation cross-section is 43.5 eV per ion pair and the one obtained from the one excitation level model is 49.1 eV/ion pair. This compares with the experimental value of Jesse and Sadanskis of 42.3 eV/ion pair [37]. This demonstrates that the one excitation level model , which is admittedly crude, tends to overestimate the amount of excitation.

Figures 12 and 13 show the flux density distributions for a 1 Kev and a 250 eV primary electron source. As indicated in table (II-2), the W-value from 250 to 1000 eV varies less than 10%. This verifies experimental indications that the W-values are essentially energy independent over this range[38]. Furthermore, since the ratio of excitation cross-section to ionization cross-section is independent of pressure, the W-value will be pressure independent in this model.

Figure 14 compares the results obtained using the binary collision theory cross-section (Vriens) with those for the modified Vriens or semi-empirical fitted cross-section for a primary source energy of 1 keV. Figure 15 compares the above two cases together with a one excitation level model case for a source energy of 500 eV.

The curves for the two models shown in Figures 14 and 15 are reasonably consistent, although some discrepancies are noted. Some further feeling for the agreement of the two can be obtained by calculating W-values from these distributions. The W-values are listed in Table II-2. Both results are close to the experimental value and are essentially independent of energy.

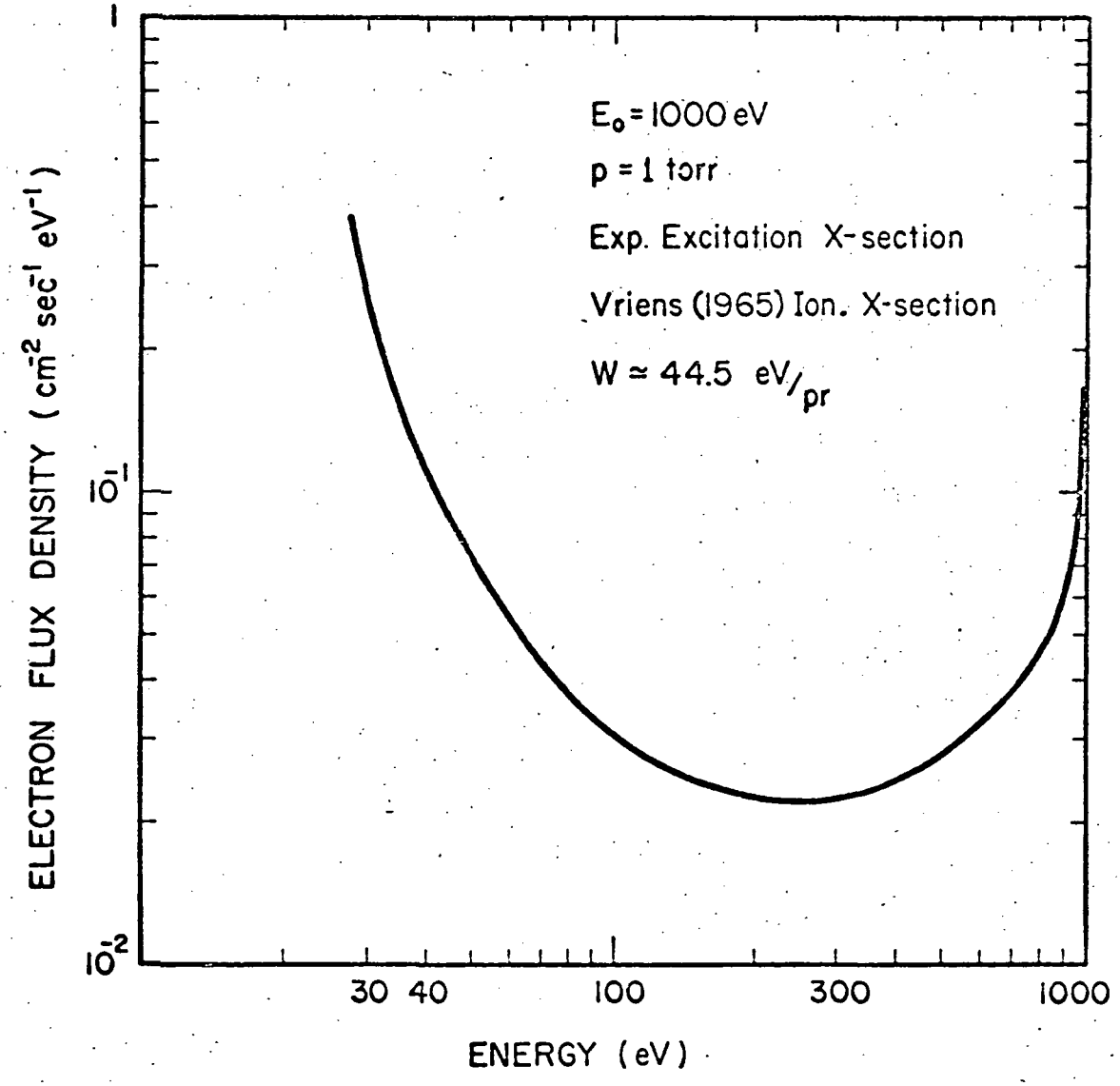

Figure 12. Electron Flux Distribution for a 1-KeV Primary Source

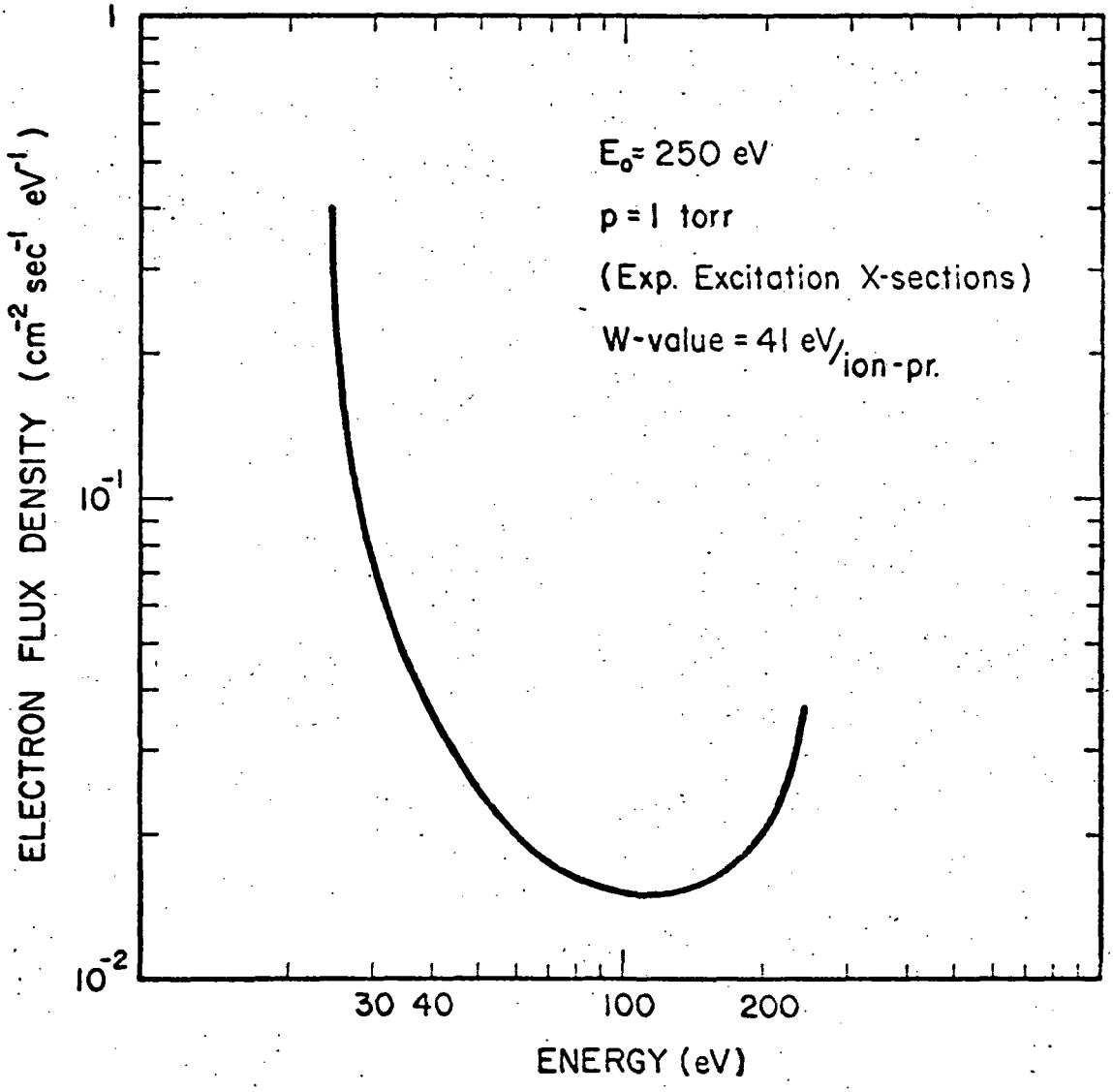

Figure 13. Electron Flux Distribution for a 250-eV Primary Source

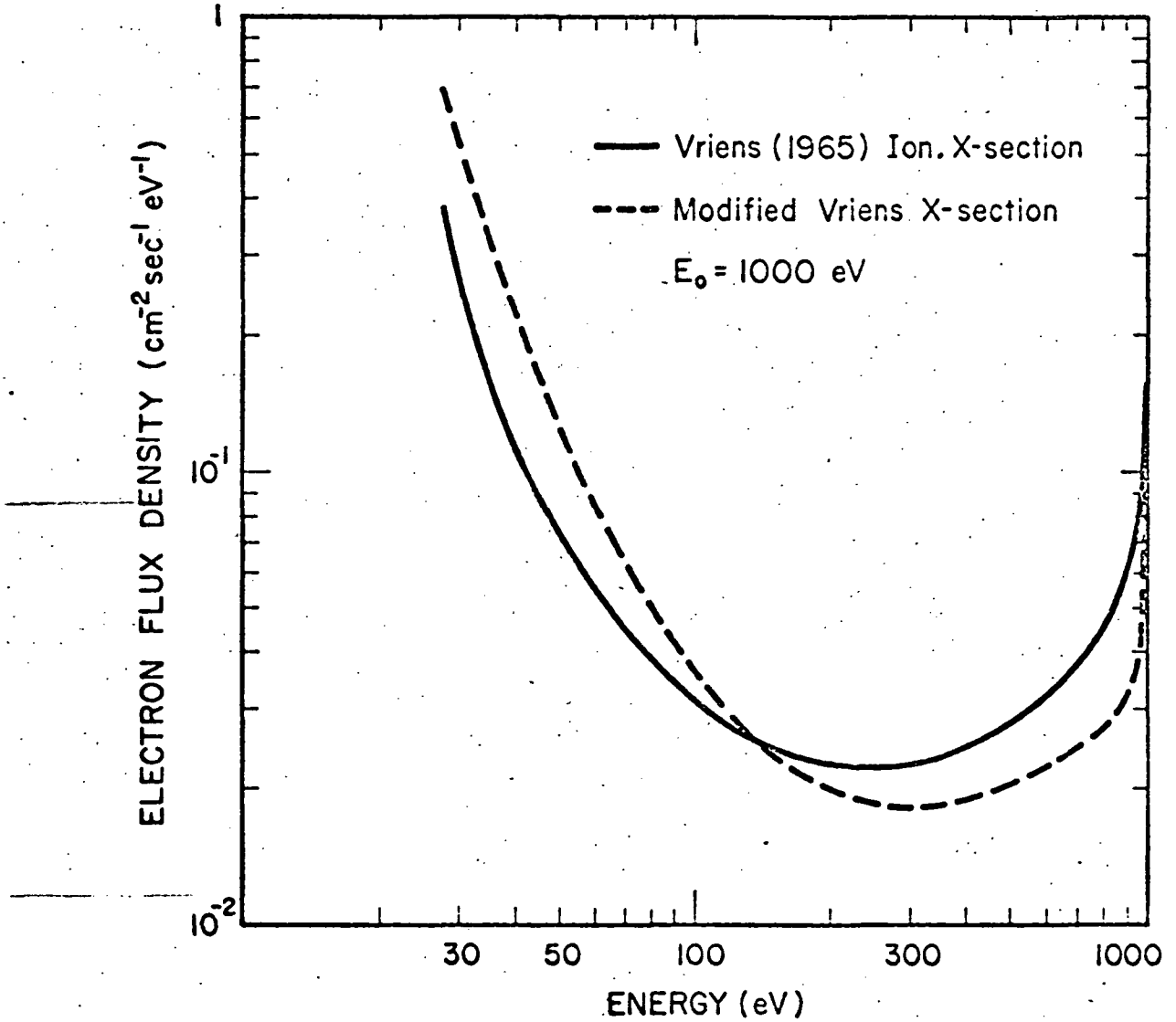

Figure 14. Comparison of Electron Flux Distributions Obtained Using Vriens Cross Sections and Fitted Vriens Cross Sections for a 1-KeV Primary Source

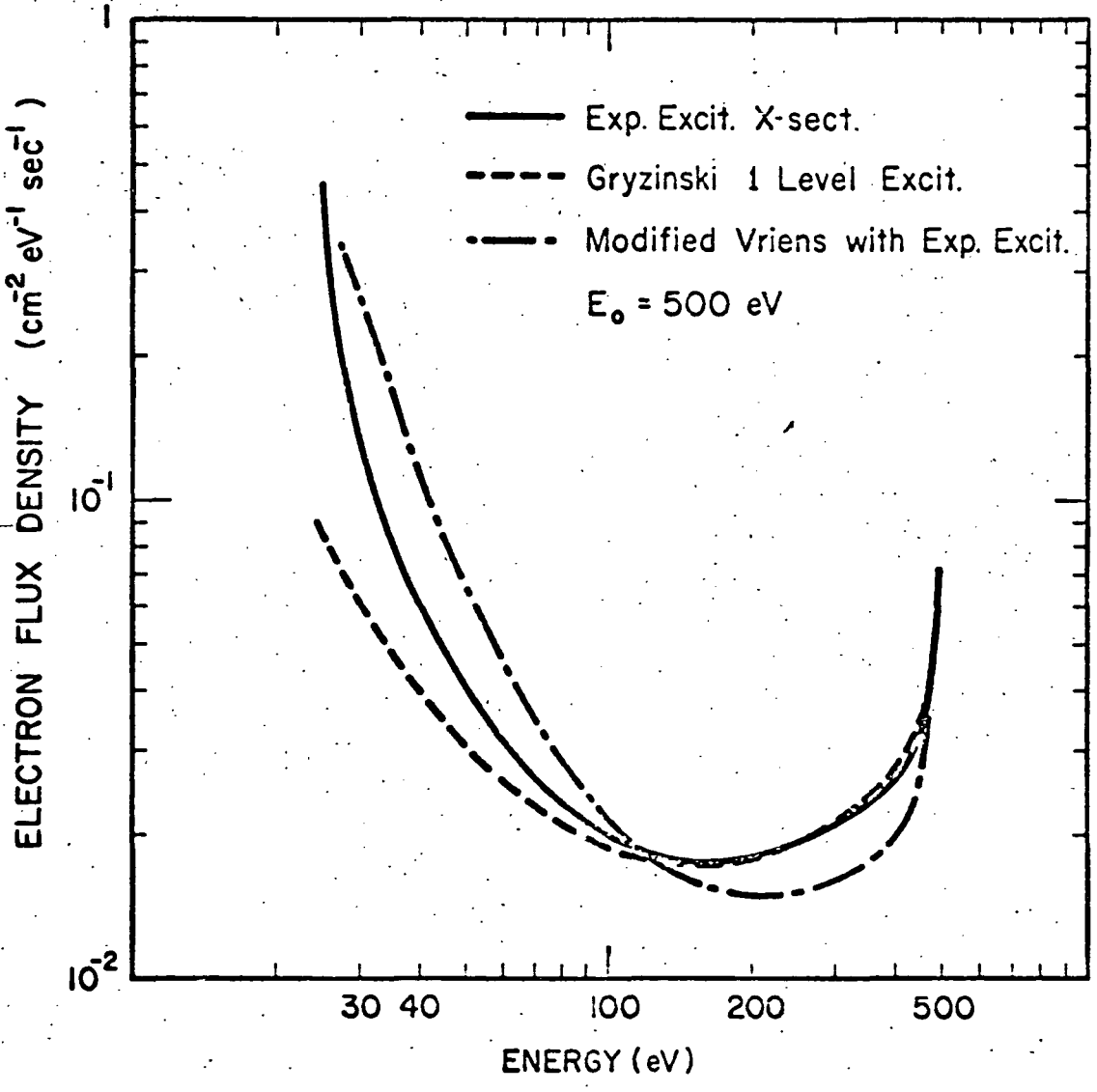

Figure 15. Comparison of Electron Flux Distributions Obtained Using Multi-level Experimental Excitation Cross Sections with 1) Vriens and 2) Fitted Vriens Cross Sections and by a 1-level Excitation Model

Table II-2. W-Values for Electrons in Helium[a]

Primary energy (eV)	Calculated W-value, eV/ion pair Vrien's cross section	Semi-empirical cross-section
1,000	41 (49.1)[b]	44
500	43.5	45
250	44.5	45

[a]The average W-value over this energy range as measured by Jesse and Sadankis is 42.3 eV/pr [37]

[b]W-value calculated with the one excitation level model.

Table II-3. W-Values for Various Noble Gases[c]

Gas	Ionization Energy (eV)	1st Excitation Energy (eV)	W-value, eV/ion pair Calculated[d]	Experiment [37]
He	24.47	19.7	49.1	42.3
Ne	21	15.7	42.9	36.6
A	15	11.2	35.6	26.4
Kr	13.99	10.0	31.2	24.1
Xe	12.13	9.0	25.6	22

[c]Primary electron energy of 1 keV

[d]One excitation level model

Thus it can be concluded that either cross section model can be used with reasonable confidence. In contrast, as observed earlier, W-values for the simple one-level model are considerably higher than the experimental values.

Figure 16 shows the electron flux density distribution for three initial energies: 1 keV, 0.5 keV, and 0.25 keV. These curves were obtained by using the six excitation cross-sections and semi-empirical form of the binary encounter collision cross-section. As expected the shapes of the curves are similar but shifted in proportion to the source energies.

As stressed earlier, we view the W-value as a means of checking the validity of the flux distribution calculation. As a matter of interest, this has been extended to noble gases other than helium. Since excitation cross-sections are incomplete, the one-excitation level model and the Gryzinski energy loss cross-sections have been used in all cases. Table (II-3) compares the results with experimental measurements. Since, as demonstrated earlier for helium, the one level model is somewhat inaccurate, the results are only expected to display trends. Indeed the calculated W-values are consistently high, but the rough agreement for this variety of gases gives confidence to the present treatment.

Figure 17 compares the present calculation for a 1000 eV primary electron distribution with some normalized results from a Monte Carlo simulation [15]. The Monte Carlo technique may be regarded as a mathematical experiment and the result is presented as points in Figure 17. The general agreement in shape is encouraging, and the discrepancies are thought to be due to the rather simplified cross-sections employed in the Monte Carlo code [15].

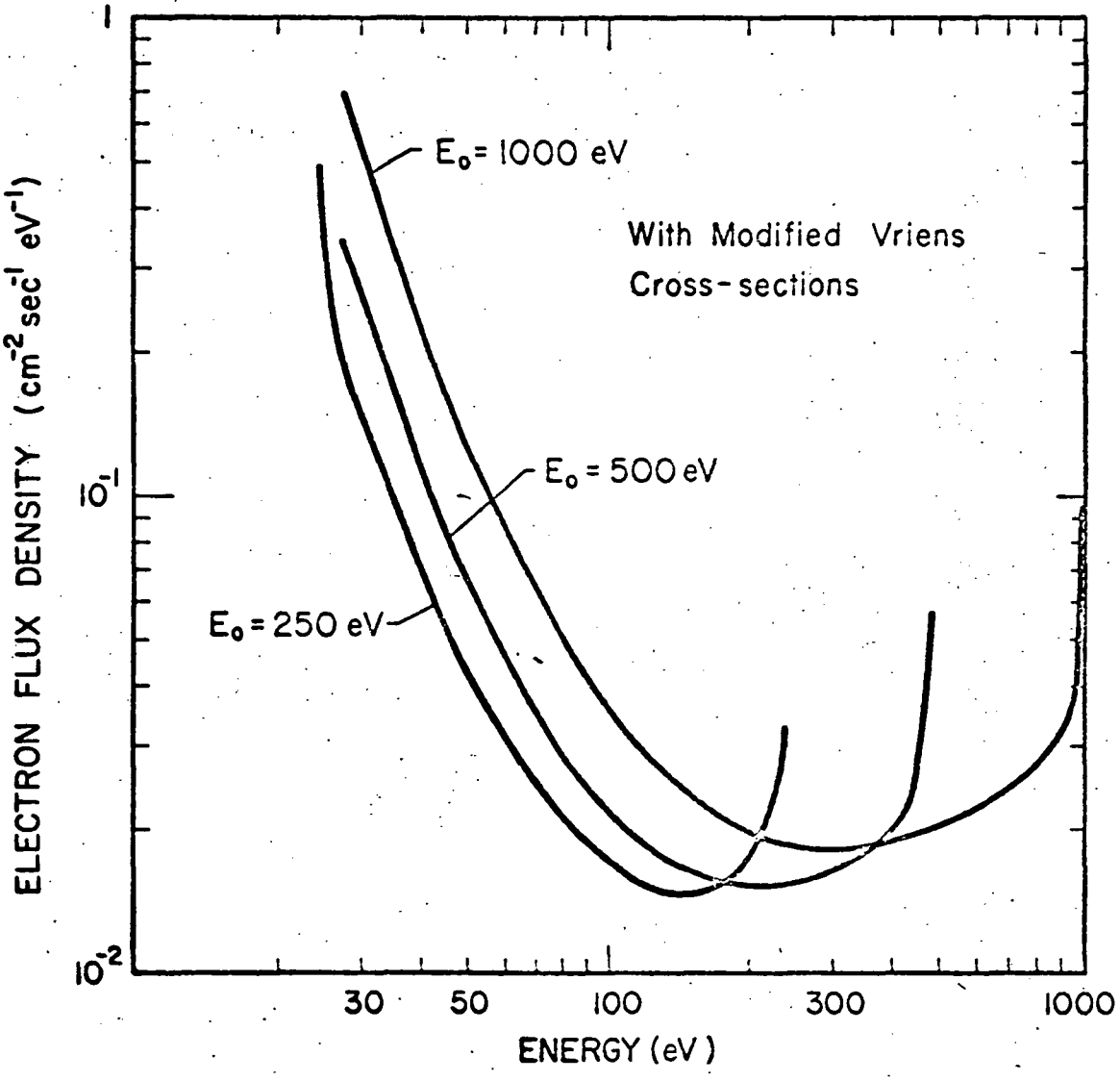

Figure 16. Electron Energy Distributions Calculated with Experimental Excitation and Fitted Vriens Cross Sections for 250, 500 and 1-KeV Primaries

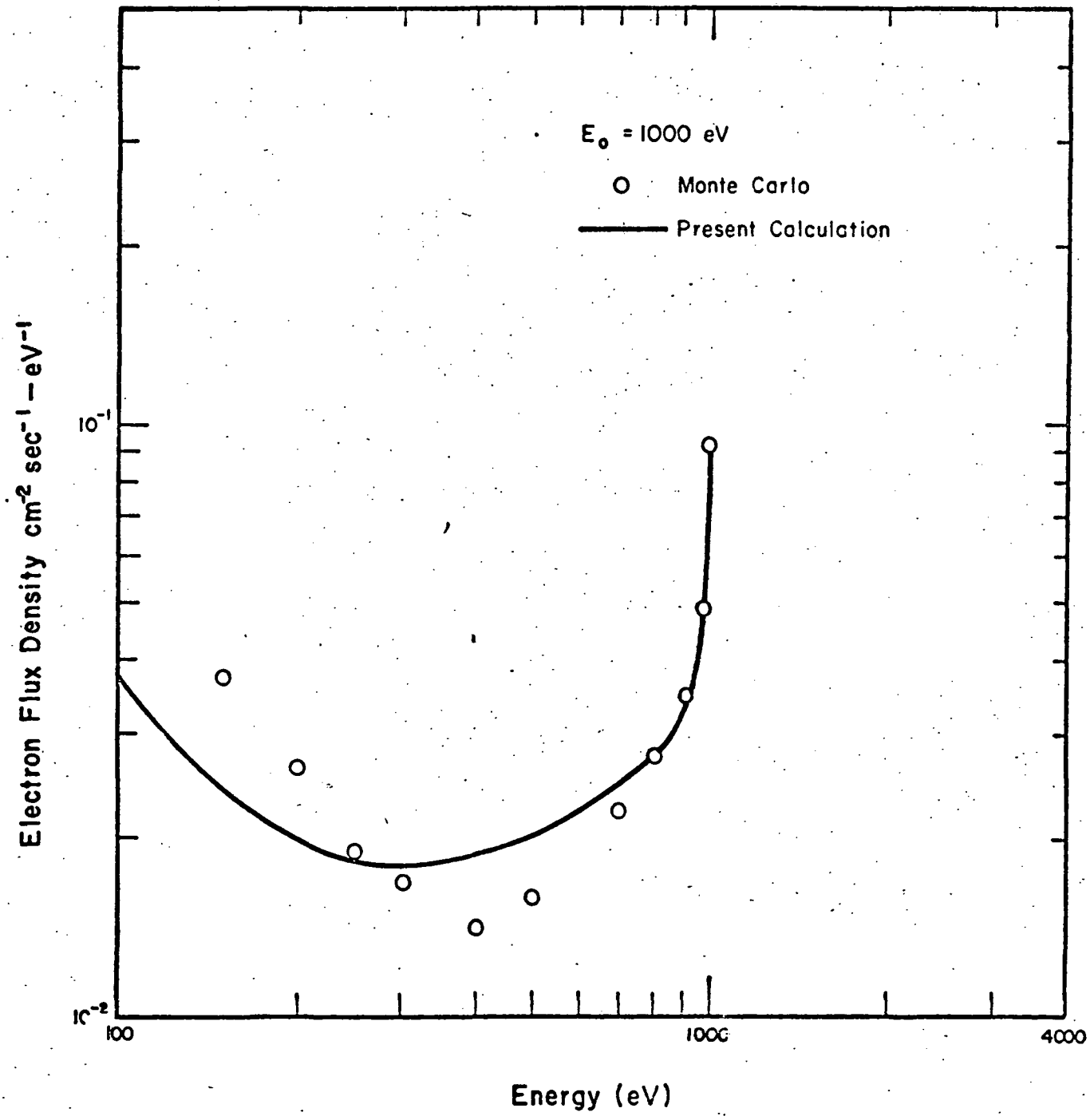

Figure 17. Comparison of Electron Flux Distributions from a Monte Carlo Calculation and the Present Calculation for 1-KeV Primary Source

2. Inclusion of Leakage

For finite media where leakage effects must be included, equation (II-28) is employed rather than equation (II-17). The numerical integration is similar however. In this case the total elastic cross-section is required and it is estimated using the first Born Approximation. As derived from Appendix C starting from the result presented by Mott and Massey[39], we obtain:

$$Q_o = \frac{4096\pi^5 m_e^2 e^4 (3\lambda^4 + 18\lambda^2 k^2 + 28k^4)}{3h^4\lambda^2(\lambda^2 + 4k^2)^3} \qquad \text{(II-31)}$$

where $k = m_e u_e / \hbar$, $\lambda = 2z/a_o$ and a_o = Bohr Radius. Values of this cross-section and some experimental measurements are compared in Figure 18 for energies above 10 eV. Then for a cylindrical system of radius 1.27 cm and length 122 cm, $1/\Lambda^2$ is estimated to be 3.6 cm^{-2} [13]. For this dimension Figure 19 compares the flux distributions obtained with leakage to that for an infinite medium with a 500 eV primary electron and 2 torr pressure. Figure 20 shows the case for a pressure of 4 torr. Comparing Figures 19 and 20 one sees that with increased pressure a finite system approaches one where leakage can be neglected. This is because at higher pressures electrons suffer more collisions before they can leak out of the system.

Figure 21 shows results for a primary electron energy of 800 eV case and a pressure of 2 torr. Comparison of Figures 19 and 21 shows that the diffusion loss is more significant for a higher energy primary source. The physical reason is that the higher energy electrons and their secondaries have a better chance of leaking out of the system. Thus for higher energy primaries one must be concerned about the leakage up to a higher pressure.

Changing $1/\Lambda^2$ is equivalent to changing the size of the system. Figure 22 shows results for three values of $1/\Lambda^2$ for the case of E_o = 800 eV

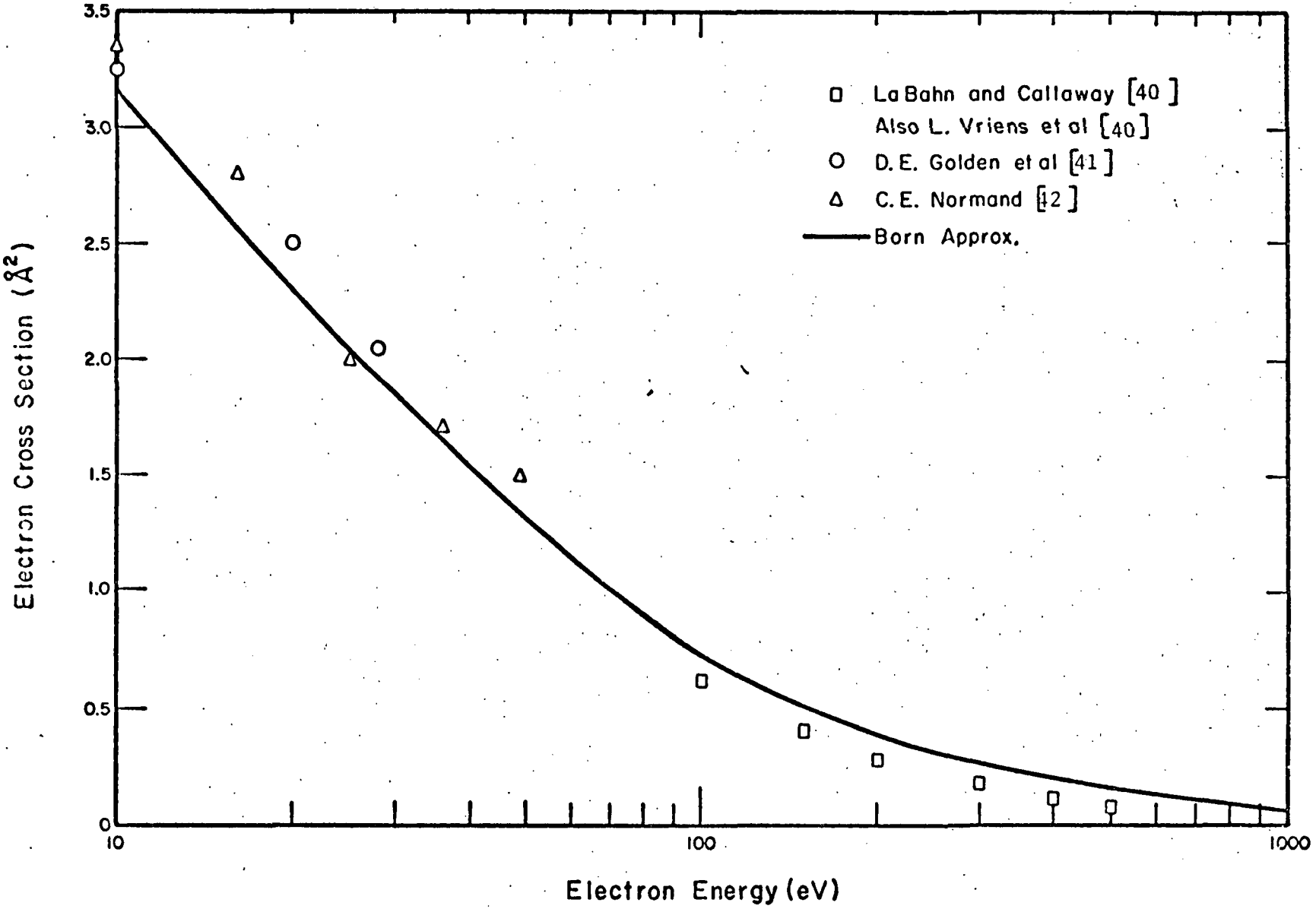

Figure 18. Comparison of Calculated Total Electron Elastic Scattering Cross Section in Helium with Measurements

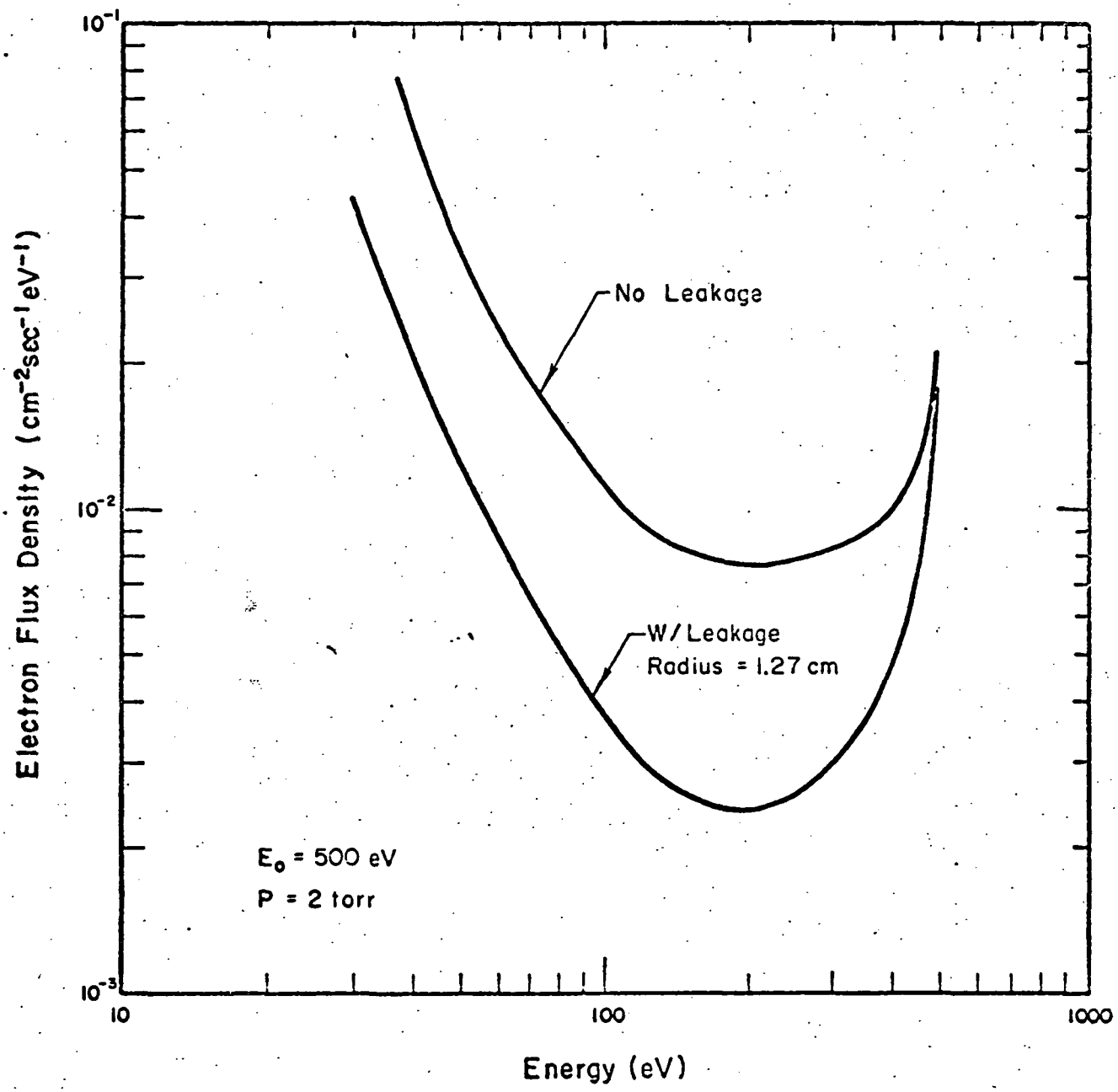

Figure 19. Comparison of Flux Distributions With and Without Leakage at p= 2 Torr, E_o= 500 eV

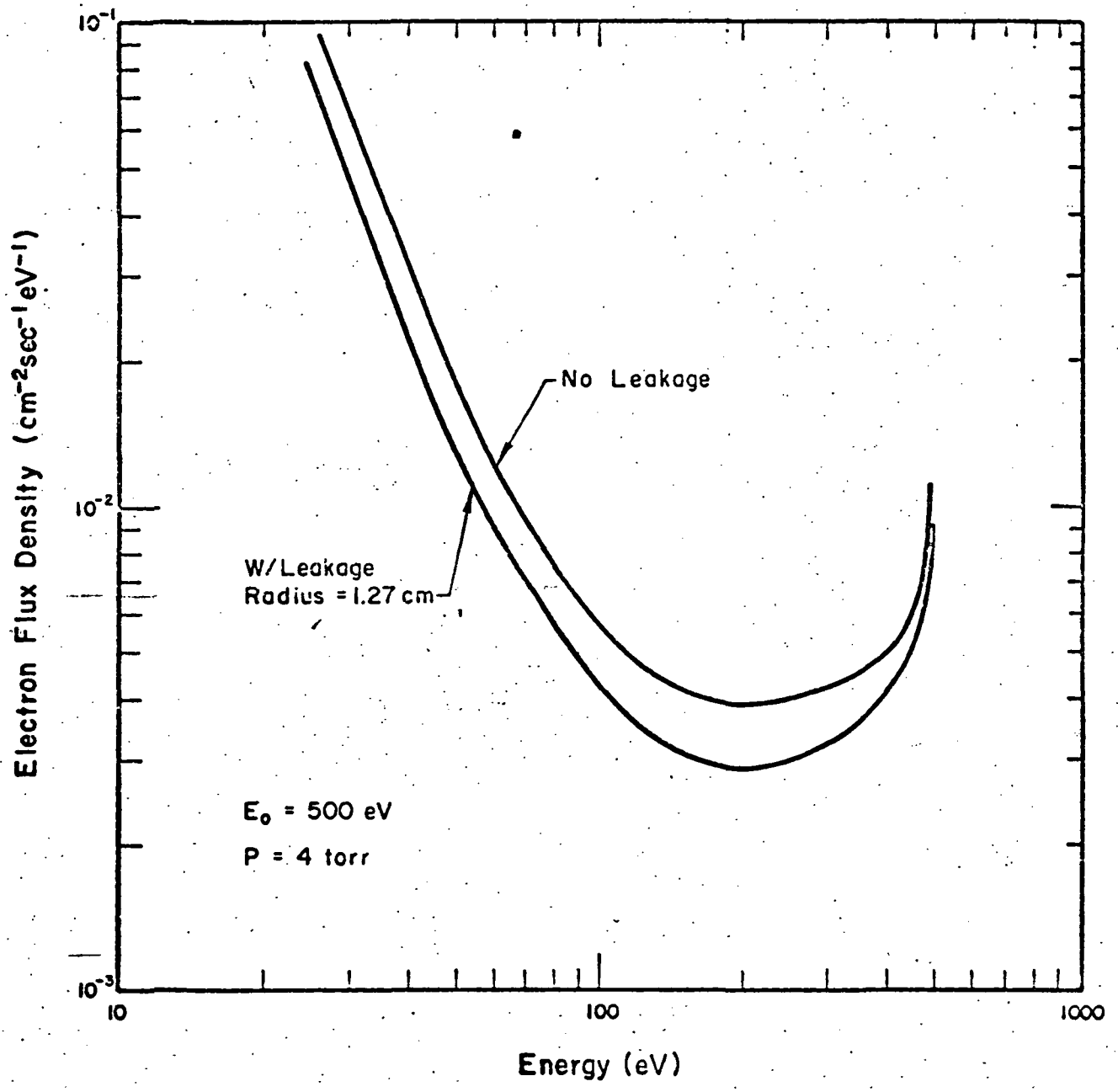

Figure 20. Comparison of Flux Distributions With and Without Leakage at p= 4 Torr, E_o= 500 eV

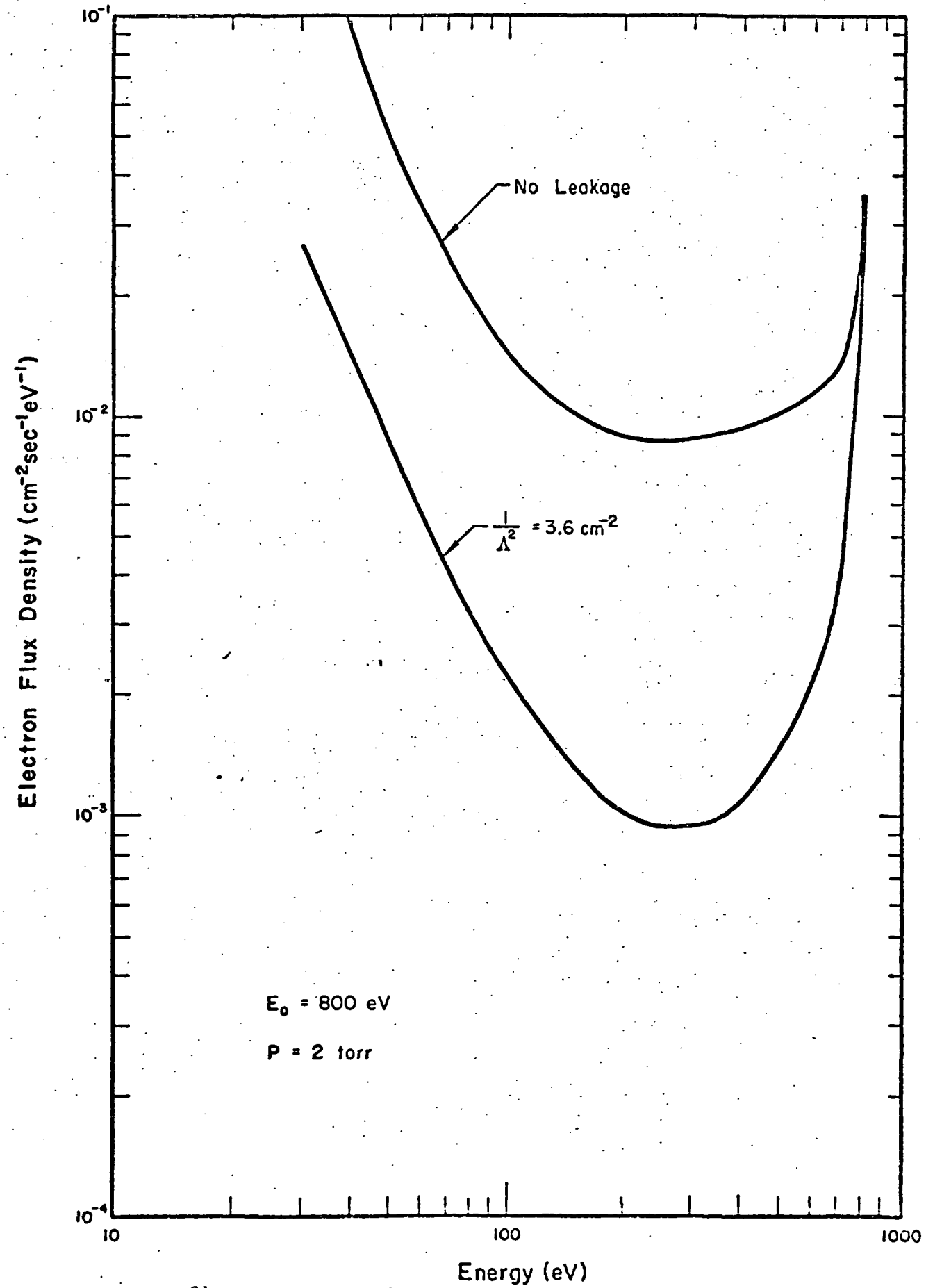

Figure 21. Comparison of Flux Distributions With and Without Leakage at p = 2 Torr, E_o = 800 eV

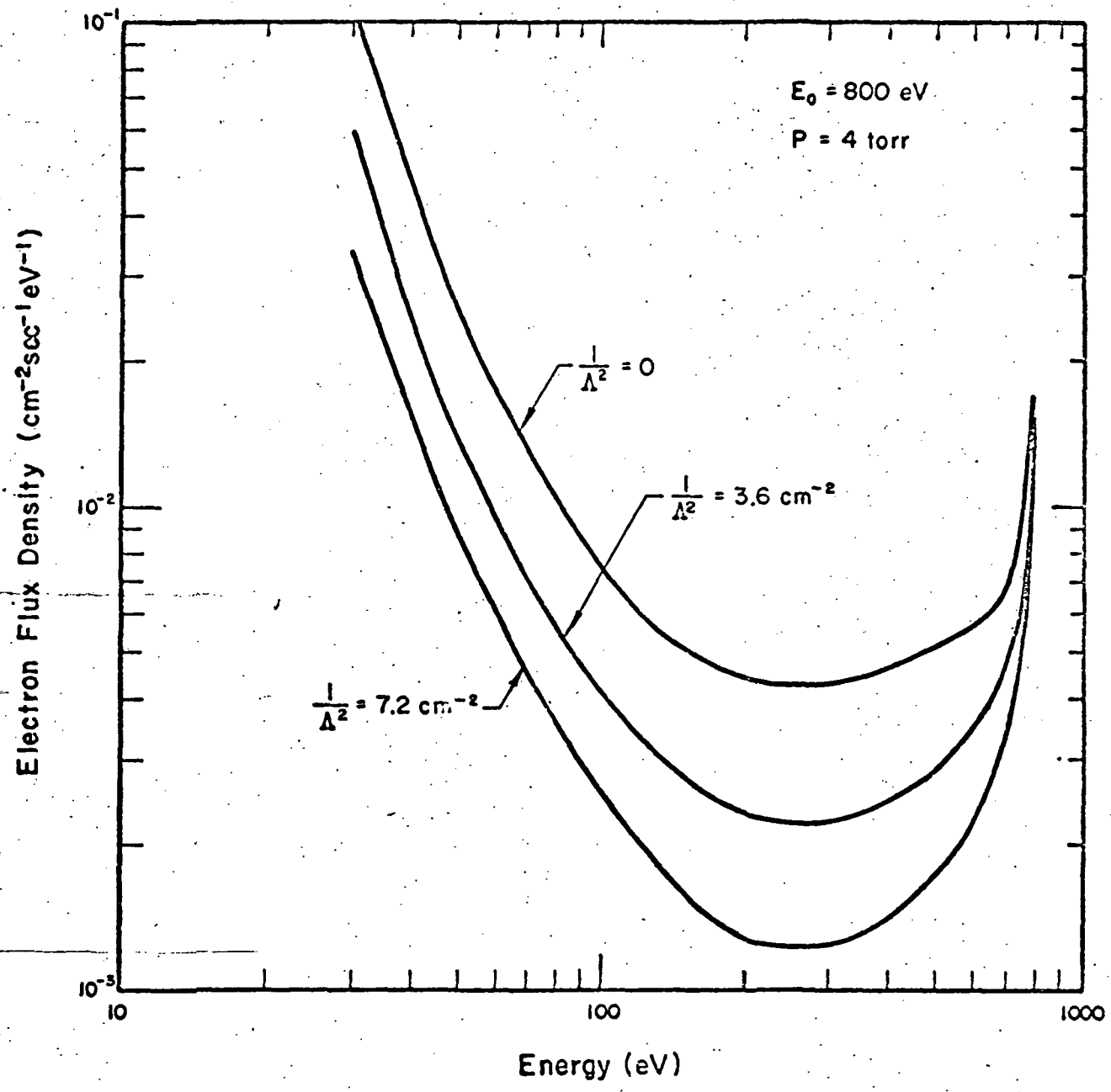

Figure 22. Comparison of Flux Distributions With E_o = 800 eV, p = 4 Torr for Three Cases of System Dimensions; $1/\Lambda^2$ = 0, 3.6 and 7.2 cm^{-2}

at 4 torr. A decrease in physical dimensions increases the leakage and shifts the flux to lower energies. The cases of $1/\Lambda^2 = 0$, 3.6 and 7.2 cm^{-2} correspond to the infinite medium, a tube radius of 1.27 cm and a tube radius of 0.88 cm, respectively.

These results are to be compared with that of Figure 23 for the case of 250 eV primary electron energy. (The gas pressure in Figure 23 is 2 torr because curves for higher pressures would overlap the infinite medium case.) A comparison of Figures 22 and 23 shows that the change of size of system has less effect on the energy spectrum in the case of a lower primary electron energy. Another observation is that the leakage term has a cumulative effect and the percentage deviation between the infinite and finite media cases becomes more significant at lower energies. For instance, for the 250 eV primary electron case, at 125 eV the difference between $1/\Lambda^2 = 0$ and $1/\Lambda^2 = 3.6$ cm^{-2} is about 22% while at 50 eV the difference is about 30%. This is because the population is progressively reduced as electrons leak out of the system during the slowing process.

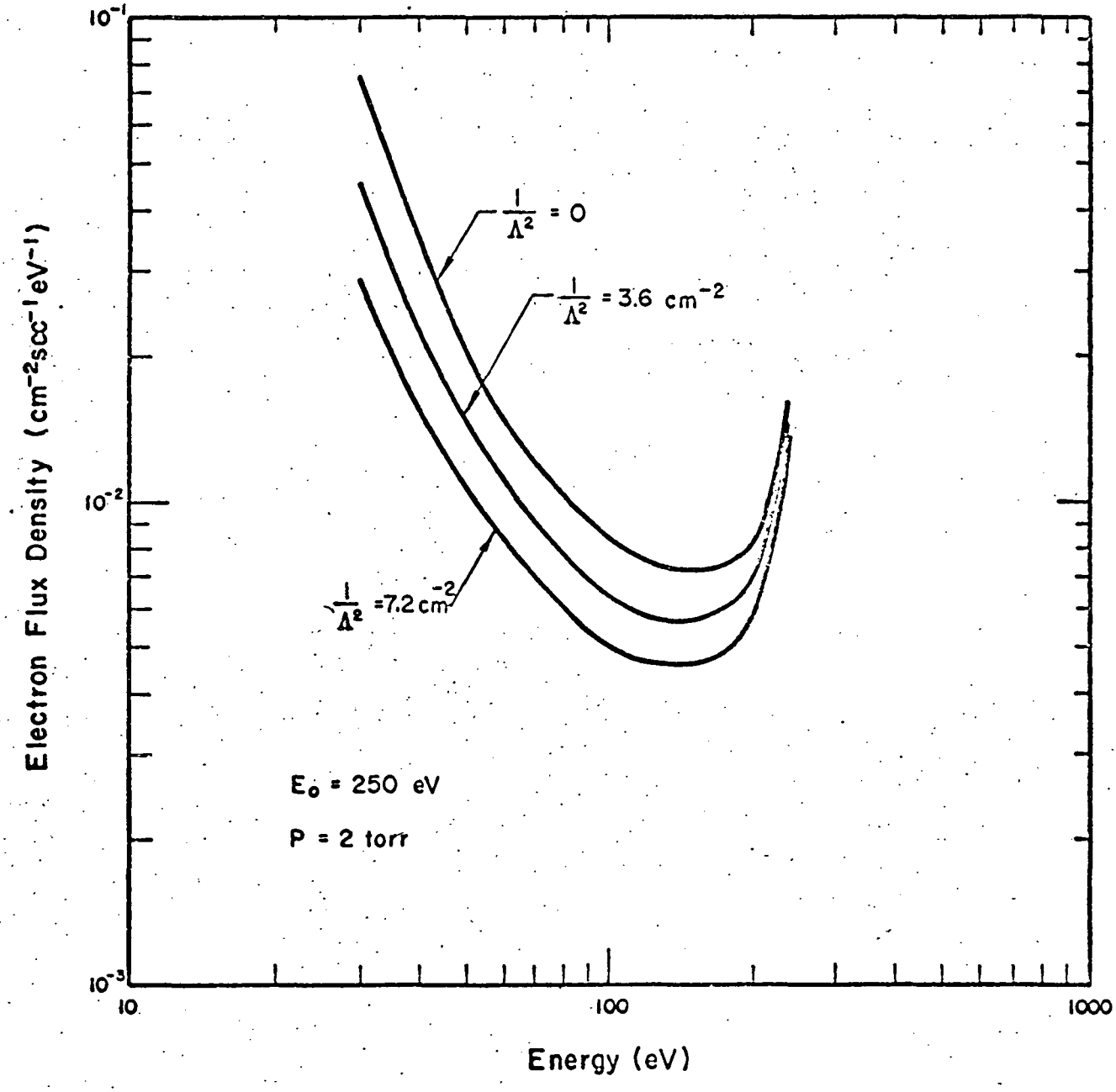

Figure 23. Comparison of Flux Distributions With E_o = 250 eV, p= 2 Torr for Three Cases of System Dimensions; $1/\Lambda^2$ = 0, 3.6 and 7.2 cm^{-2}

CHAPTER III

THE ELECTRON ENERGY DISTRIBUTION BELOW THE FIRST EXCITATION POTENTIAL ENERGY OF HELIUM

A. A Model for Thermalization in Helium

In a weakly ionized plasma, one can expect to neglect electron-electron and electron-ion interactions during thermalization. The validity of this assumption will be examined later in this chapter for the specific physical situations of interest. In conventional gaseous discharges, electron-electron interactions are thought to play an important role in bringing the energy distribution closer to a Maxwellian. However, in the present case, it will be shown that the absence of an electric field allows the distribution to collapse into a nearly Maxwellian form.

Due to the absence of ionization and excitation collisions, below the first excitation energy, the electrons in an energy interval are populated mainly by elastic collisions and depopulated by recombination with ions, leakage and scattering out of that energy interval. The steady state equation taking into account of these processes is:

$$-D(\mathcal{E})\nabla^2\Phi(\mathcal{E}) + \Sigma_r(\mathcal{E})\Phi(\mathcal{E}) = \int_0^\infty \Sigma_s(\mathcal{E}'\to\mathcal{E})\Phi(\mathcal{E}')d\mathcal{E}' - \Sigma_s(\mathcal{E})\Phi(\mathcal{E}) \qquad \text{(III-1)}$$

where $D(E)$ = diffusion coefficient

$\Phi(E)$ = electron flux distribution

$\Sigma_r(E)$ = macroscopic electron-ion recombination in cross-section

$\Sigma_s(E)$ = total macroscopic scattering cross-section

$\Sigma_s(E' \to E)$ = macroscopic scattering cross-section of going into interval at E from E'.

$S(E)$ = direct electron source from high energy inelastic scattering.

In equation (III-1), the diffusion approximation notation has been used (see Appendix D). Because of the small amount of energy less per elastic collision it is difficult to solve equation (III-1) by numerical integration techniques as was done in the high energy region. Instead, one can make use of the fact that energy loss per collision is small and expand $\Phi(E)$ in moments of $(E'-E)$. This procedure is similar to the "heavy gas model"[43] in neutron thermalization. It should be noted that the assumption of small energy loss per collision breaks down when electron-electron or electron-ion collisions become significant. This model is, therefore, valid only in a weakly ionized plasma.

In the absence of leakage and recombination, the principle of detail balance[44] shows that $\Phi(E) = M(E)$, where $M(E)$ is a Maxwellian distribution. Thus for the case where there is recombination and leakage, it is convenient to define $\Phi(E)$ as $M(E)\psi(E)$ and solve for the correction factor $\psi(E)$. With this substitution equation (III-1) becomes:

$$-\mathcal{D}(E)\nabla^2\Psi(E)M(E) + \Sigma_r(E)\Psi(E)M(E) = \int_0^\infty \Sigma_s(E'\to E)\Psi(E')M(E')\,dE' - \Sigma_s(E)\Psi(E)M(E) \qquad \text{(III-2)}$$

Normalization is such that $\int_0^\infty \Phi(E)\,dE = n_e$, where n_e is the total primary and secondary electron density. Electrons are assumed to be born at higher energies so electrons enter the low energy region by slowing and an explicit source is not included in (III-2). If a low energy source term were included, equation (III-2) would be inhomogeneous. However, the solution for the inhomogeneous case can be obtained from the solutions of the present homogeneous equation by the method of variation of parameters as shown in Appendix G.

Applying the principle of detail balance to the Maxwellian factor of the distribution, we obtain:

$$E' e^{-E'/kT} \Sigma_s(E' \to E) = E\, e^{-E/kT} \Sigma_s(E \to E') \tag{III-3}$$

The integral on the R.H.S. of equation (III-2) becomes:

$$\int_0^\infty \Sigma_s(E' \to E)\psi(E')M(E')\,dE' = M(E)\int_0^\infty \Sigma_s(E \to E')\psi(E')\,dE' \tag{III-4}$$

and substitution back into equation (III-2) gives:

$$-D(E)\nabla^2\psi(E) + \Sigma_r(E)\psi(E) = \int_0^\infty \Sigma_s(E \to E')\psi(E')\,dE' - \Sigma_s(E)\psi(E) \tag{III-5}$$

Expanding $\psi(E')$ around $E' = E$ in the integral of equation (III-5) by a Taylor series, one obtains:

$$\psi(E') = \sum_{n=0}^{\infty} \frac{(-1)^n}{n!} \frac{d^n\psi(E)}{dE^n} (E - E')^n \tag{III-6}$$

With this expansion, the integral on the R.H.S. of equation (III-5) becomes:

$$\int_0^\infty \Sigma_s(E \to E')\psi(E')\,dE' = \int_0^\infty \Sigma_s(E \to E') + \sum_{n=1}^{\infty} \overline{\Delta E^n}\, \Sigma_s(E) \frac{d^n\psi(E)}{dE^n} \frac{(-1)^n}{n!} \tag{III-7}$$

where, $\overline{\Delta E^n} = \frac{1}{\Sigma_s(E)} \int_0^\infty \Sigma_s(E \to E')(E - E')^n\,dE'$

The assumption next used is that the energy loss due to elastic scattering between electrons and neutral atoms is small. This is reasonable despite a large scattering cross section due to the large mass difference. The energy E' is therefore close to energy E.

For $\mu = \frac{m_e}{M} << 1$, where M is the mass of gas atom and m_e is the mass of electron and assuming isotropic scattering, the moments of ΔE are given by[43]:

$$\overline{\Delta E'} = 2\mu(2T - E) + \mathcal{O}(\mu^2)$$

$$\overline{\Delta E^2} = 4\mu kTE + \mathcal{O}(\mu^2)$$

and

$$\overline{\Delta E^n} \leq \mathcal{O}(\mu^2) \qquad \text{for } n \geq 3 \tag{III-8}$$

where T is the gas temperature.

In the case of elastic collisions between electrons and neutral atoms, the terms with order larger than μ^2 are not retained, and equation (III-7) becomes:

$$\int_0^\infty \Sigma_s(E\to E')\Psi(E')dE' = \Sigma_s(E)\Psi(E) + \Sigma_s(E)\left[2\mu(2kT-E)\right]\frac{d}{dE}\Psi(E) + \frac{1}{2}\Sigma_s(E)\left[4\mu E kT\right]\frac{d^2}{dE^2}\Psi(E) \qquad \text{(III-9)}$$

Also equation (III-5) becomes:

$$-D(E)\nabla^2\Psi(E) = -\Sigma_r(E)\Psi(E) + \tfrac{2}{3}\Sigma_s(E)\left[(2kT-E)\frac{d}{dE}\Psi(E) + EkT\frac{d^2}{dE^2}\Psi(E)\right] \qquad \text{(III-10)}$$

Changing the notation back to $\Phi(E)$, where $\Phi(E) = \psi(E)M(E)$, Appendix H shows that equation (III-10) can be written as:

$$-D(E)\nabla^2\Phi(E) + \Sigma_r(E)\Phi(E) = \tfrac{2}{3}\Sigma_s(E)\left[\Phi(E) + E\frac{d}{dE}\Phi(E) + EkT\frac{d^2}{dE^2}\Phi(E)\right] \qquad \text{(III-11)}$$

To proceed in solving equation (III-11), we must assign specific forms to the cross-sections and the diffusion coefficient. In the case of helium, the elastic scattering cross-section is reasonably constant in this low energy range[45]. If we assume a constant recombination coefficient over the thermal range, the recombination collision cross-section is =(1/velocity), i.e. 1/u. Although a weakly ionized gas is assumed throughout this development, for the low energy portion, it can be assumed that diffusion leakage is governed by the ambipolar diffusion coefficient.

One must be cautious that some of these assumptions may not be entirely valid in certain pressure ranges or if the model is applied to gases other than helium. Also, as examined in detail in later sections, the degree of

ionization must be below a certain critical value for equation (III-11) to be valid. However, in general, when electron neutral atom scattering dominates, and when the moments of averaged energy loss can be cut-off at n = 2, equation (III-11) is accurate. This equation can be applied to gases other than helium by use of appropiate cross-sections and coefficients. If an analytic solution cannot be found, equation (III-11) can still be solved numerically. This is not necessary for helium, however, since with some simplifying assumptions, an analytic solution is possible. While the assumption may lead to some inaccuracy, this technique is preferred since considerable physical insight is obtained.

B. Series Solution of the Thermalization Equation

With the assumptions that the total elastic scattering cross-section is a constant and that the recombination cross-section is an inverse function of the velocity, as shown in Appendix H, equation (III-11) becomes:

$$y\frac{d^2\Phi(y)}{dy^2} - [1 - zy^2]\frac{d}{dy}\Phi(y) + [4y - gy - \Delta]\Phi(y) = 0 \qquad \text{(III-12)}$$

where

$$y = \sqrt{E/kT}$$

$$\Delta = \frac{\Sigma_r(kT)}{3\Sigma_s}$$

and

$$g = \frac{D_a}{\Lambda^2 3\Sigma_s}$$

Here D_a is the ambipolar diffusion coefficient, and Λ is the characteristic first fundamental mode diffusion length defined in Appendix F. Equation (III-12) is solved by expanding $\Phi(y)$ in polynomials of y, i.e.;

$$\Phi(y) = y^2 e^{-y^2} S(y)$$

where,

$$S(y) = \sum_{l=0}^{\infty} A_l y^l \qquad \text{(III-13)}$$

The Maxwellian distribution is used as a multiplier because for $g = \Delta = 0$, i.e. no leakage and absorption, the solution of equation (III-12) is a Maxwellian as expected. Appendix (H) gives the coefficients of the series S(y) to be:

$$A_0 = 4/\sqrt{\pi}$$

$$A_1 = \Delta A_0/3$$

and

$$A_\ell = \frac{1}{\ell(\ell+2)}\left[2(\ell-2+3/2)A_{\ell-2} + \Delta A_{\ell-1}\right] \qquad \text{(III-14)}$$

Appendix (H) gives the first four coefficients to illustrate the form of A_ℓ. It is noted that terms with higher orders of Δ and g appears later in the series. The assumption of weak absorption and leakage is not a necessary one for the series to converge. However, for the physical cases considered, g and Δ are much less than one. In these cases, one can expand S(y) in Δ and g and retain the terms of first few orders in g and Δ. The series S(y) for keeping terms up to second order in g and Δ is:

$$S(y) = A_0\left[1 + \Delta\mu_1(y) + \Delta^2\mu_2(y) + g\eta_1(y) + g^2\eta_2(y) + g\Delta\chi(y)\right] \qquad \text{(III-15)}$$

The series $\mu_1(y)$, $\mu_2(y)$, $\eta_1(y)$, $\eta_2(y)$ and $\chi(y)$ rapidly converge for $y \leq 5$ and they have been derived in Appendix (H). The final form of $\Phi(y)$ is given as:

$$S(y) = A_0 y^2 e^{-y^2}\left[1 + \Delta\sum_{n=0}^{\infty}\frac{y^{2n+1}}{(2n+1)\Gamma(n+5/2)} + \right.$$

$$\frac{\Delta^2}{4}\sum_{n=1}^{\infty}\frac{y^{2n}}{n(n+1)}\left[\sum_{k=0}^{\infty}\frac{(k+1)!}{(2k+1)\Gamma(n+5/2)}\right] + g\left[\sum_{n=1}^{\infty}b_{2(n-1)}y^{2n}\right] +$$

$$\left. g^2\left\{\sum_{n=2}^{\infty}\left[d_{2n} + c_{2n}\right]y^{2(n+1)} + d_4 y^4\right\} + \Delta g\left[\tfrac{1}{2}\left(\tfrac{1}{3}+\tfrac{1}{8}\right)\sum_{n=1}^{\infty}e_{2n-1}y^{2n+1}\right]\right]$$

(III-16)

where, $b_0 = 1/8$, $b_{2n} = b_{2(n-1)} \frac{n-1}{n(n+1)}$,

$$d_4 = 1/4.6.8 \ , \quad d_{2(n+1)} = d_{2n} \frac{z(zn)}{(2n+2)(2n+4)} \ ,$$

$$c_4 = b_4/48 \ , \quad c_{2(n+1)} = c_{2n}/(2n+2)(2n+4) \ ,$$

$$e_1 = 1 \ , \quad e_{2n-1} = e_{2n-3} \frac{2(2n-1)}{(2n+1)(2n+3)} \ .$$

C. Range of Validity

Electron self interactions and electron-ion interactions have been neglected in the present calculations. This is valid for a weakly ionized gas, and the purpose of the present calculation is to examine the maximum degree of ionization allowable. To do this relaxation times are considered to obtain a first estimate of the limit. The ratio of the electron-ion relaxation time τ_{ei} and the electron-electron relaxation time τ_{ee} for singly charged ions is approximately: $\tau_{ee}/\tau_{ei} \approx 1/2\sqrt{2}$ [46]. It is sufficient, therefore, to compare τ_{ee} with τ_{en}, the electron-neutral relaxation time. The former is given by [47]:

$$\tau_{ee} \approx \frac{25.8 \sqrt{\pi} \epsilon_0^2 m_e^{1/2} (kT)^{3/2}}{e^4 n_e \ln \Lambda} \qquad \text{(III-17)}$$

where $$\Lambda = \frac{12\pi (\epsilon_0 kT/e^2)^{3/2}}{n_e^{1/2}}$$

and τ_{en} is given by [48]:

$$\tau_{en} \approx \frac{1}{\frac{8}{3} v_e N_n Q_m} \ . \qquad \text{(III-18)}$$

where Q_m is the momentum transfer cross-section, U_e is the speed of electron, N_n is the neutral atom density and ξ the mass ratio 2m/M. Using these results, we obtain figure 24 which shows the fractional ionization when the two relaxation times are equal. For this calculation, the momentum transfer cross sections were taken from O'Malley[45], and since $\ell n\ \Lambda$ is insensitive to electron density or energy, approximate values for it from Spitzer[47] were used. Holt and Hasskel[48] have used a similar curve to define a weakly ionized plasma. They show a critical value of 10^{-4} for the fractional ionization of helium at one torr and 300°K. There, they considered only the directional relaxation. When the mass ratio is added to account for the energy relaxation, figure (24) is found to be in good agreement.

It is noted from figure 24 that as the energy increases, the fractional ionization limit is not quite so stringent. At low energies, the charged-particle self-interaction tends to enhance thermalization into a Maxwellian form. Therefore, if the distribution obtained without the inclusion of charged-particle self-interaction is already close to a Maxwellian form in an energy region below a few kT, the fractional ionization restriction need not be extended to this region.

For electrons above about 0.5 eV, comparison of the $\tau_{ee} = \tau_{en}$ curve with figure (G-4) of Appendix G shows that with a tube radius of 1.27 cm and gas pressure of one torr, charged-particle self-interaction becomes important for a neutron flux above $\sim 5 \times 10^{13}$ cm^{-2} sec^{-1}. For gas pressures higher than 20 torr, the fractional ionization limit decreases and the neutron flux limit can be raised.

D. Numerical Results and Discussion

The choice of some of the parameters required for evaluation of

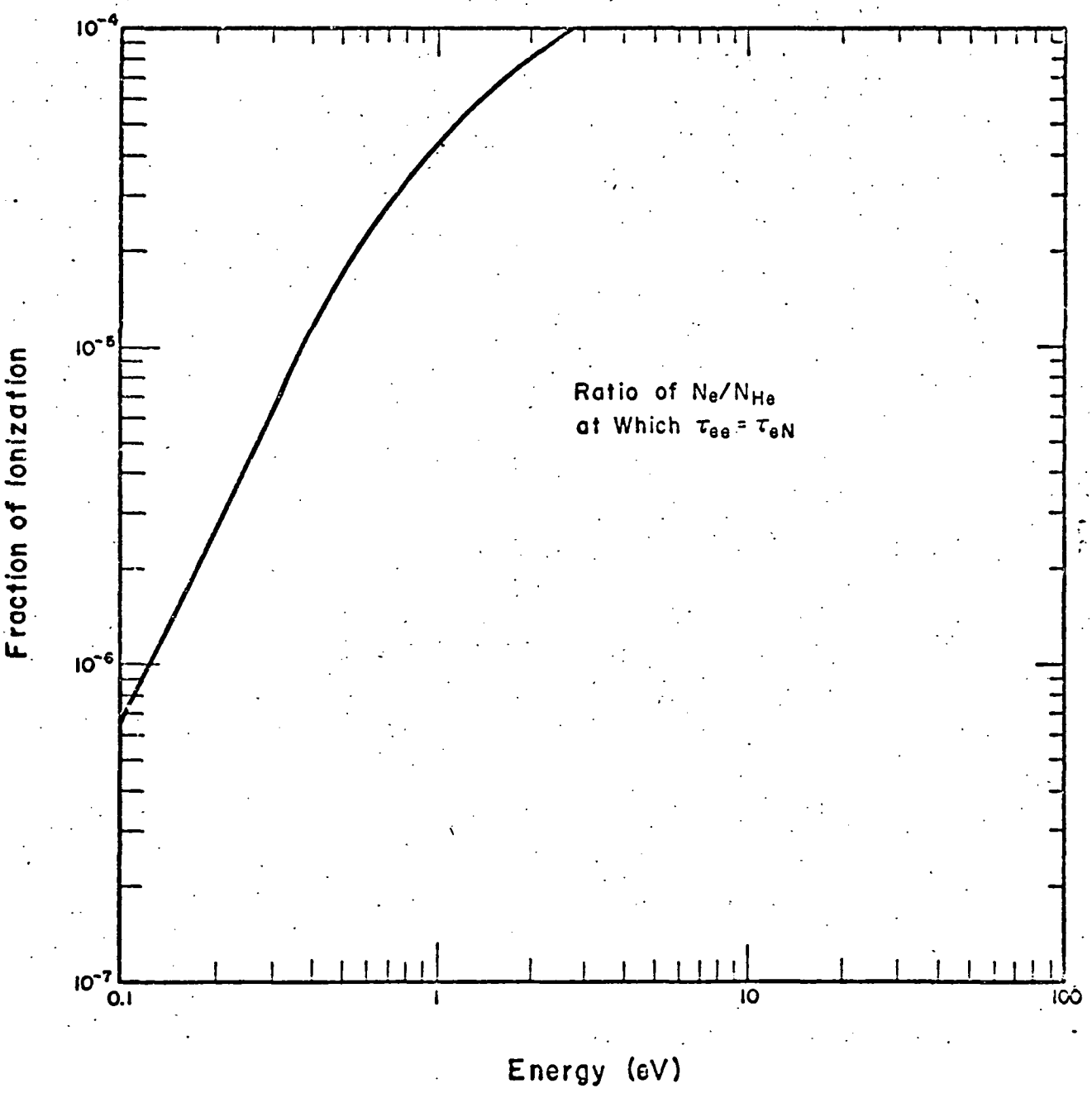

Figure 24. Fraction of Ionization Defining a Weakly Ionized Plasma

equation (III-16) is not definite, partly due to uncertainties in experimental observations. For helium at low energies, the recombination coefficient is taken as 4×10^{-9} cm^3-sec^{-1} [49], the ion diffusion coefficient as $D_2^+ p = 840$ cm^2-torr/sec[50] and the elastic scattering cross-section as 17.6×10^{-16} cm^2 [45]. With these parameters, Figures 25 and 26 show the normalized electron distribution for three pressures. The normalization is such that; $\int_0^\infty f(y)\, dy = 1$, where $y = \sqrt{\frac{E}{kT}}$. The ion density for a given neutron flux and pressure condition is first calculated through the procedure of Appendix G. The resultant leakage and recombination rates were then used as parametric inputs to equation (III-16).

A Maxwellian distribution is included for reference. It is observed that the distributions shift to a higher energy tail at lower pressures. This is because that at low pressures, electrons are more likely to leak out of the system before they can reach lower energies. At higher pressures, the energy deposition rate of the heavy-charged particles increases, resulting in higher ion densities. However, the neutral atom density also increases causing more electron-neutral scattering which reduces leakage. As a result the distribution approaches a Maxwellian form. The shape of the distribution, not much deviated from a Maxwellian, has also been confirmed by the Monte Carlo simulation of B. Wang and G. Miley[15].

Figures (27) and (28) show cases where the tube size has been increased to a radius doubling Λ^2. Then, for the same neutron flux, the distributions for the three different pressures lie much closer together. This is attributed to the fact that the energy deposition rate by heavy-charged particles is essentially independent of the tube size but leakage has been greatly reduced by the larger tube size.

Figure (29) shows an extreme case of changing the tube size at a low

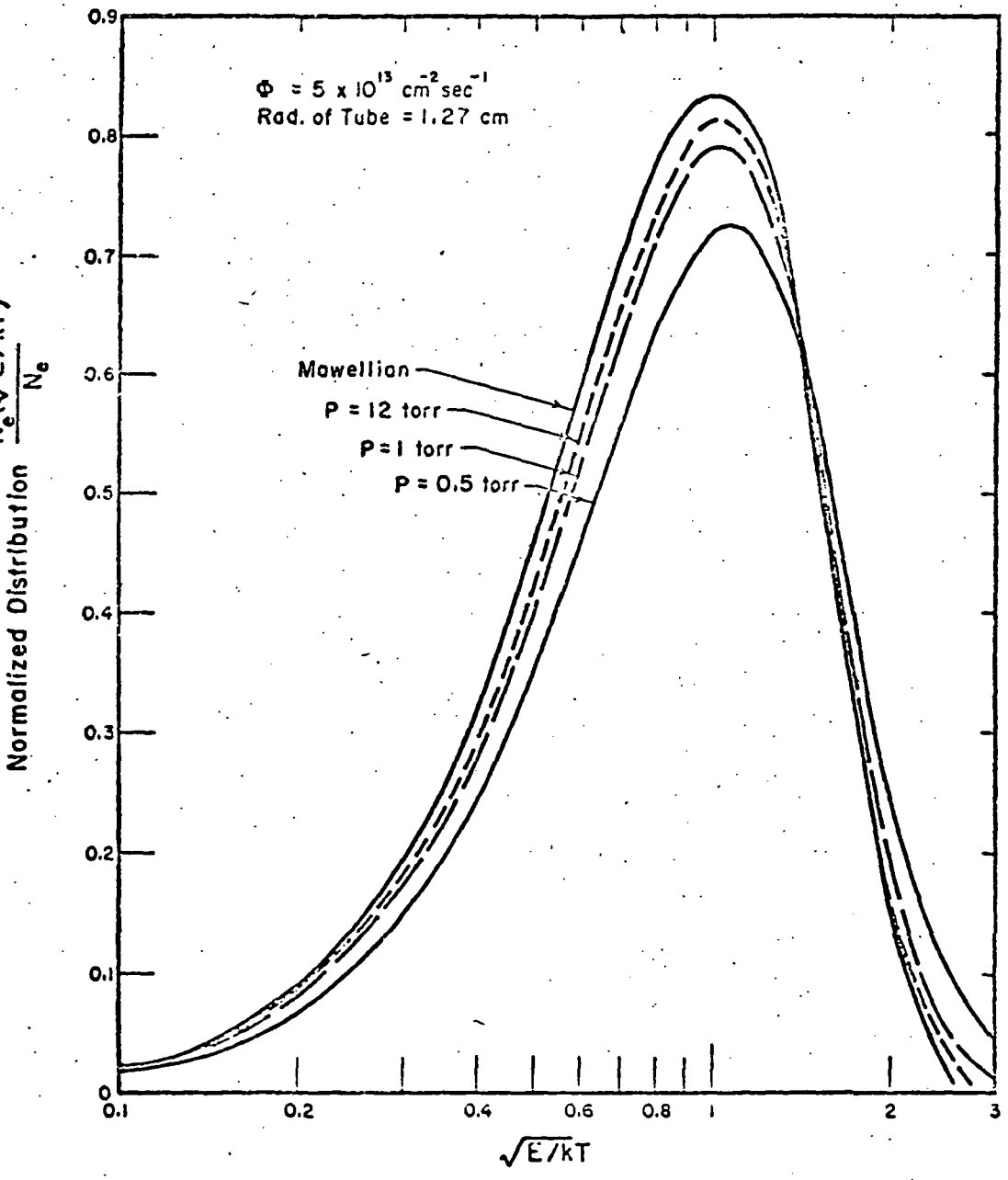

Figure 25. Electron Energy Distributions for Pressures of 0.5, 1, and 12 Torr and a Tube Radius of 1.27 cm.

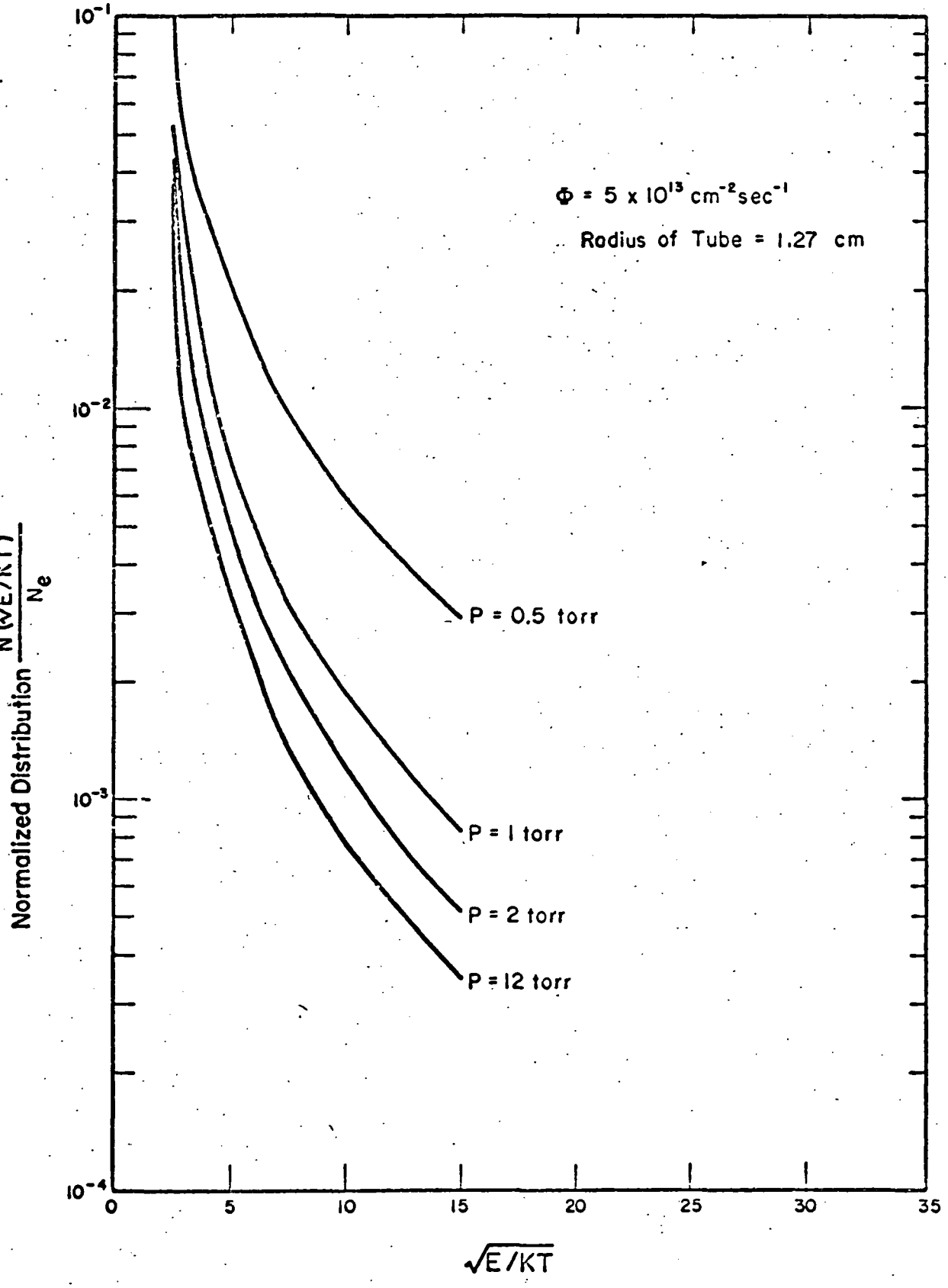

Figure 26. Electron Energy Distributions for Pressures of 0.5, 1 and 12 Torr and a Tube Radius of 1.27 cm.

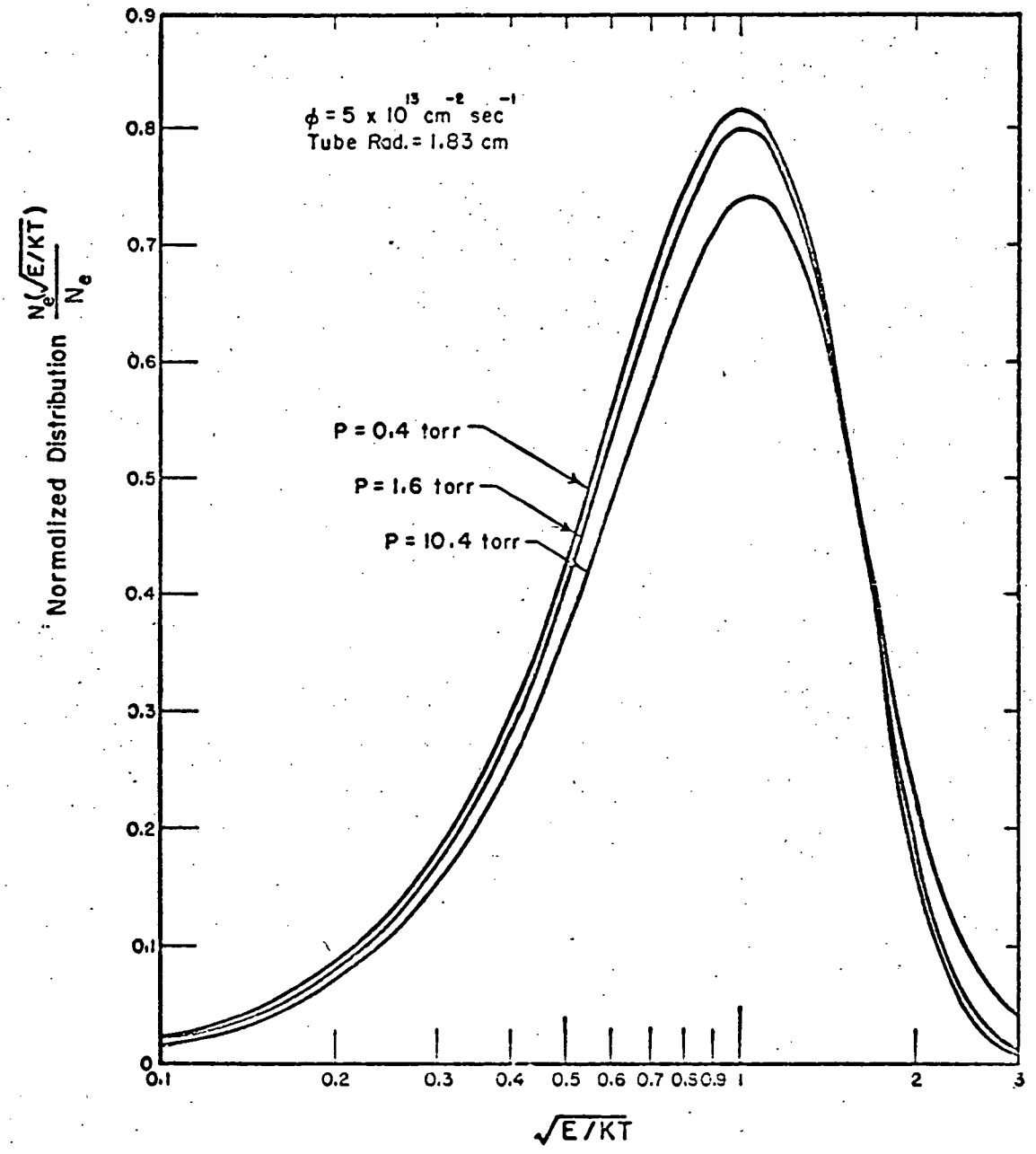

Figure 27. Electron Energy Distributions for Pressures of 0.4, 1.6 and 10.4 Torr and a Tube Radius of 1.83 cm.

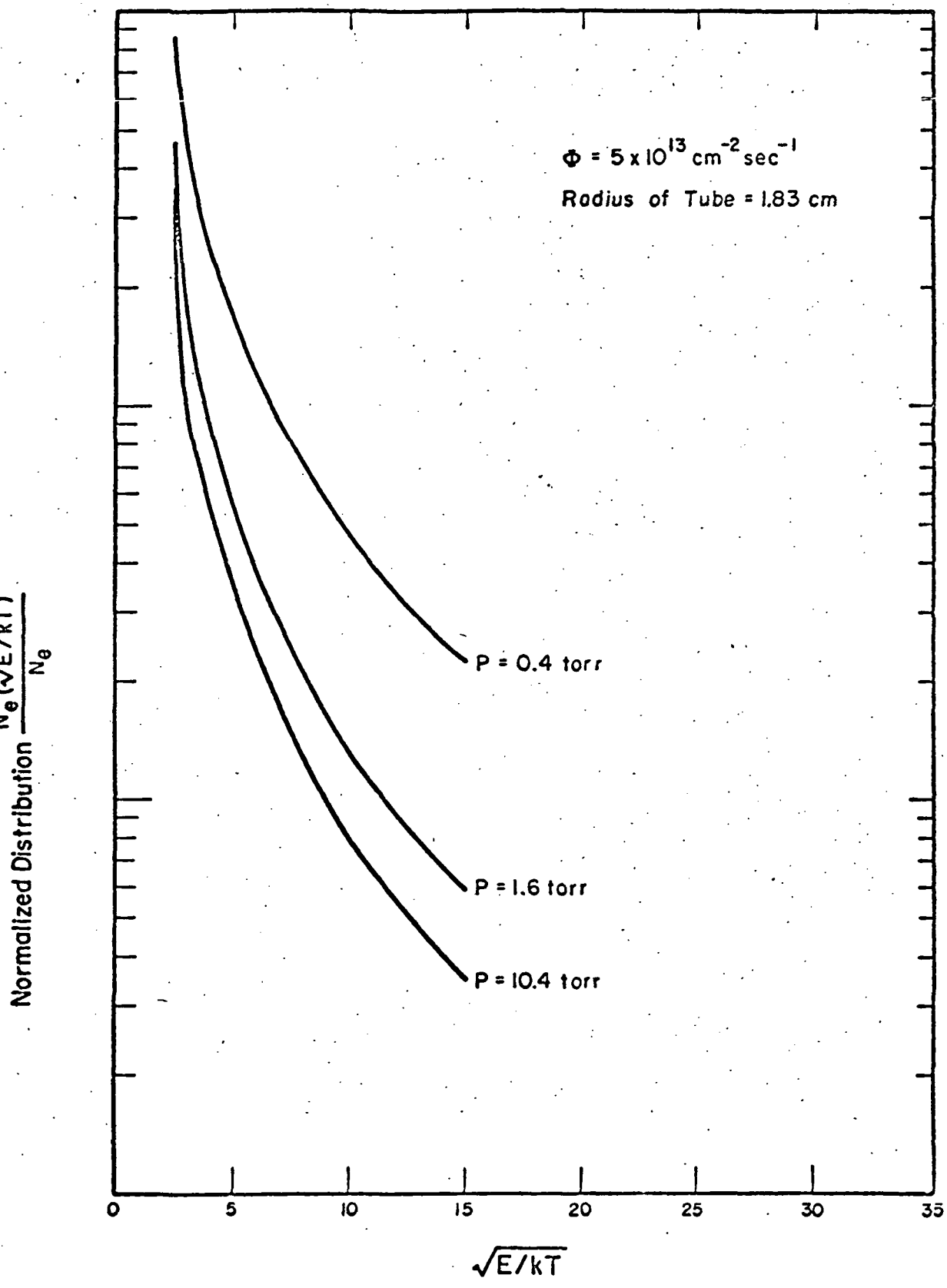

Figure 28. Electron Energy Distributions for Pressures of 0.4, 1.6 and 10.4 Torr and a Tube Radius of 1.83 cm.

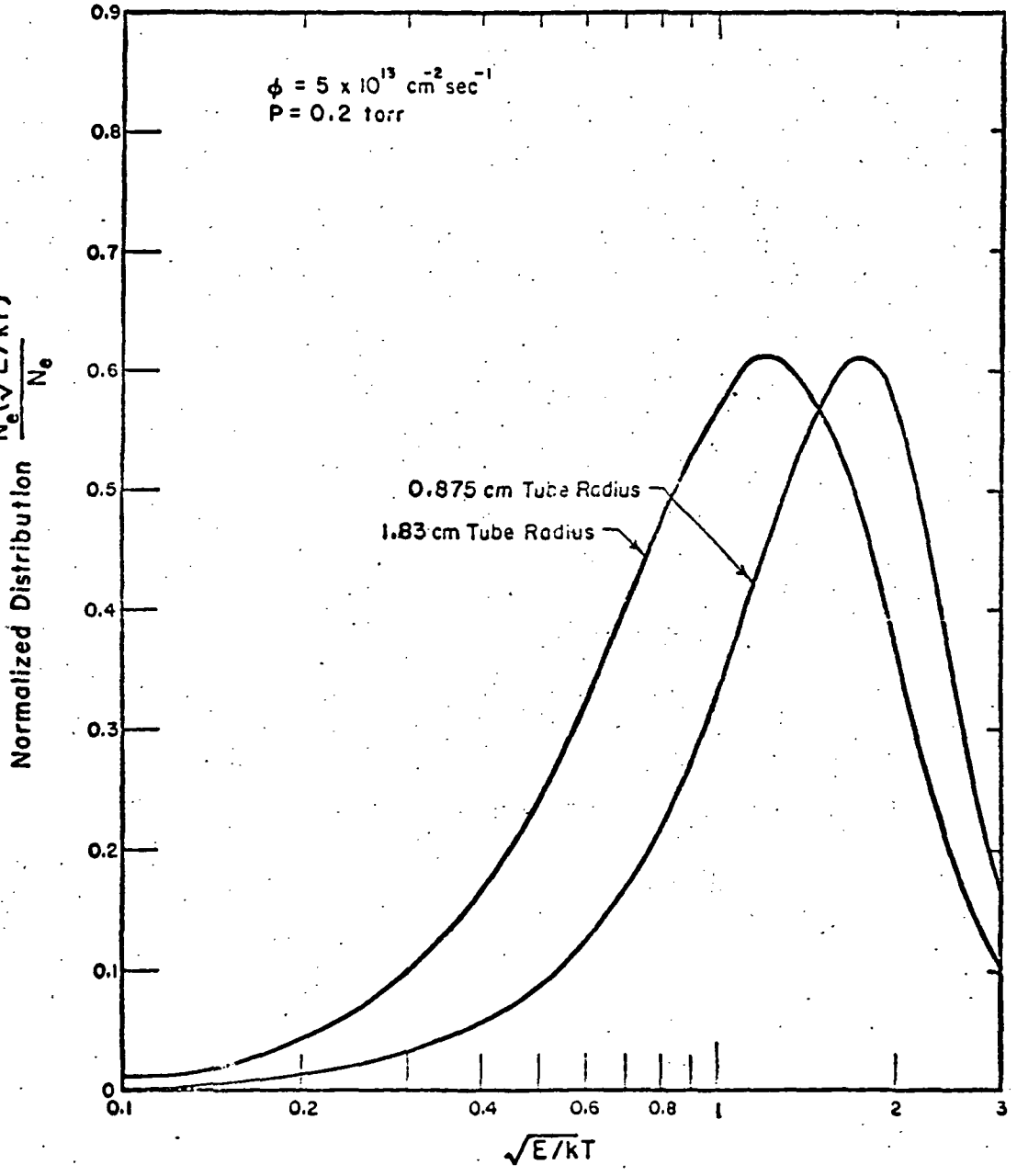

Figure 29. Comparison of Electron Energy Distributions for Tube Radii of 0.875 and 1.83 cm. for Helium at 0.2 Torr

pressure of 0.2 torr. In this case the shift to a higher energy is significant when the tube radius is cut in half. Again, this shift is due to the failure of electrons to reach lower energies as leakage increases.

A more extreme case of neutron flux of 5×10^{14} cm^{-2} sec^{-1} is shown in Figure (30). In this case, charged-particle self-interaction neglected in the present treatment, should be included. However, this figure is included to illustrate the dramatic shift in the distribution for a high heavy-charged particle energy-deposition rate. The peaks shift to about 1.4 to 2 kT. This is more pronounced in the case of low pressure of 0.2 torr where the leakage rate is larger. Reducing the pressure shifts the distribution in a manner similar to that which occurs as the tube diameter is reduced. However, the distribution is not a unique function of d_p (diameter pressure). This is because, although the leakage term has this form, the other terms such as recombinations do not have such a dependency.

Figure (31) shows the joining of the low energy portion of the distribution with the high-energy portion developed in Chapter II. The flux distribution in the higher energy region is an inverse function of pressure, as can be observed from equation (II-10) or from the stopping-power approximation of Appendix A. For the energy range 5 kT to 20 eV, a recombination cross section[51] of $E^{-3/2}$ has been used. The collision density, $\Sigma(E)\dot{\Phi}(E)$ cm^{-3} sec^{-1}, is a continuous function, but abrupt changes in cross section can result in a discontinuity of $\Phi(E)$. Such an effect is observed at 20 eV due to the abrupt charge in cross sections used in the two energy regions. Similar discontinuities also appear in other studies[52] and they can be eliminated entirely by use of a finer energy division in the numerical computation or by adopting smoothed cross sections.

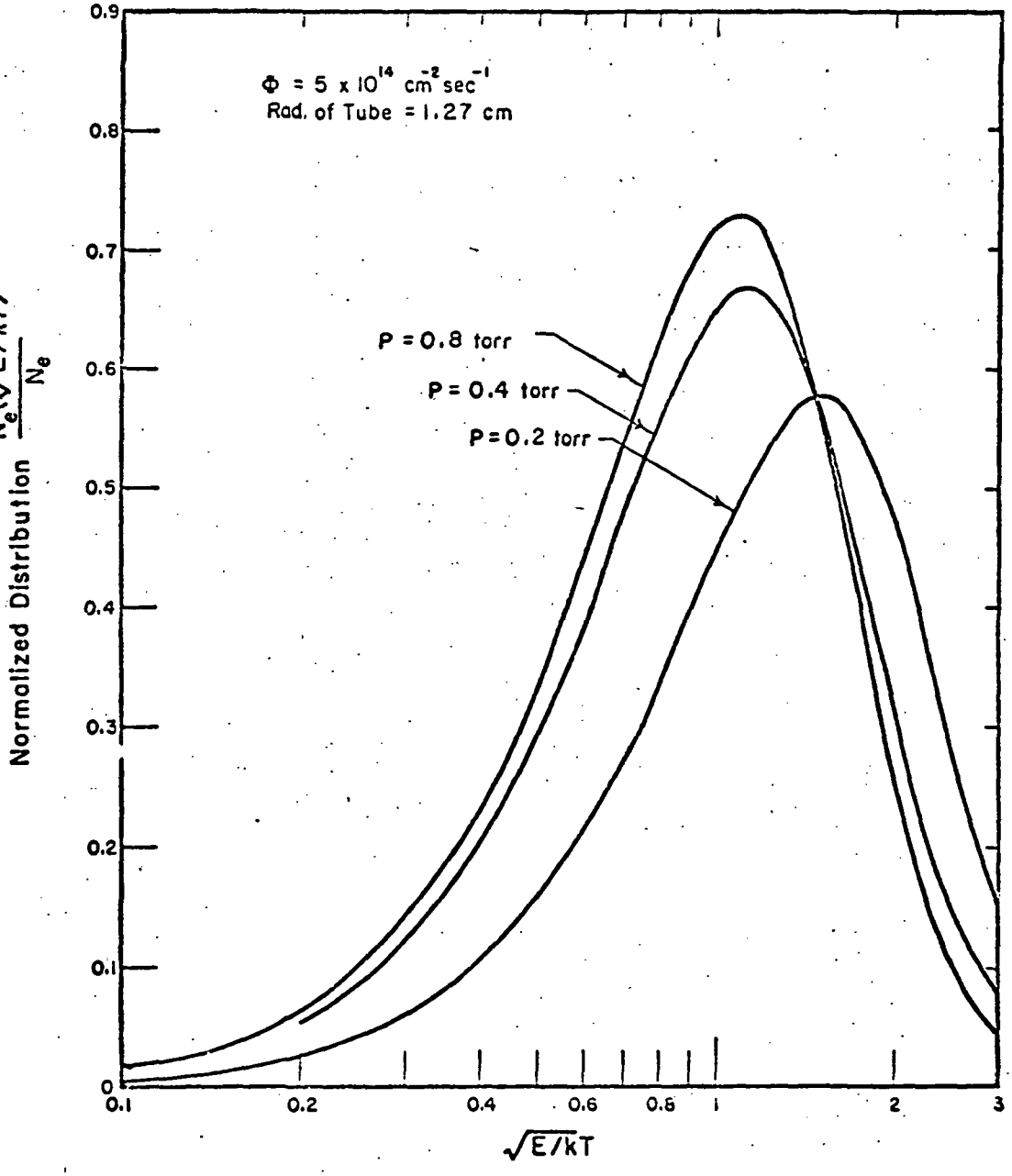

Figure 30. Comparison of Electron Energy Distributions for Pressures of 0.2, 0.4 and 0.8 Torr With a Neutron Flux of 5×10^{14} cm^{-2}-sec^{-1}

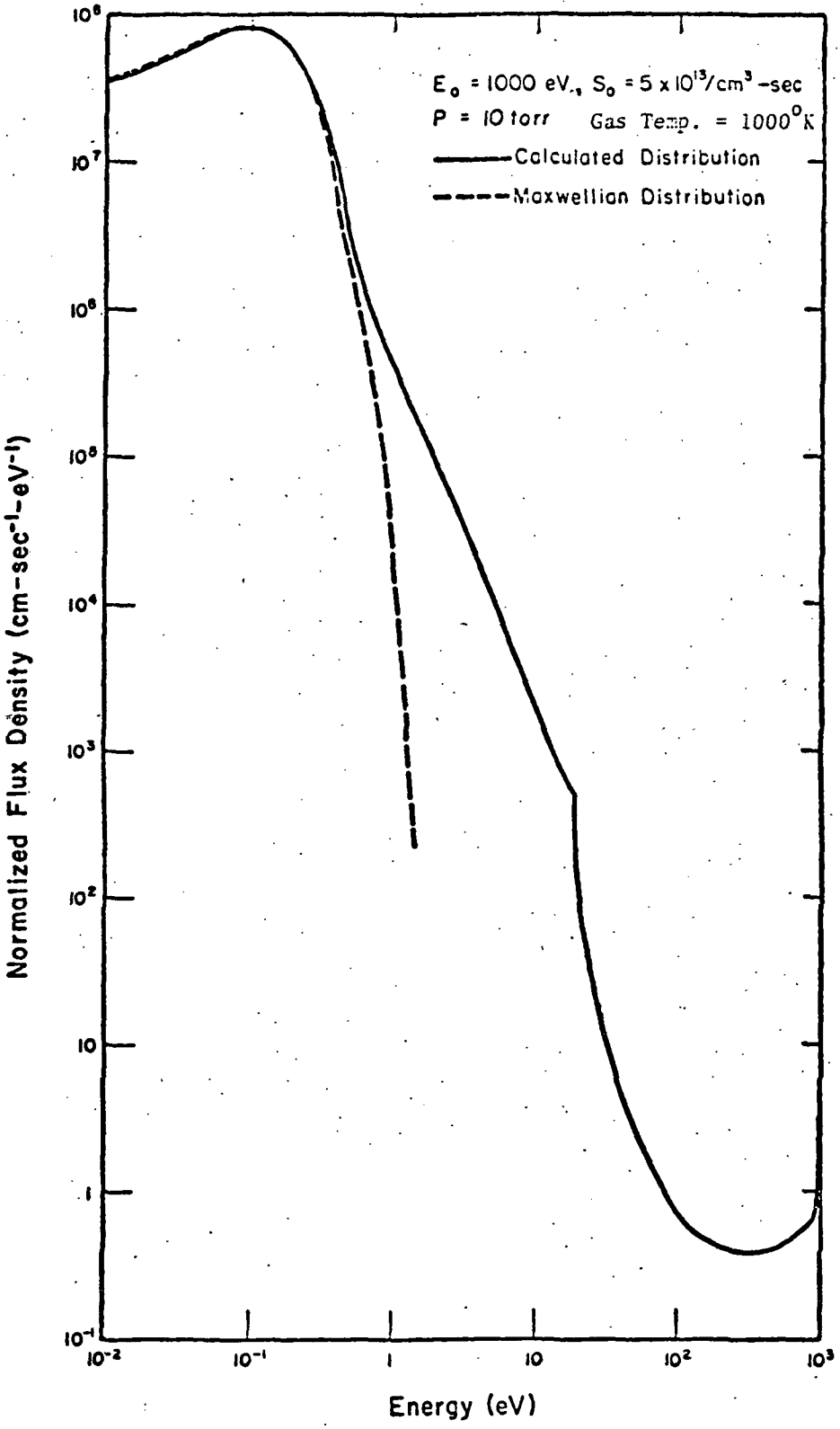

Figure 31. Comparison of Maxwellian and Calculated Distributions for a 1-KeV Source

CHAPTER IV

ENERGY DISTRIBUTION IN THE PRESENCE OF AN ELECTRIC FIELD

A. The Model

The total energy distribution of electrons due to an external source superimposed on a plasma with an applied direct current electri field will be considered. A uniform field, E, is assumed and spatial effects due to finite geometry and leakage are not included. The uniform field is often good in the positive column of a discharge tube, but it will not be applicable in other regions such as the cathode fall or the sheaths near the electrodes while the field is changing rapidly. Nor will it be applicable to some electrode configurations where the field strength varies rapdily throughout the system, like the case where a center wire of a tube is used as one of the electrodes.

In moderate to low E/p cases, which shall be assumed, the electrons above the ionization energy of the gas atoms are not influenced by the field as they slow down. In particular, Appendix I demonstrates that for E/p less than 10 $V\text{-}cm^{-1}\text{-}mm^{-1}$, the energy gained from the field can be neglected comparing with the energy loss via inelastic collisions. This is the largest field considered here and is a reasonable upper limit for other reasons also. Most of the applications of interest (see Chapter I) involve smaller fields. Also the assumption of a weakly ionized plasma places a similar limitation on the field strength, since higher E/p values, like larger external source strengths, would result in additional ionization and too large a fractional ionization. Finally, leakage is neglected here, and as shown in previous chapters, this is consistent with either large systems or high pressures, and the latter implies smaller E/p values.

With this restriction on E/p, the electron distributions developed in Chapter II, for high energy or slowing down region, is therefore applicable here. In the lower energy region, i.e. below excitation potential of the gas atoms, the energy gained from the field becomes comparable to the electron energy. Thus a new treatment of the distribution is required for this region. In doing this the electron source due to slowing down from the high energy portion and the sink due to recombination will be included.

B. Balance Equation for the Low Energy Region

The steady-state Boltzmann Equation with a d.c. elastic field corresponding to Equation (II-1) is:

$$\nabla_{\vec{r}} \cdot \vec{u} f(\vec{r},\vec{u}) - \frac{e\vec{E}}{m_e} \cdot \nabla_{\vec{u}} f(\vec{r},\vec{u}) = \left(\frac{\delta f(\vec{r},\vec{u})}{\delta t}\right)_{coll.} \qquad \text{(IV-1)}$$

Following Allis[53], the distribution function is expanded in spherical harmonics. Retaining the first two terms of the expansion, we obtain:

$$f(\vec{r},\vec{u}) = f_o(\vec{r},\vec{u}) + \vec{f}_1(\vec{r},\vec{u}) \cdot \vec{u}/u \qquad \text{(IV-2)}$$

where,
$$4\pi f_o(\vec{r},\vec{u}) = \int f(\vec{r},\vec{u})\, d\Omega$$
$$\frac{4\pi}{3} \vec{f}_1(\vec{r},\vec{u}) = \int f(\vec{r},\vec{u})\, \vec{u}\, d\Omega$$

Substituting equation (IV-2) into equation (IV-1), one arrives at two coupled equations[53]:

$$\frac{u}{3} \nabla_{\vec{r}} \cdot \vec{f}_1(\vec{r},\vec{u}) - \frac{e\vec{E}}{6u^2} \cdot \frac{d}{du} u^2 \vec{f}_1(\vec{r},u) = \left(\frac{\delta f_o(\vec{r},\vec{u})}{\delta t}\right)_c \qquad \text{(IV-3)}$$

$$- \frac{e\vec{E}}{m_e} \frac{d}{du} f_o(\vec{r},\vec{u}) = \left(\frac{\delta \vec{f}_1(\vec{r},\vec{u})}{\delta t}\right)_c \qquad \text{(IV-4)}$$

where
$$\left(\frac{\delta f_o(\vec{r},\vec{u})}{\delta t}\right)_c = \left(\frac{\delta f_o}{\delta t}\right)_{elastic} + \left(\frac{\delta f_o}{\delta t}\right)_{inelastic},$$

$$\left(\frac{\delta f_o}{\delta t}\right)_{elastic} = \frac{2m_e}{M+m_e} \frac{1}{u} \frac{d}{d(u^2)} \left[u^3 \nu_c \left(f_o + \frac{2kT}{m_e} \frac{d}{d(u^2)} f_o\right)\right]$$

= the net rate of influx of electrons due to elastic collisions in the velocity element $d^3\vec{u}$

$\left(\frac{\delta f_o}{\delta t}\right)_{inelastic}$ = the net rate of production (loss) due to inelastic collisions in the velocity element $d^3\vec{u}$

$\left(\frac{\delta \vec{f}_1}{\delta t}\right)_c$ = rate of momentum influx into the velocity element $d^3\vec{u}$

T = gas temperature

and ν_c = momentum transfer collision frequency.

If the first-fundamental-mode diffusion approximation and uniform spatial properties are assumed, $f(\vec{r},\vec{u})$ becomes spatially independent. Then, combining equations (IV-3) and (IV-4), we obtain a second order differential equation for $f_o(\vec{u})$:

$$-S + \left(\nu_r + \frac{u^3}{3\Lambda^2 \nu_c}\right) f_o + \frac{1}{4\pi u^2} \frac{d}{du} G = 0 \qquad \text{(IV-5)}$$

where S = total source rate from primary δ-electrons and ionized secondaries into the velocity element $d^3\vec{u}$.

ν_r = recombination frequency

Λ = characteristic length of the system from diffusion approximation

and $$G = -\frac{4\pi}{3} u^3 \nu_c \left(\mu_c \frac{1}{mu} \frac{d}{du} f_o + \frac{3m}{M+m} f_o\right)$$

with $$\mu_c = \left(\frac{eE}{m_e}\right)^2 \frac{1}{\nu_c^2}$$

Omitting the source and neglecting spatial losses and recombination while assuming $[m/(m+M)]\, kT \ll (\frac{eE}{m})^2/\nu_c^2$, Nigham[3] solved equation (5) numerically for N_2, CO and CO_2 gases. However, for present purposes, a formal expression for f_o can be obtained from equation (IV-5), (see Appendix J), as:

$$f_o(u) = \exp[-B(u)]\left[\text{const.} + \int_o^u \frac{\exp[B(u')]S'(u')\,du'}{A(u')}\right] \qquad \text{(IV-6)}$$

where $B(u) = \int_0^u \left[\frac{mc^4}{M\lambda(c)} / A(c)\right] dc$,

$$A(c) = \frac{F^2 c \lambda(c)}{3} + \frac{mkTc^3}{M\lambda(c)} ,$$

$$S'(u') = \int_0^{u'} [\nu_n f^o(c) - \alpha(c)] c^2 \, dc$$

$\lambda(c) = c/\nu_c(c) \approx$ mean free path

$\alpha(c)$ = electron production rate in velocity element $d^3\bar{u}$

and $F^2 = \left(\frac{eE}{m}\right)^2$

The assumptions of (m+M) ≈ M and no leakage losses have been made.

Equation (IV-6) can be solved by a simple numerical integration provided that an approximate form of $f^o(u)$ can be obtained for the calculation of $S'(u')$. The case without external electron sources or recombination has been solved by Druyvestyen[2], Smit[54] and others[55],[56]. Their results have been used as the initial estimate of $f^o(u)$, and a corrected form of $f^o(u)$ is obtained for the present case of interest where a source and sink are present.

This procedure was used in preference to the direct numerical solution of equation (IV-5) for two reasons. First, a Monte Carlo simulation for the case with an electric field shows that the distribution is rather close to that of Smit[54]. Second, the numerical solution of equation (IV-5), such as used by Nigham, is also a first order approximation since a two-term expansion of $f(\bar{r},\bar{u})$ was used but eventually only the first term was calculated.

C. Numerical Results and Discussion

The uncorrected f(u) for no source or recombination, similar to that discussed by Deuyvesteyn[2], was used to estimate the rate of recombination and rate of ionization. With the assumption that $\left(\frac{eE}{m}\right)^2 \frac{1}{\nu_c^2} \gg \frac{m}{M} kT$,

f(u) becomes a function of $\frac{eE}{m}\lambda(c)$ or E/p. Following the work of Smit[54], $\lambda(c)$ is assumed to be a constant for electron energies below 5 eV while from 5 to 19.8 eV, $\lambda(c)$ is assumed to be proportional to c. From 19.8 to 24.7 eV, Smit has obtained f(u) represented in Bessel functions. Druywesteyn et al[2] show that these Bessel functions can be approximated by an exponential function and this simpler form for f(u) has been used from 19.8 to 24.7 eV.

The total electron density n_e, is first estimated by substituting the uncorrected form of the distribution into the appropiate rate equation, namely:

$$\beta n_e^2 - P/W - n_e \int_U^\infty f(E/p,\varepsilon)\,\sigma_i(\varepsilon)\,d\varepsilon = 0 \qquad \text{(IV-7)}$$

where β = recombination coefficient

p = rate of energy deposition by heavy-charged particles

W = energy required to create an ion pair

$f(E/p,\varepsilon)d\varepsilon$ = normalized distribution in energy interval dE at ε

$\sigma_i(\varepsilon)$ = ionization cross section from Vriens.

The first term of equation (IV-7) represents the total rate of recombination sink S_k, and the last two terms represent the total rate of electron production S. To compute the differential source rate $\alpha(u)du$, we use the differential energy loss cross-section $\sigma(\Delta E)$ of Stabler[25] such that:

$$4\pi\alpha(u)u^2du = \alpha(E)dE = S\sigma(\chi)d\chi \qquad \text{(IV-8)}$$

where $\chi = \Delta E - u$, and the normalization is such that:

$$\int_0^\infty S\sigma(\chi)\,d\chi = S \qquad \text{(IV-9)}$$

For computation of the differential recombination rate, the uncorrected form of f(u) is again used. Equation (IV-6) has been evaluated with these sink and source rates to obtain a first order correction to the distribution.

Numerical values for the source were selected to represent typical ionization rates due to heavy-charged particle energy deposition. Figure (32) illustrates the distributions for a neutron flux of 5 x 10^{13} $cm^{-1}sec^{-1}$ in E/p = 3, 4, 6 and 8 V-cm^{-1}-mm^{-1}. The nomalization is such that $\int_0^{25} n(E)dE = 1$. The population over 25 eV is considered to be negligible in this normalization. Figure (33) illustrates the distributions for the same E/p values with a neutron flux of 5 x 10^{14} $cm^{-2}sec^{-1}$. The deviation from an uncorrected Druyvesteyn-type distribution is largest when the neutron flux is high and E/p is low. Two such cases are compared with the unperturbed distributions in Figure (34). In general, the perturbations are not too large and the use of unperturbed distributions in the source and sink integrals is justifiable. This is especially true in the case of the smaller neutron flux with E/p larger than 4 V-cm^{-1}-mm^{-1}.

The perturbation is examined more closely in Figure (34) which compares the E/p = 3 and 4 V-cm^{-1}-mm^{-1} cases for no source or sink with the cases where the neutron flux is 5 x 10^{14} $cm^{-2}sec^{-1}$. It is seen that as E/p increases, the deviation decreases. This is because in higher electric fields, the distribution is more dictated by the field than the electrons slowing down from higher energies. The ratio of electric field strength and the source strength, then, determines the importance of the inclusion of source and sink in the calculation.

The average velocity $\bar{u}$ can be computed from the distribution obtained. This random velocity is also proportional to the drift velocity[51]. The average electron flux $\bar{u}\, n_e$, therefore is proportional to the current density. A plot of the average flux vs. E/p is shown in Figure (35). This has the same characteristics as the V-I measurements of Ganley[57] in the enhancement of CO_2 lasers by nuclear radiation experiment. Although an exact comparison cannot be made due to the different gases involved, the trends in Figure (35) do agree with the measurement in CO_2.

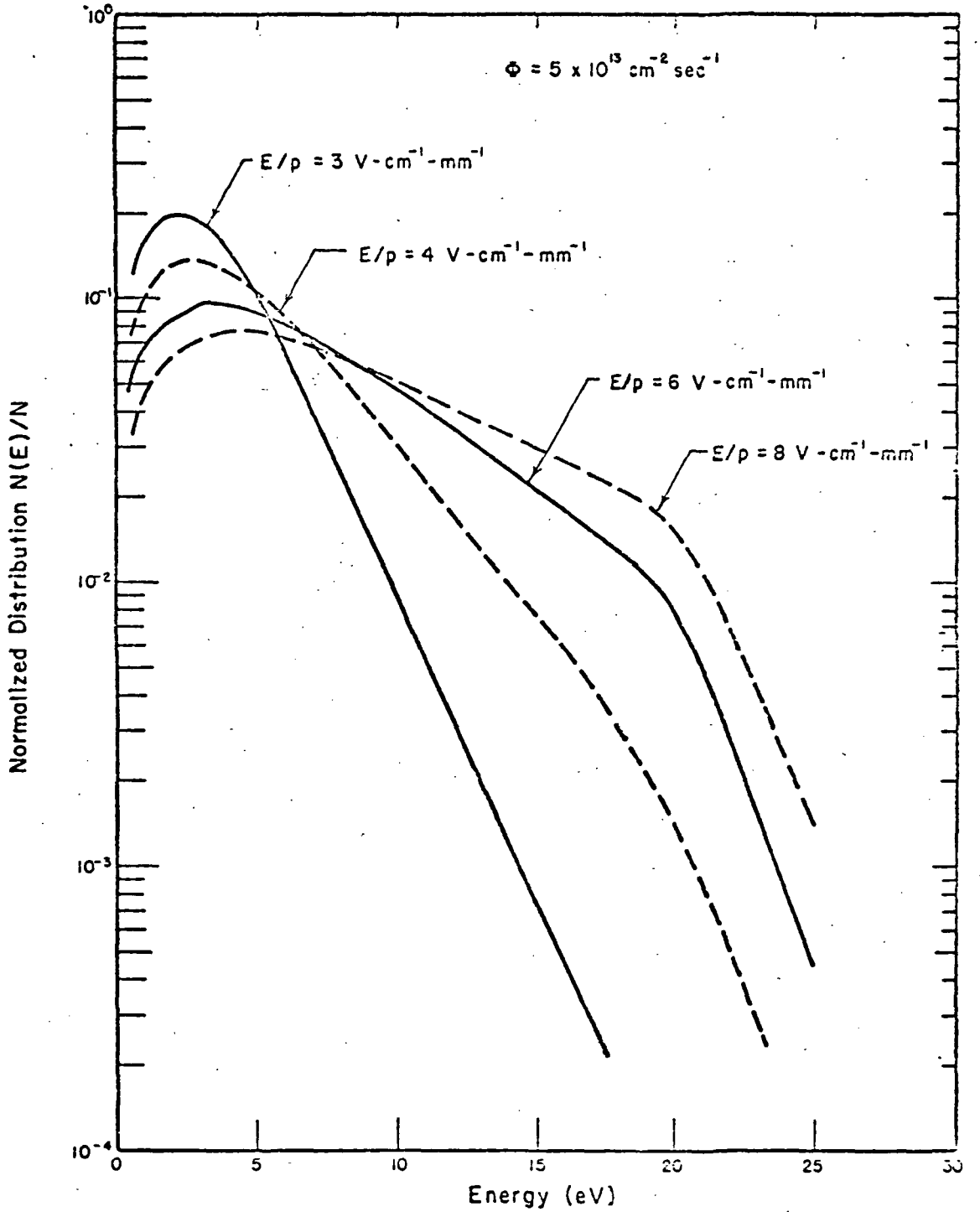

Figure 32. Normalized Distributions in Electric Fields, for E/p = 3, 4, 6 and 8 Volt-cm^{-1}-mm^{-1} and a Neutron Flux of 5 x 10^{13} cm^{-2}-sec^{-1}

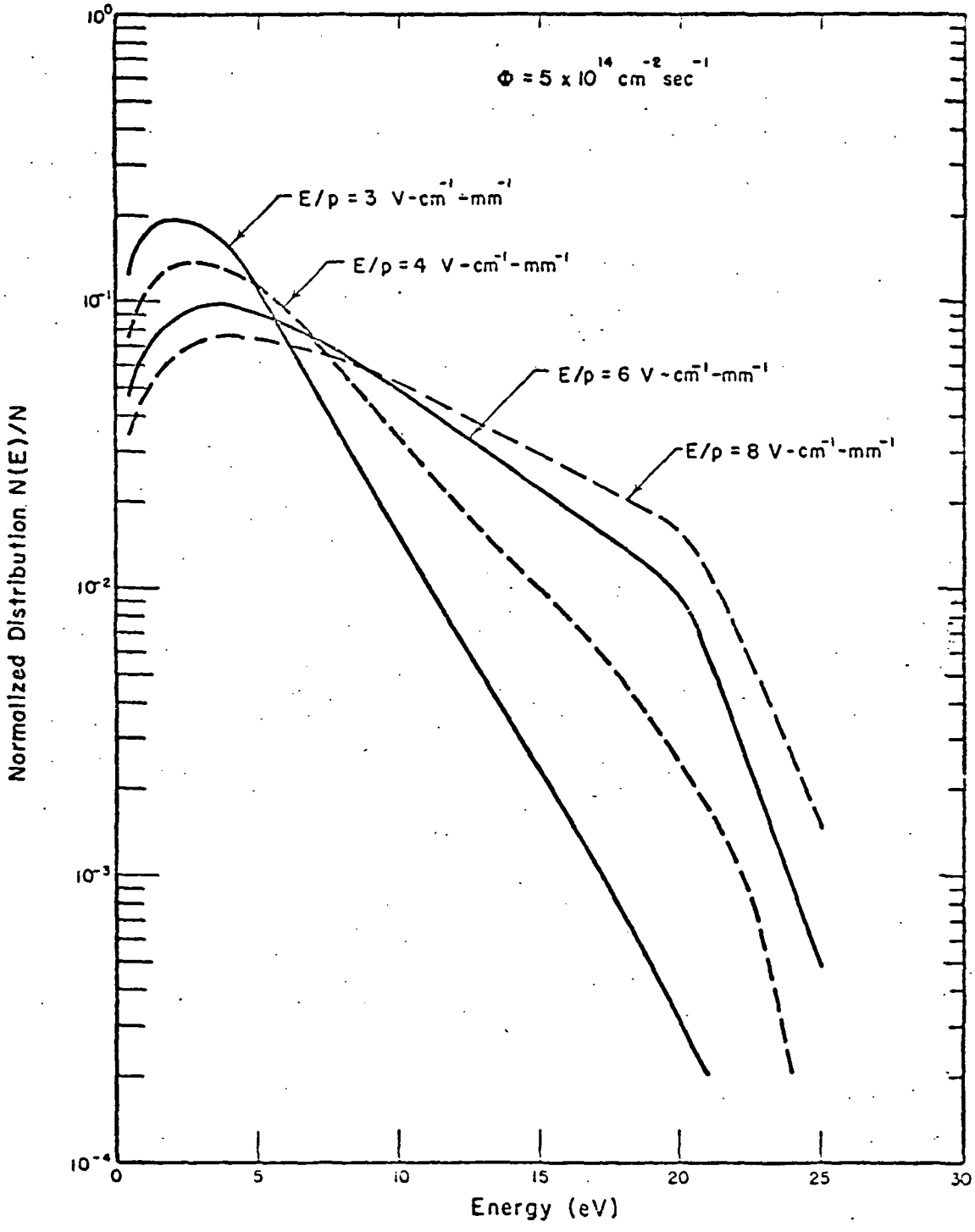

Figure 33. Normalized Distributions in Electric Fields for E/p = 3, 4, 6 and 8 Volts-cm^{-1}-mm^{-1} and a Neutron Flux of 5 x 10^{14} cm^{-2}-sec^{-1}

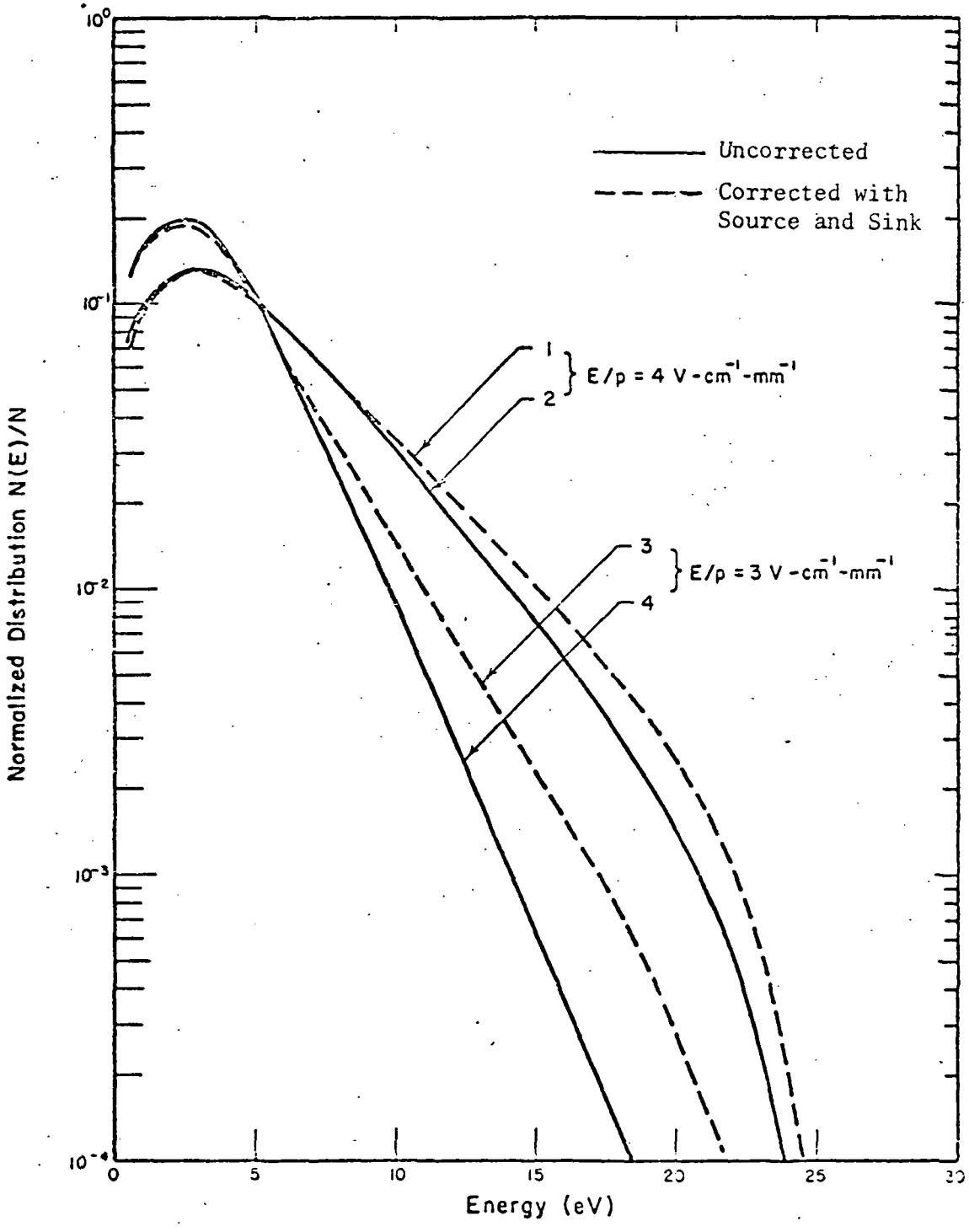

Figure 34. Comparison of Normalized Distributions in Electric Fields for With and Without a Source and Sink

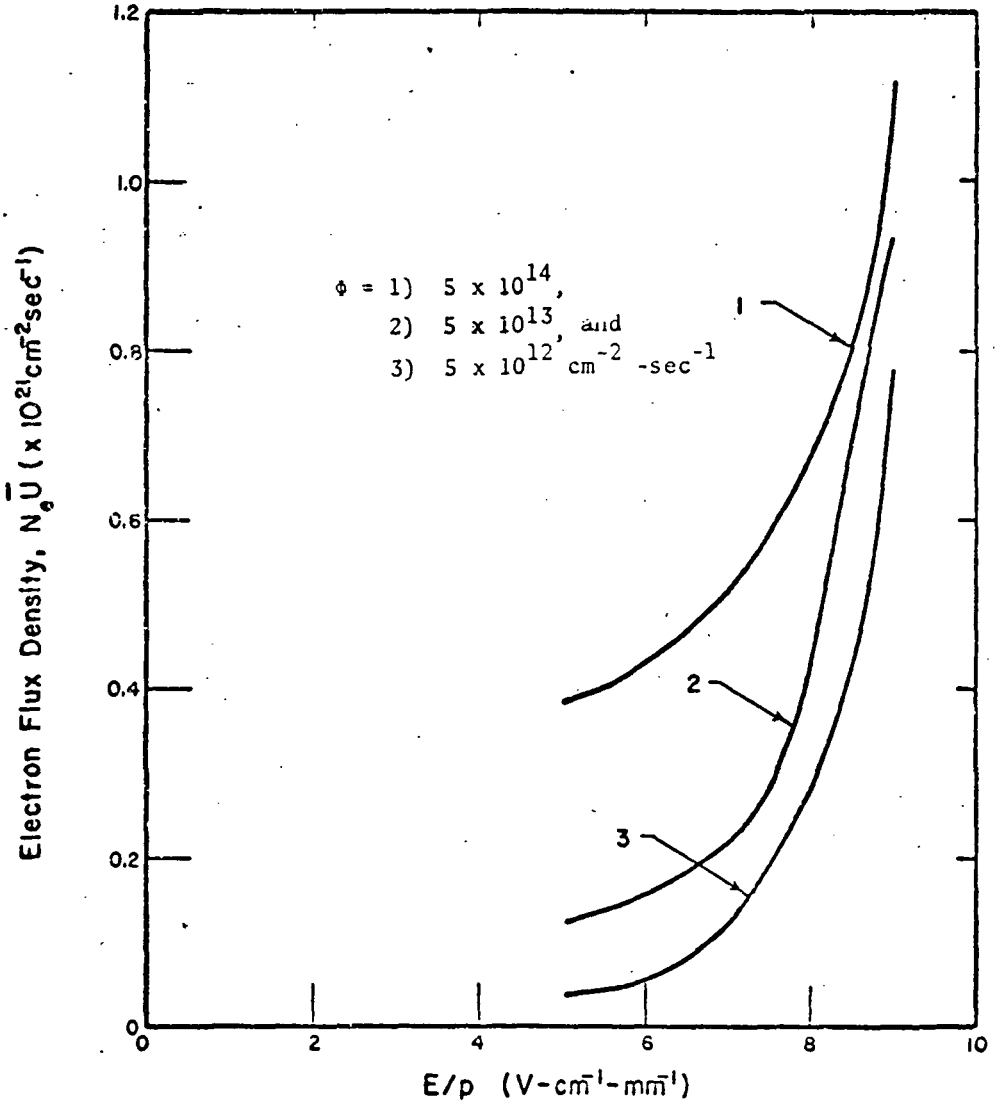

Figure 35. Electron Flux Densities as a Function of E/P for Three Cases of Neutron Fluxes

It is concluded that for neutron flux of less than 5×10^{13} cm^{-3}-sec^{-1} (equivalent to a primary source of about 5×10^{14} 1-keV electrons in 10-torr helium) the distribution is close to that arrived at by Druyvestyen or Smit. This has also been demonstrated by a Monte Carlo calculation[15] where only moderate deviations are observed only for primary electron (1 keV) source rates of 10^{16} cm^{-3}-sec^{-1} or above. It should be noted, however, that in the case of helium, excitation and ionization potentials are relatively high. Larger perturbations can be expected in the cases such as molecular gases, where lower energy levels are involved. For those cases where deviations become severe, equation (IV-6) is not accurate unless a better estimate of f_o is available for the source and sink integrals. A numerical solution of equation (IV-5) would then be necessary.

CHAPTER V

CONCLUSIONS AND SUGGESTIONS FOR FUTURE EXTENSIONS

A. Summary of Present Work

1. General Remarks

The energy distribution of electrons in helium resulting from a continuous high energy source has been analytically studied. The main purpose of the study is to provide a method to analyse the problem. Within the illustrated constrains, such as the degree of ionization, and with appropriate changes in reaction rates, the method can be extended to cover other gases or gas mixtures. A set of physical parameters, such as dimensions of the system, gas pressures, and primary source rates were used to illustrate numerical results of the analytic methods developed. These parameters were consistent with experiments of J. Guyot et al.[13] in studying noble gas plasmas created by nuclear irradiations. Again, within the specified constrains, these parameters can be changed to suit new situations as they arise.

If analytic results are not feasible when new parameters are introduced, the basic equations of the present study are still valid and may be tackled on a purely numerical basis. As shall be detailed later, the present work complements the Monte Carlo simulation of the problem and it may be of advantage to incorporate both methods in a single program. However, some of the specific results of the present analysis shall be pointed out first.

2. The Analysis of the Distribution in the High Energy Region

For energies above the excitation potential of helium, the inelastic collisions were found to be the dominate process in the slowing down of electrons. The balance equation has been set up for this region with the appropriate slowing-past kernels calculated (equation II-28). These kernels were

derived from energy-loss cross-sections. The solutions for the flux distributions were numerically obtained from the balance equation. They are critically dependent on the slowing-past kernels and therefore accurate cross-sections are necessary. The slowing-down past kernels and appropiate limits developed here are uniquely suitable for this energy range accounting for the secondary electrons.

The W-values in helium were calculated to check the validity of the flux calculation and to determine the appropiate cross-sections to use. Vriens' energy-loss cross-sections were used. Emperical parameters were introduced to force the integral of these cross-sections to agree with experimental total ionization cross-sections. The W-value calculations alone do not clearly demonstrate the superiority of the fitted cross-sections but they do indicate that when individual excitations were considered, the agreement is better than the case when a one-excitation level model was used. W-values calcuated for a 1-KeV primary source using the six largest excitation cross-sections were 41 eV per ion pair using the fitted Vriens cross-sections This is to be compared with the W-value of 42.3 eV per ion pair measured by Jesse et. al.[37]

The effect of leakage was included through a first-fundamental model, diffusion-approximation leakage term. The effect of change of pressure and system size is observed, and the shift in the distribution also clearly illustrates the effect of leakage (Figures 21-23). It is shown that the flux depression due to leakage is more severe for higher energy primaries, for smaller systems and for lower pressures.

These flux distributions cannot be obtained if only the thermalized swarm is considered. For a source rate of $10^{13}cm^{-3}\text{-}sec^{-1}$, 1-KeV primaries,

the Maxwellian tail at 50 eV would underestimate the flux density presently calculated at that energy by a factor below 10^{-4}. If the approximation of flux $\simeq$ const./$\langle \frac{dE}{dx} \rangle$ were used, it would overestimate the flux density at 50 eV by a factor of more than 7. The flux distribution presently calculated would therefore provide a much more accurate electron reaction rate than other crude approximations.

3. The Distributions at the Lower Energy Region

For low energies, a model similar to the "heavy gas" model in neutron physics was found to be applicable. This model is uniquely suitable for the presence of a high energy electron source. The fraction of ionization or the primary source rate beyond which charged-particle coulomb interaction cannot be ignored has been determined through an analysis of relaxation times. For a 1.27-cm radius boron-coated tube at 1 torr, this limit corresponds to a neutron flux of $5 \times 10^{13} cm^{-2}\text{-}sec^{-1}$.

For the cases without an electric field, the distribution is found to be close to a Maxwellian with deviations due to leakage and recombination. A shift to a higher average energy due to the inability of higher energy electrons to thermalize is noted. For the cases with an externally imposed direct current electric field, it is found that the high-energy electrons are not appreciably influenced by a moderate field of $E/p \leq 10$. The low energy distributions are close to the results of Druyvestyen when no external sources are present. However, for a large primary electron source rate, corresponding to a neutron flux of 5×10^{14} $cm^{-2}\text{-}sec^{-1}$, deviations from the Druyvestyen results can be observed. Finally, the enhancement of current densities in the presence of a primary electron source are noted.

For cases both with and without the field, the model results in a second order differential equation. Solutions were obtained by a series

expansion and a perturbation approximation. Numerical solution of these equations may be more appropriate in cases (for instance, in the presence of molecular gases) where the algebra becomes too involved or when the deviation from a Maxwellian or Druyvestyen distribution becomes too large.

Many of the results obtained in the present study agree with a Monte Carlo simulation reported by B. Wang, and these are pointed out more specifically below.

4. Comparison With Monte Carlo Results

The Monte Carlo simulation[32] and the present work show the same general shapes in the high energy region. In the presence of an electric field, the Monte Carlo result show that for the case of E/p = 10 V-cm^{-1}-mm^{-1}, the distribution in the high energy region is not influenced by the field. For the low energy region, the distributions can be approximated by a Maxwellian or for the cases with fields, by a Druyvestyen distribution. Deviations from those were observed when the source rates are extremely high. ($>10^{16}$ cm^{-3}-sec^{-1}, 1-keV electrons). These deviations have the same trend as the deviations of the present calculations relative to source rates, pressures.

5. Concluding Remarks on the Methods

Numerical results under various specific parametric conditions were calculated from the equations developed for the entire energy range below the source energy. W-value comparisons and comparisons with a Monte Carlo simulation show these specific results to be in good agreement. Comparisons with temperature measurements by micro-wave techniques[58,59] are not made because in the presence of a high energy source, the thermalized condition is not assumed. As indicated, the important high energy region is indeed found to be highly non-Maxwellian. The agreement of current enhancement in the presence of a high energy source with Ganley's[57] observations has been

noted although no numerical comparisons were made because of the differences in gases and reactions involved.

The basic equations are generally valid for other gases and physical parameters; however, the accuracy of results depends heavily on the cross-sections and kernels. For the high-energy region, equation (II-28) can be used provided slowing-past kernels are derived accordingly from accurate cross-sections. For the low-energy region, equations (IV-5) and (III-11) account for the presence of source and sink for the cases with and without an electric field superimposed respectively. These equations can be numerically solved without any of the approximations used in the present analysis, i.e. the series expansion used in solving equation (III-11) and the perturbation method used in solving equation (IV-5). In fact, these techniques were successful in the present case partly due to the specific circumstances involved, such as cross-sections in helium, pressure ranges, electric field strengths and system sizes.

B. Future Extensions

It is suggested that future work should concentrate on applying the methods developed here nad in the direct confirmation of their validity through experimental observations. Some examples are:

1. The electron energy distributions can be calculated by the methods developed for the appropiate gas or gas mixtures. These distributions can then be used to find electron reaction rates for a set of rate equations describing the plasma kinetics. The emission spectrum from a certain excited state, for instance, could then be measured to varify the calculated excited state density. This provides an accurate check of the calculated electron energy distribution.

2. The energy distributions also provide a starting point in several applied calculations in a radiation-induced laser application. The electron energy distributions can be used to determine possible inversion of excited states by solving the rate equations described above. In a nuclear light-bulb reactor, the appropriate distribution can be used to calculate the radiative emission spectrum from the fuel region and from the buffer-gas region. This sets up a criterion for the addition of seeded gases to prevent harmful radiations from reaching the wall structure. However, for a complicated situation such as the gaseous core reactor, Monte Carlo calculations may be a valuable supplement to the present methods.

3. The present method can be used to complement a Monte Carlo calculation. Because of the small electron population in the high-energy region, in a Monte Carlo simulation, a proper treatment of this region results in a relatively large number of sample particles in the lower energy region. Weighting factors may help, but the calculation may still be prohibitively expensive. The present analytic method handles the high-energy region with good efficiency, but involves complicated expansions and approximations in the low-energy region. Thus there is a strong motivation to combine the methods. The present method would be used to generate a distribution in the high energy region while a Monte Carlo calculation would provide more accurate results in the lower energy region.

The present calculational technique might also aid the Monte Carlo calculation by providing an initial input. The convergence of a Monte Carlo code depends on an estimated initial input. A good initial input can be obtained through the present calculation to assure a rapid convergence of the code.

APPENDIX A

Approximate Flux Using a Continuous Slowing Down Model With No Secondaries

U. Fano[4], using transform techniques on the flux conservation equation, demonstrated that to a first approximation, the flux is related to the inverse of the stopping power. This can also be shown by expanding the flux in the particle balance equation. In the absence of secondaries, the balance equation becomes;

$$\Phi(E')\Sigma(E') = \int_0^\infty k(E'+\tau,\tau)\Phi(E'+\tau)d\tau + S_p\delta(E-E_o) \tag{A1}$$

where $\Sigma(E')$ is the total collisional loss cross-section, $k(E'+\tau,\tau)$ is the probability of a particle of energy $(E'+\tau)$ losing an energy of amount τ from energy, and $S_p\delta(E-E_o)$, the primary electron source, is taken as a delta function at E_o with source strength S_p.

If $\Phi(E)$ and $k(E,\tau)$ are slowly varying functions of energy, the first two terms of a Taylor expansion give:

$$\Phi(E')\Sigma(E') \doteq \Phi(E')\int_0^\infty k(E',\tau)d\tau + \frac{\partial\Phi(E')}{\partial E'}\int_0^\infty k(E',\tau)\tau\,d\tau + S_p\delta(E-E_o) \tag{A2}$$

In the absence of absorption,

$$\int_0^\infty k(E',\tau)d\tau = \int_0^{E'} k(E',\tau) = \Sigma(E') \tag{A3}$$

Multiplication of equation A2 by dE' and integration yields:

$$0 = \int_0^E \tau\,d\tau \int_E^\infty dE' \frac{\partial}{\partial E'}\Phi(E')k(E',\tau) + S_p \tag{A4}$$

and since

$$\lim_{E\to\infty} \Phi(E)k(E,\tau) = 0 \tag{A5}$$

we obtain:

$$\Phi(E) \doteq \text{const} \Big/ \int_0^E k(E',\tau)\tau\,d\tau \tag{A6}$$

Equation (A-6) agrees with the result U. Fano[4] obtained by Laplace transforming equation (A-1).

APPENDIX B

Derivation of an Integral Form of the Collision Density Balance Equation

After an ionization collision, two identical electrons will emerge. To have an accounting system we shall label the one with larger energy as the "primary" electron and the one with the smaller energy of the two, the "secondary". The collision density balance equation for a δ-function source of electrons at energy E_o is:

$$\Sigma_c(E)\,\Phi(E) = \int_{E+U_1}^{E+\Delta} \Sigma_c(E' \to E)\,\Phi(E')\,dE' + S_s(E) + S_p\,\delta(E-E_o) \qquad \text{(B-1)}$$

where $\Sigma_c(E' \to E)$ is the differential cross-section of scattering into energy E from energy E'.

U_1 = first excitation potential of the gas atoms

$\Delta = E + U$ if $2E + U \leqslant E_o$, and $\Delta = E_o - E$ if $2E + U \geqslant E_o$.

The "secondary" source term takes the form:

$$S_s(E) = \int_{2E+U}^{E_o} \Sigma_s(E' \to E)\,\Phi(E')\,dE' \qquad \text{(B-2)}$$

where $\Sigma_s(E' \to E)$ is the probability per electron track length that the "secondary" electron emerges with an energy in dE at E.

We shall divide the energy range into two cases:

Case 1. If $2E + U \quad E_o$, then $S_s(E) = 0$ and $\Delta = E_o - E$.

Integrating equation (B-1) from E to E_o, we obtain,

$$\int_E^{E_o} \Sigma_c(E'')\,\Phi(E'')\,dE'' = \int_E^{E_o} dE'' \int_{E''+U_1}^{E_o} \Sigma_c(E' \to E'')\,\Phi(E')\,dE' + S_p \qquad \text{(B-3)}$$

Now consider the double integral on the R.H.S. of equation (B-3). Since for E'' in the range of $E_o - U_1$ to E_o, $\Sigma_c(E' \to E'') \equiv 0$, we have

$$\int_{E}^{E_0} dE'' \int_{E''+U_1}^{E_0} \Sigma_c(E' \rightarrow E'') \Phi(E') dE' = \int_{E}^{E_0-U} dE'' \int_{E''+U_1}^{E_0} \Sigma_c(E' \rightarrow E'') \Phi(E') dE'$$

$$= \int_{E+U_1}^{E_0} dE' \Phi(E') \int_{E}^{E'+U_1} dE'' \Sigma_c(E' \rightarrow E'') \quad \text{(B-4)}$$

where we have interchanged the order of integration. Combining equations (B-3) and (B-4), we obtain

$$\int_{E}^{E_0} \Phi(E') dE' \int_{E_{min}}^{E'-U_1} \Sigma_c(E' \rightarrow E_1) dE_1 = \int_{E+U_1}^{E_0} dE' \Phi(E') \int_{E}^{E'-U_1} dE_1 \Sigma_c(E' \rightarrow E_1) + S_p \quad \text{(B-5)}$$

where E_{min} is the minimum energy above which electrons with energy E' can slow down. Note that we have changed the notation of dummy variables inside the integrals. Breaking up the LHS of equation (B-5) gives:

$$LHS = \int_{E}^{E+U_1} \Phi(E') dE' \int_{E_{min}}^{E'-U_1} \Sigma_c(E' \rightarrow E_1) dE_1 + \int_{E+U_1}^{E_0} dE' \Phi(E') \int_{E_{min}}^{E'-U_1} \Sigma_c(E' \rightarrow E_1) dE_1 \quad \text{(B-6)}$$

so equation (B-5) becomes

$$\int_{E}^{E+U_1} \Phi(E') dE' \int_{E_{min}}^{E'-U_1} \Sigma_c(E' \rightarrow E_1) dE_1 + \int_{E+U_1}^{E_0} dE' \Phi(E') \left[\int_{E_{min}}^{E'-U_1} \Sigma_c(E' \rightarrow E_1) dE_1 \right.$$

$$\left. - \int_{E}^{E'-U_1} \Sigma_c(E' \rightarrow E_1) dE_1 \right] = S_p$$

or,

$$\int_{E}^{E+U_1} \Phi(E') dE' \int_{E_{min}}^{E'-U_1} \Sigma_c(E' \rightarrow E_1) dE_1 + \int_{E+U_1}^{E_0} \Phi(E') dE' \int_{E_{min}}^{E} \Sigma_c(E' \rightarrow E_1) dE_1 = S_p \quad \text{(B-7)}$$

Consider the L.H.S. of equation (B-7). The flux $\Phi(E')$ in the first integral lies in the range from E to E + U, and any inelastic collision will slow the electron down past energy E; as for the remaining integrals, E_1 is in energy range E_{min} to E and Σ_c $(E' \rightarrow E_1)$ accounts for all collisions that slow the electron down past energy E. Therefore, the LHS of equation (B-7) represents

the total rate of slowing down past energy E.

Case 2. If $(2E + U) < E_o$; in this case $\Delta = E + U$ and

$$S_s(E) = \int_{2E+U}^{E_o} \Sigma_s(E' \rightarrow E'') \Phi(E') dE' \tag{B-8}$$

Integration of equation (B-1) from E to E_o gives:

$$\int_E^{E_o} \Sigma_c(E'') \Phi(E'') dE'' = \int_E^{\frac{E_o - U}{2}} dE'' \int_{E''+U_1}^{2E''+U} dE' \Phi(E') \Sigma_c(E' \rightarrow E'')$$

$$+ \int_{\frac{E_o-U}{2}}^{E_o} dE'' \int_{E''+U_1}^{E_o} dE' \Phi(E') \Sigma_c(E' \rightarrow E'') + \int_E^{E_o} S_s(E') dE' + S_p \tag{B-9}$$

Consider the RHS of (B-9). The first two integrals cover the areas (1) and (2) in the sketch of Fig. B-1. This is equal to areas [(1) + (2) + (3)] - (3), i.e. the first two integrals become:

$$\int_{E+U_1}^{E_o} \Phi(E') dE' \int_E^{E'-U_1} dE'' \Sigma_c(E' \rightarrow E'') - \int_{2E+U}^{E_o} \Phi(E') dE' \int_E^{\frac{E'-U}{2}} dE'' \Sigma_c(E' \rightarrow E'') \tag{B-10}$$

But, for the second integral, $\Sigma_c(E' \rightarrow E'')$ is equal to zero for the region of E'' since no "primary" electron can slow down past $(E' - U)/2$. The integral therefore vanishes in area (3). Then equation (B-9) becomes:

$$\int_E^{E_o} \Sigma_c(E'') \Phi(E'') dE'' = \int_{E+U_1}^{E_o} \Phi(E') dE' \int_E^{E'-U_1} dE'' \Sigma_c(E' \rightarrow E'') + \int_E^{E_o} S_s(E') dE' + S_p \tag{B-11}$$

Equation (B-11) is identical to equation (B-5) except for the "secondary" production rate term. Using equation (B-7), equation (B-11) can be written as:

$$\int_E^{E+U_1} \Phi(E') dE' \int_{E_{min}}^{E'-U_1} \Sigma_c(E' \rightarrow E_1) dE_1 + \int_{E+U_1}^{E_o} \Phi(E') dE' \int_{E_{min}}^{E} \Sigma_c(E' \rightarrow E_1) dE_1 =$$

$$S_p + \int_E^{E_o} S_s(E') dE' \tag{B-12}$$

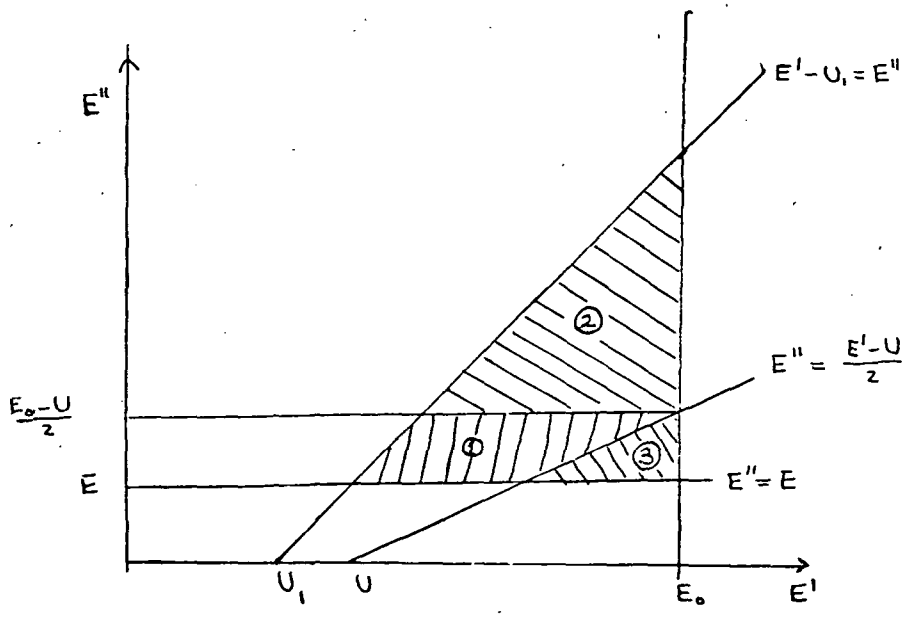

Figure B-1 Sketch of Area Covered in the Collision Integral

Here the LHS is equal to the total rate of slowing down past energy E while the RHS equals the total rate of production above energy E. This is the same as:

$$\sum_j \int_E^{E_o} \Phi(E') K_j(E', E)\, dE' = S_p + \int_E^{E_o} S_s(E')\, dE' \qquad \text{(B-13)}$$

where $K_j(E',E)$ = probability per track length of slowing down past energy E through a j^{th} type collision.

This shows that in both cases the differential form of the balance equation (Equation (B-1)) and the integral form of the balance equation are equivalent.

APPENDIX C

Comparison of Average Energy Loss Due to Elastic and Inelastic Collisions For High Energy Electrons in He

For elastic collisions, we consider the first Born approximation cross-sections[59,60]:

$$I(\theta) = \left| \frac{8\pi^2 m_e}{h^2} \int_0^\infty \frac{\sin kr}{kr} V(r) r^2 dr \right|^2 \qquad \text{(C-1)}$$

where $k = \frac{2m_e U}{h} \sin\theta/2$

For helium, Hylleraas[61] has employed a variational method to obtain the following wave function:

$$\psi_0 = \left(z^3/\pi a_0^3\right) e^{-z(r_1+r_2)/a_0} \qquad \text{(C-2)}$$

with the potential:

$$V(r) = -2e^2 \left(\frac{1}{r} + \frac{z}{a_0}\right) e^{-2zr/a_0} \qquad \text{(C-3)}$$

where $z = 1.69$, and a_0 is the Bohr radius. From this, the differential scattering cross-section becomes

$$I(\theta) = \frac{4m_e^2 e^4 A (2\lambda^2 + k^2)^2}{h^4 (\lambda^2 + k^2)^4} \qquad \text{(C-4)}$$

where $\lambda = 2\ z/a_0$, A = atomic weight.

The fractional energy loss due to elastic collisions is related to the angle of scattering by[1]

$$\frac{\Delta E}{E} = \frac{2m}{M} (1 - \cos\theta) \qquad \text{(C-5)}$$

where m/M is the mass ratio between the colliding particle. From equations (C-4) and (C-5) the average fractional loss per track length becomes:

$$\left\langle \frac{\Delta E}{E} \right\rangle = \int_0^{\pi} \left(\frac{\Delta E}{E} \right) I(\theta) 2\pi \sin\theta \, d\theta$$

$$= 2\pi \left(\frac{2m}{M} \right) \frac{4m^2 e^4 A}{\hbar^4} \int_0^1 8x^3 \frac{(2a + bx^2)^2}{(a + bx^2)^4} \, dx$$

$$= 8\pi \left(\frac{2m}{M} \right) \frac{4m^2 e^4 A}{\hbar^4} \left[\frac{1}{b^2} \lg \frac{a+b}{b} + \frac{1}{6b^2} - \frac{a}{b^2(a+b)} \right.$$

$$\left. + \frac{a^2}{4b^2(a+b)^2} - \frac{a^3}{6b^2(a+b)^3} \right] \qquad \text{(C-6)}$$

where $a = \lambda^2$,

$$b = \left(\frac{2mv^2}{\hbar} \right)^2 = \frac{8mE}{\hbar^2}$$

After rearranging the constants, we obtain:

$$\left\langle \frac{\Delta E}{E} \right\rangle = \pi e^4 \left(\frac{m}{M} \right) \frac{A}{E^2} \left\{ \lg \left[1 + \left(\frac{k}{\beta} \right)^2 \right] + \frac{1}{6} - \frac{k^2}{k^2 + \beta^2} \right.$$

$$\left. + \frac{1}{4} \frac{k^2}{(k^2 + \beta^2)^2} + \frac{k^6}{6(k^2 + \beta^2)^3} \right\} \qquad \text{(C-7)}$$

where $\beta = v/c$ and $k = \frac{1}{4}(1/137)^2$

and we have used the fact that $\lambda^2 = \left(\frac{e^2}{\hbar c} \right)^2 \frac{1}{4} \left(\frac{1}{\beta} \right)^2$

$$= \left(k/\beta \right)^2 .$$

For inelastic collisions, we consider the Möller cross-section[ ]

$$k_m(E, \tau) d\tau = \frac{2\pi N_e r_0^2}{\beta^2} \left\{ \frac{1}{\tau^2} + \frac{1}{(E-\tau)^2} - \frac{(2 + \frac{1}{E})}{(E+1)} \left[\frac{1}{\tau} + \frac{1}{E-\tau} + \frac{1}{(E+1)^2} \right] \right\} \qquad \text{(C-8)}$$

where E and z are the incident energy and energy loss for the collision respectively, in units of $M_o C^2$. The average fractional loss per track length

becomes:

$$\left\langle \frac{\Delta E}{E} \right\rangle_{inel.} = \int_{\bar{Q}}^{E'/2} k_m(E,\tau) \frac{\tau}{E} d\tau$$

$$= \int_{\bar{Q}}^{E'/2} \frac{2\pi N_e r_o^2}{\beta^2 E} \left\{ \frac{1}{\tau} + \frac{\tau}{(E-\tau)^2} - \frac{(2+\frac{1}{E})}{(1+E)^2} \left[1 + \frac{\tau}{E-\tau} \right] + \frac{\tau}{(1+E)^2} \right\} \qquad \text{(C-9)}$$

where $r_o = e^2/mc^2$, and $\bar{Q}$ is a constant determined from stopping power theory. For U << C, $\bar{Q}$ equals Bethe's[16] $Q_{min} = \frac{(Uz)^2}{2\ MU^2}$. The upper limit is arrived at from the consideration of indistinguishability of electrons. Changing the energy units to electron volts and integrating (C-9), we find

$$\left\langle \frac{\Delta E}{E} \right\rangle = \frac{2\pi N_e e^4}{E^2} \left\{ 2 - \frac{E}{E-\bar{Q}} + \lg \frac{E}{2\bar{Q}} + \lg \frac{E/2}{E-\bar{Q}} + \frac{(2E+mc^2)mc^2}{(E+mc^2)^2} \lg \frac{E/2}{E-\bar{Q}} + \frac{1}{(E+mc^2)^2} \left(\frac{E^2}{8} - \frac{\bar{Q}^2}{2} \right) \right] \qquad \text{(C-10)}$$

Comparison of equations (C-7) and (C-10) demonstrates that in the energy range where Born approximation and Möller's cross-section are valid, the average energy losses due to inelastic and elastic scattering differ by a factor of magnitude about m/M. This justifies the neglect of elastic collisional losses in that energy range.

APPENDIX D

Slowing Down Kernels from Binary Encounter Collision Theory

The binary collision theory neglects the influence of the atomic nucleus and treats inelastic collisions as an interaction between two electrons alone. When two interacting particles obey the inverse square law, the problem is exactly soluble in wave mechanics, and the solution yields the same scattering law as the classical theory[39]. If, however, the two interacting particles are identical, as in the case for electrons, symmetrical and antisymmetrical wave functions in the space-coordinates of the electrons must be used. Therefore, if the corresponding cross sections are σ^+ and σ^- and θ is the angle between the spin directions of the electrons, the total cross section is[39]

$$\sigma = \frac{1}{4}(1-\cos\theta)\sigma^+ + \frac{1}{4}(3+\cos\theta)\sigma^- \tag{D-1}$$

If one assumes unpolarized electrons, this reduces to

$$\sigma = \frac{1}{4}\sigma^+ + \frac{3}{4}\sigma^- \tag{D-2}$$

L. Vriens' model of two interacting electrons with exchange and interference gives[20]:

$$\sigma_{\Delta E}\, d\Delta E = \frac{\pi e^4}{E_3}\left[\left(\frac{1}{\Delta E^2} + \frac{4E_3}{3\Delta E^3}\right) + \left\{\frac{1}{(E_3-E_2-\Delta E)^2} + \frac{4E_2}{3(E_3-E_2-\Delta E)^3}\right\} - \frac{\Phi''}{\Delta E(E_3-E_2-\Delta E)}\right]$$

$$\text{for } E_3' > E_2 \tag{D-3}$$

and

$$\sigma_{\Delta E}\, d\Delta E = \frac{\pi e^4}{E_3}\left[\left(\frac{1}{\Delta E^2} + \frac{4}{3}\,\frac{E_3'}{\Delta E^3}\right) + \left\{\frac{1}{(E_3 - E_2 - \Delta E)^2} + \frac{4\,E_3'}{3\,|E_3 - E_2 - \Delta E|^3}\right.\right.$$

$$\left.\left. - \frac{\Phi'}{\Delta E\,|E_3 - E_2 - \Delta E|}\right]\left(\frac{E_3'}{E_2}\right)^{1/2} d\Delta E \quad , \quad \text{for} \quad E_3' \leq E_2 \qquad \text{(D-4)}$$

where the terms are defined in the text. The value of Φ' is $\simeq 1$ for $E_1 >> R$. In the following integrations, we shall approximate Φ' by a constant. This is consistent with the assumption that Vriens made in arriving at his total ionization and excitation cross-sections.

For the case of ionization collisions, consider E_1 to be the incident energy and $E_1 - \Delta E$ and $\Delta E - U$ to be the exit energies after ionization, U being the ionization potential (Fig. D-1)

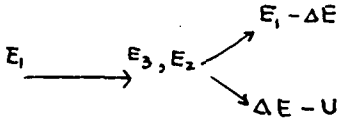

Fig. (D-1) Electron Energies in an Ionization Collision

The two emerging electrons are indistinguishable and the maximum energy loss possible is $(E_1 + U)/2$. The minimum energy loss that an incident electron can suffer and still slow down past energy E from energy E' is E' - E. The slowing-past kernel due to ionization collisions is then obtained by integrating Vriens' differential cross-section through these limits. Thus, for $(E' + U)/2 \geq E' - E \geq U$;

$$K_I(E', E) = \int_{E'-E}^{(E'+U)/2} N_e\, \sigma_{\Delta E}\, d\Delta E$$

$$= \frac{N_e \pi e^4}{E_3}\left\{\frac{1}{E' - E} - \frac{1}{E_3 - E_2} - \frac{2E_2}{3}\left[\frac{1}{(E'-E)^2}\right.\right.$$

$$\left.\left. + \frac{1}{(E_3 - E_2)^2}\right] - \frac{\Phi''}{(E'+U)}\ln\left(\frac{E+U}{E'-E}\right)\right\}$$

where

$$\Phi'' = \cos\left\{\frac{\sqrt{R}}{(E_2 - E_1)^{1/2}} \ln\frac{E+U}{E'-E}\right\} \qquad \text{(D-5)}$$

and N_e is the total number of valance electrons in helium. For more complicated atoms, one has to sum over each different electrons in the shells with their appropriate ionization potentials and averaged kinetic energies. An approximate method suggested by Vriens is to simply multiply by the number of electrons in the outer valance shells.

If, however, $E' - E \leq U$, any ionization collision will show the electron from energy E' past energy E. Therefore, for $(E' - E) \leq U$;

$$K_I(E',E) = \int_U^{\frac{E'+U}{2}} N_e \sigma_{\Delta E}\, d\Delta E$$

$$= \frac{N_e \pi e^4}{E_3}\left\{\frac{1}{U} - \frac{1}{E'} + \frac{2}{3}E_2\left[\frac{1}{U^2} - \frac{1}{E'^2}\right] - \frac{\Phi''}{E+U}\ln\frac{E'}{U}\right\} \qquad \text{(D-6)}$$

This is, as one would expect, identical to the total ionization cross-section and is consistent with the ionization cross-section given by Vriens and others. The two slowing-down kernels (D-5) and (D-6) are continuous at $E' - E = U$. For $E' - E \geq (E' + I)/2$ or $E' \leq U$, the slowing down kernel $K_I(E',E) = 0$.

The binary collision model assumed that an excitation to level n takes place when the energy loss ΔE is such that, $U_n \leq \Delta E \leq U_{n+1}$, where U_n and U_{n+1} are excitation potentials of levels n and n+1 respectively. In the case of helium where the final state depends on the spin orientation, we will apply the following approximation. Mott and Massey give the excitation cross-section for an arbitrary angle θ between spin directions of interacting electrons to be[39]:

$$Q_e(\theta) = Q_{de} + Q_{ee} + (1+\cos\theta)\,Q_{int}. \qquad \text{(D-7)}$$

where de, ee and int denote contributions due to direct, exchange, and interference. For parallel spins, $Q_e(0) = Q_{de} + Q_{ee} + 2\,Q_{int}$ and for antiparallel spins, $Q_e(\pi) = Q_{de} + Q_{ee}$. However, direct excitation only occurs in the singlet mode while exchange excitation can be either singlet or triplet. If one assumes one half of electrons have opposite spins and the other have parallel spins; then

$$Q_e = \tfrac{1}{2} Q_e(\pi) + \tfrac{1}{2} Q_e(0) = Q_e(\pi/2)$$

$$= Q_{de} + Q_{ee} + Q_{int} \qquad \text{(D-8)}$$

From this we deduce that,

$$Q_{singlet} = Q_{de} + \frac{Q_{ee}}{2} \quad \text{and} \quad Q_{triplet} = \frac{Q_{ee}}{2} \qquad \text{(D-9)}$$

In general the excitation to the n^{th} cross-section is calculated according to:

$$Q_{ex}(n) = \int_{U_n}^{U_{n+1}} \sigma_{\Delta E}\, d\Delta E \qquad \text{(D-10)}$$

Since only ΔE, the loss of energy is considered, there is no distinction between levels when one considers the kernel of slowing down past a certain energy. One can therefore group all the excitations into one level and consider an excitation range, i.e. one considers excitation to have occurred if $U_1 \leq \Delta E \leq U_i$ where U_1 is the first excitation potential energy and U_i, the ionization potential. We refer to the slowing down past kernel due to excitation derived through this model as the one level excitation model.

For $E' - E \geq U_1$, no excitation collision can bring an electron from energy E' down past energy E and the slowing down past kernel $K_{ex}(E',E) = 0$. For $E' \geq U_1$ and $U_i \geq E' - E \geq U_1$

$$K_{ex}(E',E) = \int_{E'-E}^{U_i} N_e \sigma_{\Delta E}\, d\Delta E$$

$$= \frac{N_e \pi e^4}{E_3}\left\{\frac{1}{E'-E} - \frac{1}{U_i} + \frac{1}{E'} - \frac{1}{E+U_i} + \frac{2E_2}{3}\right.$$

$$\left.\left[\frac{1}{(E'-E)^2} - \frac{1}{U_i^2} + \frac{1}{E'^2} - \frac{1}{(E+U_i)^2}\right] - \frac{\Phi'''}{(E'+U_1)} \ln\left[\frac{U_i(E+U_i)}{(E'-E)E'}\right]\right\}$$

where

$$\Phi''' \approx \cos\left\{\left(\frac{R}{E_1+U_1}\right)^{1/2} \ln \frac{E'-U_i-U_1}{U_1}\right\} \qquad \text{(D-11)}$$

For $E' \geq U_i$ and $U_1 \geq E' - E$, any excitation collision will bring the electron down past energy E from energy E', and

$$K_{ex}(E',E) = \int_{U_1}^{U_i} N_e \sigma_{\Delta E}\, d\Delta E$$

$$= \frac{N_e \pi e^4}{(E'+W)}\left[\left(\frac{1}{U_1} - \frac{1}{U_i}\right) + \left(\frac{1}{E'} - \frac{1}{E'+U_i-U_1}\right) + \frac{2E_2}{3}\right.$$

$$\left.\left\{\frac{1}{U_1^2} - \frac{1}{U_i^2} + \frac{1}{E'^2} - \frac{1}{(E'+U_i-U_1)^2}\right\} - \frac{\Phi'''}{E'+U_1} \ln\left\{\frac{U_i(E'+U_i-U_1)}{E'U_1}\right\}\right] \qquad \text{(D-12)}$$

This agrees with Vriens' one-level total excitation cross-section.

The secondary production kernel is defined as the probability per track length that an electron with energy E' is going to produce two electrons with energies both larger than E. This (Fig. D-1) imposes the requirement that $\Delta E - U \geq E$ or $E' \geq 2E + U$. For energy $E' \geq 2E + U$, after an ionization collision, at least one of the electrons will emerge with energy larger than E. For both to emerge with energies larger than E, the minimum energy loss of the incident electron must be E + U. The maximum loss of energy due to the indistinguishibility of electrons, cannot exceed $\frac{1}{2}(E' + U)$. The kernel

for secondary production $K_s(E',E)$ is; for $E' > 2E + U$;

$$K_s(E',E) = \int_{E+U}^{\frac{1}{2}(E'+U)} \sigma_{\delta E}\, d\delta E$$

$$= \frac{N_a \pi e^4}{(E_i+W)} \left\{ \frac{1}{E+U} - \frac{1}{E'-E} + \frac{2E_2}{3} \left[\frac{1}{(E+U)^2} - \right.\right.$$

$$\left.\left. \frac{1}{(E'-E)^2} \right] - \frac{\Phi''}{E'+U} \ln \left[\frac{E'-E}{E+U} \right] \right\} \qquad \text{(D-13)}$$

and $K_s(E',E) = 0$ for $E' < 2E + U$.

APPENDIX E

Determination of the Number of Secondary Electrons Produced Per δ-ray

First, we shall show explicitly that in an energy range below the first excitation potential but above an energy where recombination is significant, i.e. between 19.5 and say 2 eV in helium, the slowing down past density q(E) is a constant. In this region, the recombination is considered to be negligibly small and in the case of helium, processes like dissociative ionization ($e + A_2 \rightarrow A^+ + A^- + e$) can be neglected [50]. Consider the collision density F(E) defined as the total number of collisions at energy E per unit energy interval;

$$F(E)dE = \int_E^{U_1} F(E')P(E' \rightarrow E)dE'dE + S_I(E)dE - S_A(E)dE \qquad (E\text{-}1)$$

where $F(E) = \Sigma_s(E)\Phi(E)$,

$S_A(E) = \Sigma_a(E)\Phi(E)$,

and $S_I(E)dE$ gives the rate of electrons arriving in dE at E from inelastic scatterings above energy U_1. $\Sigma_s(E)$ and $\Sigma_a(E)$ are macroscopic elastic and recombination cross-sections and $P(E' \rightarrow E)dE$ is the probability that an electron scattering at energy E' will arrive in energy interval dE at E. Integration of equation (E-1) from 0 to E where E is below U_1 gives

$$\int_0^E F(E'')dE'' = \int_0^E dE'' \int_{E''}^{U_1} F(E')P(E' \rightarrow E'')dE' + \int_0^E [S_I(E'') - S_A(E'')]dE'' \qquad (E\text{-}2)$$

The shaded area in sketch is the area of integration for the double integral

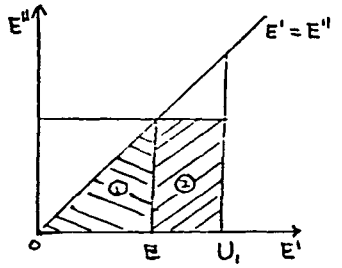

Figure E-1 Sketch of Area Covered in a Collisional Integral

on the R.H.S. of equation (E-2). Changing the order of integration, we write the double integral as a sum of integrations over the two shaded areas (1) and (2); i.e.;

$$\int_0^E dE'' \int_{E''}^{U_1} F(E') P(E' \to E'')\, dE' = \int_0^E dE' F(E') \int_0^{E'} P(E' \to E'')\, dE'' + \int_E^{U_1} dE' F(E') \int_0^E P(E' \to E'')\, dE'' \qquad \text{(E-3)}$$

But

$$\left.\begin{aligned} &\int_0^{E'} P(E' \to E'')\, dE'' = 1 \\ \text{and} \quad &\int_0^E P(E' \to E'')\, dE'' = K(E', E) \end{aligned}\right\} \qquad \text{(E-4)}$$

where K(E',E) is the probability that an electron slows down past energy E after collision at E'. From equations (E-2), (E-3) and (E-4);

$$\int_0^E F(E'')\, dE'' = \int_0^E dE' F(E') + \int_0^{\bar{E}} S_I(E')\, dE' - \int_0^E S_A(E')\, dE' + \int_0^{U_1} dE' F(E') K(E', E) \,, \qquad \text{(E-5)}$$

or

$$\int_E^{U_1} dE' F(E') K(E', E) + \int_0^E S_I(E')\, dE' = \int_0^E S_A(E')\, dE' \qquad \text{(E-6)}$$

But the L.H.S. of equation (E-6) is exactly the definition of q(E); i.e. the rate that electrons slow down past energy E or appear at energies below E. From this;

$$q(E) = \int_0^E S_A(E')\, dE' \qquad \text{(E-7)}$$

However, above a certain energy E_1, recombination is not significant, so we obtain

$$q(E) = \int_0^{E_1} S_A(E')\, dE' \qquad \text{(E-8)}$$

and q(E) is not a function of E in this range. This value of q(E) represents the total number of electrons slowing down per unit volume and time and can be used to calculate the W-value of a gas. From equation (E-6)

$$q_0(E = U_1) = \int_0^{U_1} S_I(E')\,dE'$$

$$= \int_0^{U_1} dE' \int_{U_1}^{E_0} \Phi(E'')\,\Sigma_{IN}(E'' \rightarrow E')\,dE''$$

$$= \int_{U_1}^{E_0} dE''\,\Phi(E'')\,K(E'', U_1) \qquad \text{(E-9)}$$

where

$$K_{IN}(E'', U_1) = \int_0^{U_1} dE'\,\Sigma_{IN}(E'' \rightarrow E')$$

≡ number of electrons produced with energies below U_1 per unit $\Phi(E'')$ at E'' around dE''.

Using the previous notation for slowing-past kernels due to excitation and ionization, we can illustrate some of the $K_{in}(E'', U_1)$ in different energy ranges:

For $E'' \geq U_i + 2U_1$, after an ionization collision only one electron could have energy less than U_1. No excitation collision is going to result in slowing down an electron past energy U_1. In this case:

$$K_{IN}(E'', U_1) = K_I(E'', E'' - U_i) - K_I(E'', E'' - U_i - U_1) \qquad \text{(E-10)}$$

where $U_i = U$, the ionization potential.

Using similar lines of argument, we obtain

$U_i + 2U_1 \geq E'' \geq U_i + U_1$:

$$K_{IN}(E'', U_1) = K_I(E'', E'' - U_i) + K_I(E'', U_1) + K_I(E'', E'' - U_i - U_1), \qquad \text{(E-11)}$$

$U_1 + U_i \geq E'' \geq 2U_1$:

$$K_{IN}(E'', U_i) = 2K_I(E'', E''-U_i) \quad , \tag{E-12}$$

$2U_1 \geq E'' \geq U_i$:

$$K_{IN}(E'', U_i) = 2K_I(E'', E''-U_i) + K_{ex}(E'', E''-U_1) \quad , \tag{E-13}$$

$U_1 \geq E'' \geq U_i$:

$$K_{IN}(E'', U_i) = K_{ex}(E'', E''-U_1) \quad , \tag{E-14}$$

$U_1 \geq E''$:

$$K_{IN}(E'', U_i) = 0 \tag{E-15}$$

The above notation follows from the one level excitation model defined in Appendix D.

APPENDIX F

Diffusion Approximation for Electron Leakage

Instead of $f(\vec{r},\vec{u},t)$ in equation (II-1), consider an equivalent form $f(\vec{r},\hat{\Omega},E,t)$ where $f(\vec{r},\hat{\Omega},E,t)\, d\, dEd\Omega$ is the number of electrons at $\vec{r}$ in $d^3\vec{r}$ whose flight direction $\hat{\Omega}$ is in the differential solid angle $d\Omega$ around $\hat{\Omega}$ and whose energy is between E and E + dE. With the differential electron flux defined as:

$$\Phi(\vec{r},\hat{\Omega},E,t)\,d\Omega\,dE = f(\vec{r},\hat{\Omega},E,t)\,v\,d\Omega\,dE \qquad \text{(F-1)}$$

The Boltzmann equation [Equation (II-1)], in the absence of an external force field, becomes

$$\frac{1}{v}\frac{\partial}{\partial t}\Phi(\vec{r},\hat{\Omega},E,t) = -\hat{\Omega}\cdot\nabla\,\Phi(\vec{r},\hat{\Omega},E,t) - \Sigma_t(E)\,\Phi(\vec{r},\hat{\Omega},E,t)$$

$$+ \iint \Sigma_s(E'\to E,\hat{\Omega}'\to\hat{\Omega})\,\Phi(\vec{r},\hat{\Omega}',E',t)\,dE'd\Omega' + S(\vec{r},\hat{\Omega},E,t) \qquad \text{(F-2)}$$

where we have replaced the collision term by the last three terms. In equation (F-2) $\Sigma_t(E)$ is the total collision cross-section at energy E and $\Sigma_s(E' \to E,\ \hat{\Omega}' \to \hat{\Omega})$ is the cross-section for a process in which an electron with energy E' and the direction Ω' is scattered into the element of solid angle $d\Omega$ around $\hat{\Omega}$ and the energy interval dE at E. The term $S(r,\Omega,E,t)$ accounts for other primary or secondary electron sources. We assume rotational symmetry around a distribution axis arbitrarily defined as the x-axis. Then the steady state form of equation (F-2) becomes:

$$\cos\Theta\,\frac{\partial}{\partial x}\Phi(x,\hat{\Omega},E) + \Sigma_t(E)\,\Phi(x,\hat{\Omega},E) = \iint \Sigma_s(E'\to E,\hat{\Omega}'\to\hat{\Omega})\,\Phi(x,\hat{\Omega}',E')\,dE'd\Omega'$$

$$+ S(x,\hat{\Omega},E) \qquad \text{(F-3)}$$

We expand the angular dependence in Legendre polynomials, i.e.;

$$\Phi(x,\hat{\Omega},E) = \sum_{m=0}^{\infty} \frac{2m+1}{4\pi} \Phi_m(x,E) P_m(\cos\theta) \tag{F-4}$$

$$S(x,\hat{\Omega},E) = \sum_{m=0}^{\infty} \frac{2m+1}{4\pi} S_m(x,E) P_m(\cos\theta) \tag{F-5}$$

and

$$\Sigma_s(E'\to E, \hat{\Omega}'\to\hat{\Omega}) = \sum_{m=0}^{\infty} \frac{2m+1}{4\pi} \Sigma_{sm}(E',E) P_m(\cos\theta_0) \tag{F-6}$$

where $\cos\theta_0 = \hat{\Omega}'\cdot\hat{\Omega}$

By the addition theorem for Legendre polynomials, $P_m(\cos\theta_0)$ can be expressed in terms of $P_m^{\ell}(\cos\theta)$ and $P_m^{\ell}(\cos\theta')$ where the P_m^{ℓ} are the associated Legendre Polynomials. Performing the angular integral of equation (F-3) and using conventional orthogonal relations one arrives at the P_N approximation[44,42]:

$$(n+1)\frac{\partial}{\partial x}\Phi_{n+1}(x,E) + n\frac{\partial\Phi_{n-1}(x,E)}{\partial x} + (2n+1)\Sigma_t(x,E)\Phi_n(x,E) =$$
$$(2n+1)\int \Sigma_{sn}(x,E'\to E)\Phi_n(x,E')dE' + (2n+1)S_n(x,E)$$

$$n = 0,1,2,\ldots. \tag{F-7}$$

Truncating the equations with n = 1, we obtain the P_1 approximation or the diffusion equation. For a homogeneous medium, this becomes[62]:

$$-D(E)\nabla^2\Phi(\vec{r},E) + \Sigma_t(E)\Phi(\vec{r},E) = \int \Sigma_s(E'\to E)\Phi(\vec{r},E')dE' + S(\vec{r},E) \tag{F-8}$$

where

$$\Phi(r,E) = \int_{4\pi} \Phi(\vec{r},\hat{\Omega},E)\,d\Omega \quad ,$$

$$S(r,E) = \int_{4\pi} S(\vec{r},\hat{\Omega},E)\,d\Omega \quad ,$$

$$\Sigma_s(E' \to E) = \int_{4\pi} \Sigma_s(E' \to E, \hat{\Omega}_o)\, d\Omega_o$$

and

$$D(E) = \frac{1}{3(\Sigma_t(E) - \Sigma_s \overline{\cos\theta_o})} \qquad \text{(F-9)}$$

In the calculation, we have made the simplying assumption of isotropic scattering so the averaged cosine of the scattering angle vanishes. This form for the diffusion coefficient is only valid when the electron motion is not influenced by electric field forces. This restricts it to large electron kinetic energies and a small degree ionization. Furthermore, the diffusion equation (F-5) carries the usual restrictions for the validity of Fick's Law[62], one being that the size of the system be large relative to the mean free path of the electrons. For a 1-cm radius tube, this restricts the gas pressure to be, roughly, above one torr.

APPENDIX G

Energy Deposition Rate and Primary δ-Ray Energy Distribution by a Two Region Model in the Plasmas Created by Nuclear Radiation

Using a two-region model, J. Guyot[63] and G. Miley[64] have derived expression for the rate of energy deposition by heavy-charged particles in gaseous media. In the experiments performed by J. Guyot[13] and T. Ganley[57], laser tubes coated with B-10 were placed in the University of Illinois TRIGA Reactor. The pulsed neutron flux falls upon the boron coating inducing the nuclear reaction $n + B \rightarrow Li + \alpha$. The heavy-charged particles traverse the and deposite their energy as they slow down.

The geometry of the system and the heavy-charged particle reactions are shown in figure (G-1) where a slab geometry is used to approximate the cylinder. For $0 \leq x \leq x_{cut}$, the rate of energy deposition $R_i(x.T_o)$ at x for the i^{th} type of heavy-charged particle with initial energy T_o is:

$$R_i(x,t) = \frac{S(T_o)T_o}{2}\left[\frac{x\lambda(T_o)}{\lambda_g^2(T_o)} J(t_1^{n+1}, t_2^{n+1}) - \frac{\tau}{\lambda_g(T_o)} J(o, t_2^{n+1})\right] \tag{G-1}$$

and for $x_{cut} \leq x \leq \lambda_g(T_o)$,

$$R_i(x,t) = \frac{S(T_o)T_o}{2}\left[\frac{x\lambda(T_o)}{\lambda_g^2(T_o)} J(o, t_2^{n+1})\right] \tag{G-2}$$

where in (G-1), (G-2); $S(T_o)$ = source rate of heavy-charged particle

x = distance from the surface of coating

$x_{cut} = \lambda_g(T_o)(1 - \tau/\lambda(T_o))$

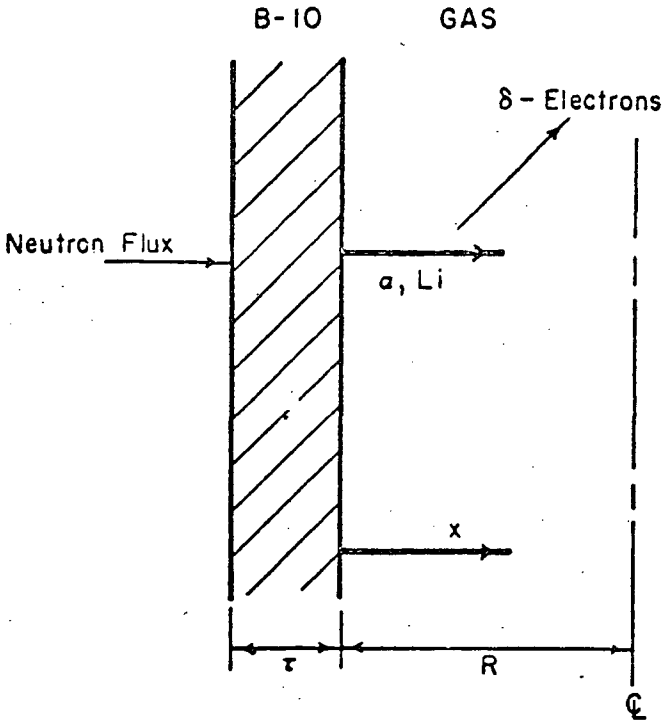

Figure G-1. Slab Geometry of the Source and Gaseous Medium Equivalent to the Actual Cylindrical Geometry

$\lambda(T_o)$ = range of heavy charged particle at T_o in the Boron Coating

$\lambda g(T_o)$ = range of heavy charged particle at T_o in the gas

τ = thickness of Boron region

$$J(u,v) = \int_u^v \frac{y^{\frac{1}{n+1}}}{(1-y)^2}\, dy$$

$$t_1 = \left(1 - x/\lambda_g(T_o)\right)^{1/n+1}$$

$$t_2 = \left(1 - \tau/\lambda(T_o) - x/\lambda_g(T_o)\right)$$

n = a fitting parameter for the slowing down and energy degradation.

For $n=0$, $J(u,v) = \left[\ell_g(1-y) - \frac{1}{1-y}\right]_u^v$

The following parameters are used in the calculation:

	T_o(MeV)	$\lambda g(T_o)$cm	$\lambda(T_o)$cm	n
α	1.459	2738.7/p	3.7×10^{-4}	0
Li	0.855	1240/p	10^{-4}	-0.25

and $S(T_o) = 450\ R\ \Phi/cm^3$ sec, where Φ is the neutron flux (cm^{-2}-sec^{-1}), R is the fraction of the type of heavy charged particles. For the production of 1.459 MeV α and 0.855 MeV Li, R = 92%. The coating thickness is 0.4 mg/cm^2.

Figure (G-2) shows the rate of energy deposition versus gas pressure at the center of the tube. The tube diameter is 2.54 cm and the neutron flux used is $\Phi = 5 \times 10^{13}$ cm^{-2} sec^{-1}. The rise in energy deposition rate as pressure increases is because of the increased slowing down efficiency as gas pressure is increased. This reaches a maximum at $\sim$ 550 torr because fewer heavy-charged particles can reach at the centerline as pressure goes higher.

The heavy-charged particle flux spectrum $F_i(x,T,T_o)$ for the i^{th} type heavy charged particle with initial kinetic energy T_o at x with kinetic energy T is given by: (133 ff. ref [64])

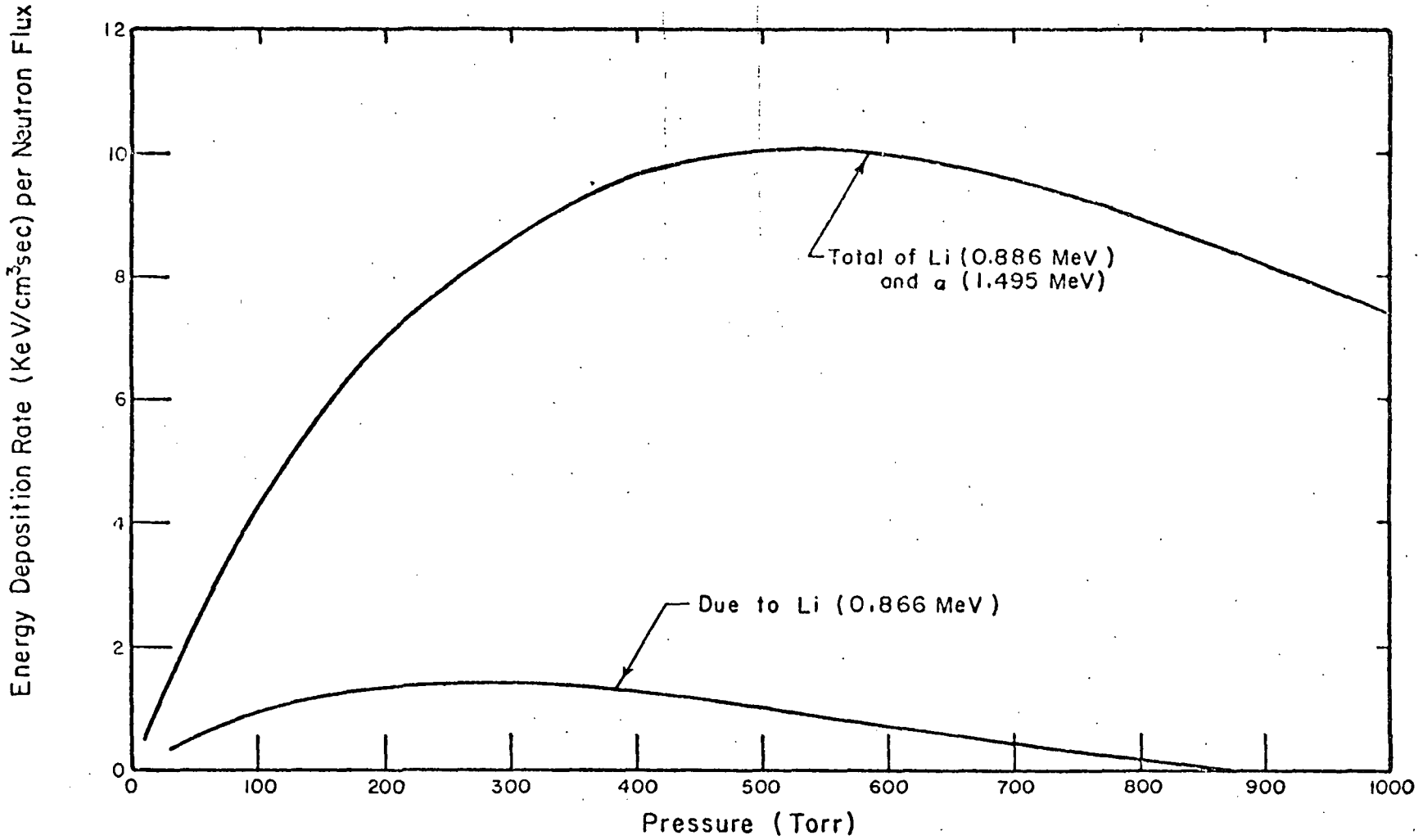

Figure G-2. Heavy-Charged Particle Energy Deposition Rate at the Center-line of the Tube

$$F_i(z,\epsilon,T_o) = \begin{cases} \dfrac{S(T_o)\tau\,(n+1)\epsilon^n}{zT_o\,(1-\epsilon^{n+1})} & \text{for } 0 \le z \le z_{crit},\ 0 \le \epsilon \le \epsilon_{crit} \\ \dfrac{S(T_o)\tau\,(n+1)\epsilon^n}{zT_o\,S}\left[1-\dfrac{z}{1-\epsilon^{n+1}}\right] & \text{for } 0 \le z \le z_{crit},\ \epsilon_{crit} \le \epsilon \le \epsilon_{max} \text{ or } z_{crit} \le z \le 1,\ 0 \le \epsilon \le \epsilon_{max} \end{cases} \tag{G-3}$$

where $\epsilon = T/T_o$, $z = x/\lambda g(T_o)$, $S = \tau/\lambda_c(T_o)$

$\epsilon_{max} = (1-z)^{1/n+1}$

$\epsilon_{crit} = (1-S-z)^{1/n+1}$

$z_{crit} = (1-S)$

The primary δ-ray electrons are created by the passage of this flux through the gas. The spatial and energy distribution of these primary δ-electrons is related to the i^{th} type heavy charged particle flux by:

$$n_i(x,E-U) = \int_{T_{thres,i}}^{T_o} F_i(x,T,T_o)\Sigma_i(T,E)\,dT \tag{G-4}$$

where $T_{thres.i}$ is the minimum kinetic energy for the i^{th} type heavy-charged particle to ionize and $\Sigma_i(E,T)$ is the probability per unit flux that a particle with energy between T and T + dT will lose an amount of kinetic energy between E and E + dE through ionization. Finally, U is the ionization potential of the gas atoms. Employing the formulation derived by M. Gryzinski for $\Sigma_i(T,E)$ and $T_{thres,i}$ (equations (6) and (8) of reference [23]), $n_i(x,E)$ has been solved for x = centerline of the tube at 1.27 cm and for 1.495 MeV α and 0.855 MeV Li ions which account for 92% of the heavy charged particles produced in the neutron irradiation of boron. Figure (G-3) shows the primary δ-electron production rate, per unit neutron flux, as a function of energy in 10 torr helium.

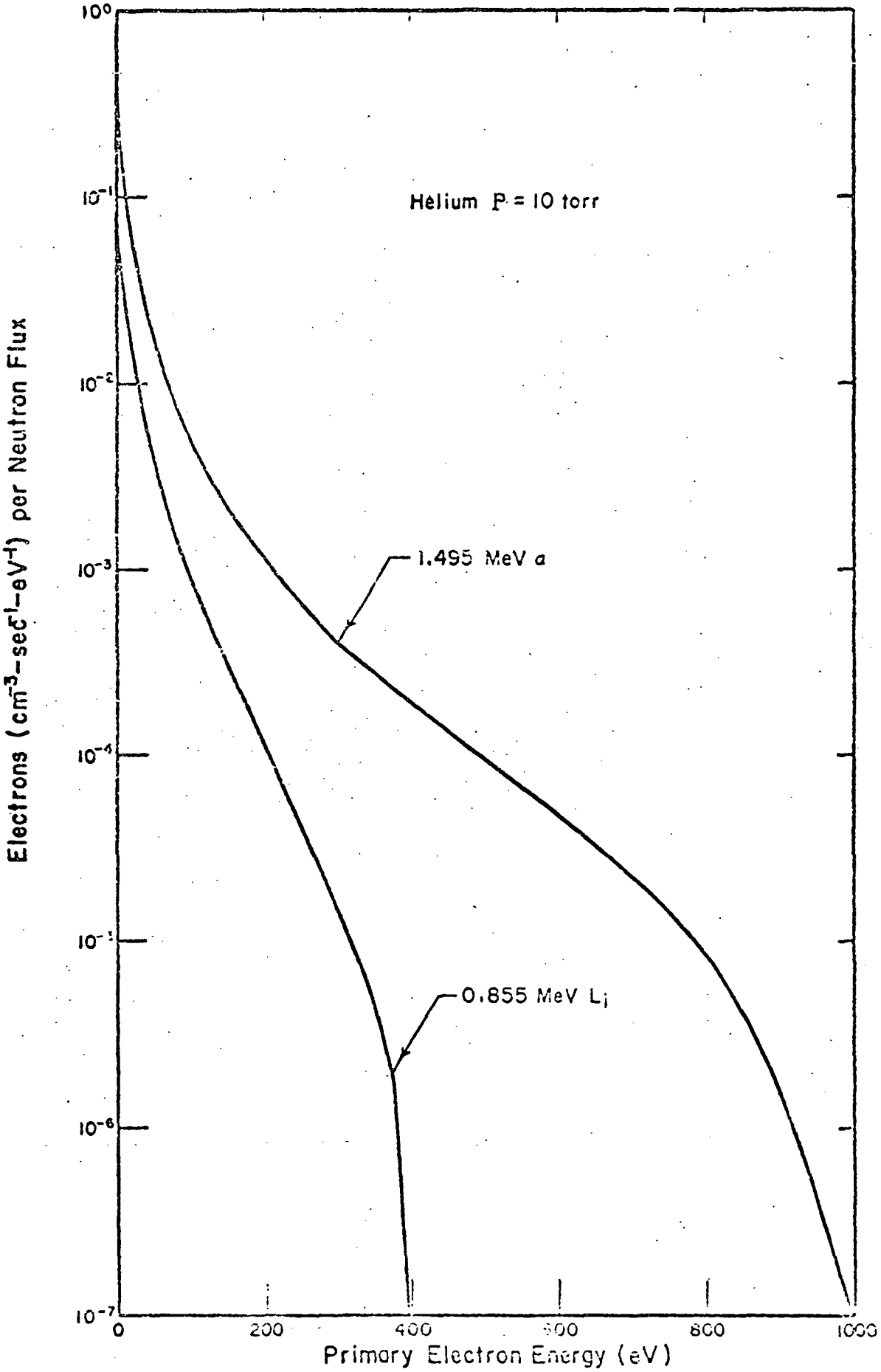

Figure G-3 Primary Electron Production Rate as a Function of Energy at the Center of Tube

The total electron density is determined by a balance of the source due to the heavy-charged particles and the losses due to recombination and leakage. The main body of electrons is assumed to be thermalized and the losses are mainly due to the recombination and diffusion leakage of thermal electrons. With this assumption, the thermal diffusion coefficient is taken to be the ambipolar diffusion coefficient. For a 1/U recombination cross-section, with only one species of ions present, the steady state electron density, n_e, is simply:

$$n_e = \frac{-D_a/\Lambda^2 + \sqrt{(D_a/\Lambda^2)^2 + 4\frac{R}{W}\alpha_R}}{2\alpha_R} \qquad \text{(G-5)}$$

where D_a = ambipolar diffusion coefficient

R = rate of energy deposition by heavy charged particle slowing down

α_R = recombination coefficient

w = energy deposition for each ion-pair production

Λ = first fundamental mode characteristic length of system

However, if molecular ion formation by three body collision is included, electron recombination is predominantly with the molecular ion. Then the electron density becomes:

$$n_e = -\frac{S_e}{2a} - \frac{D_2^+}{2\Lambda^2\alpha_R} + \left[\eta\frac{S_e}{a\alpha_R} + \frac{D_2^+ S_e}{\Lambda^2 a\alpha_R} + \left(\frac{S_e}{2a} + \frac{D_2^+}{2\Lambda^2\alpha_R}\right)^2\right]^{1/2} \qquad \text{(G-6)}$$

where $a = \frac{D_1^+}{\Lambda^2} + \eta$

$S_e = R/w$ = rate of electron production/volume [cm^{-3}-sec^{-1}]

D_1^+, D_2^+ = ambipolar diffusion coefficients for the atomic ions and molecular ions, respectively [cm^2/sec]

η = coefficient of molecular ion formation through three body collisions [1/sec]

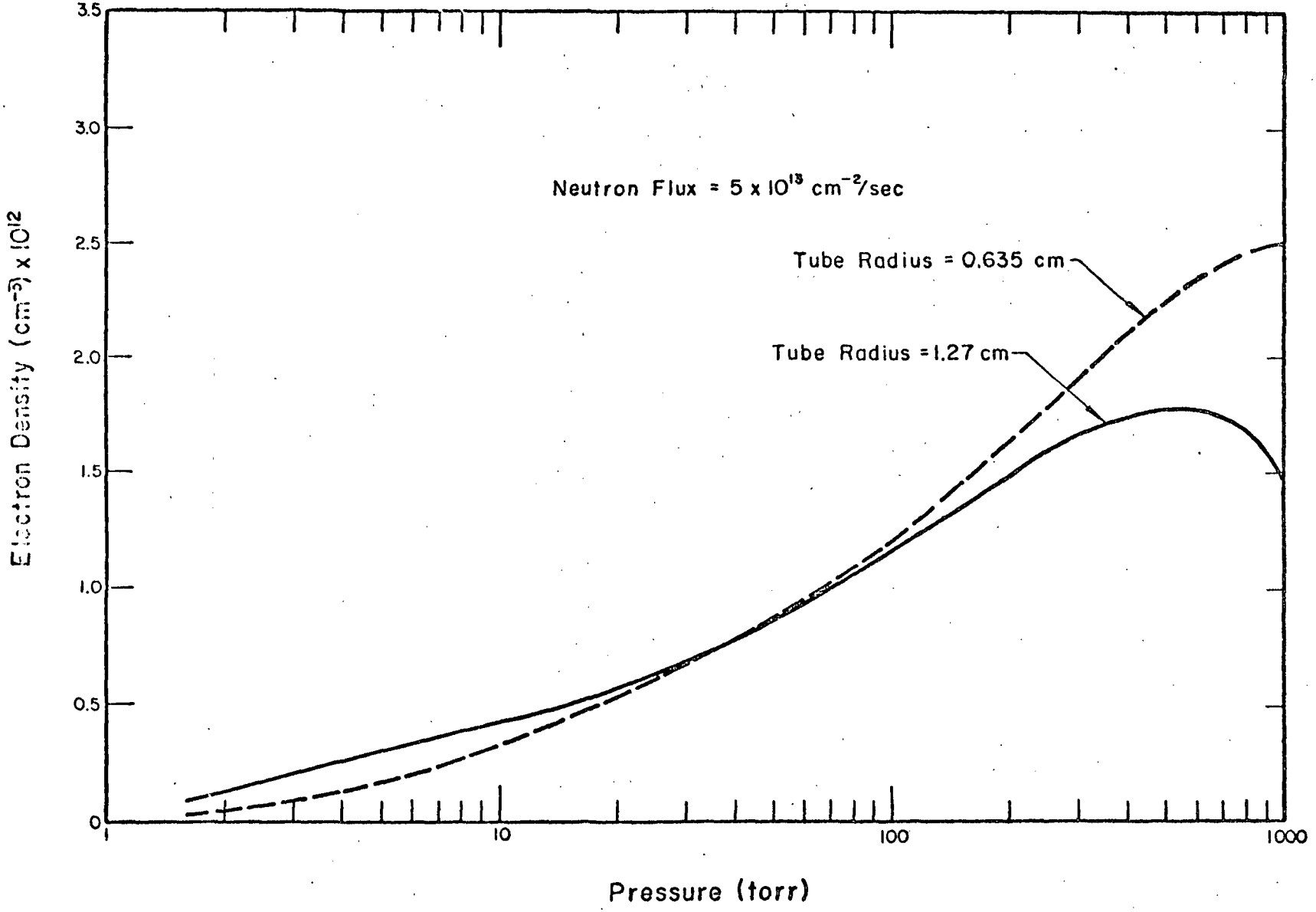

Figure G-4 Electron Density vs Pressure at the Center of Tube for Tube Radii = 0.635, 1.27 cm and a Neutron Flux of 5 x 10^{13} cm^{-2}-sec^{-1}

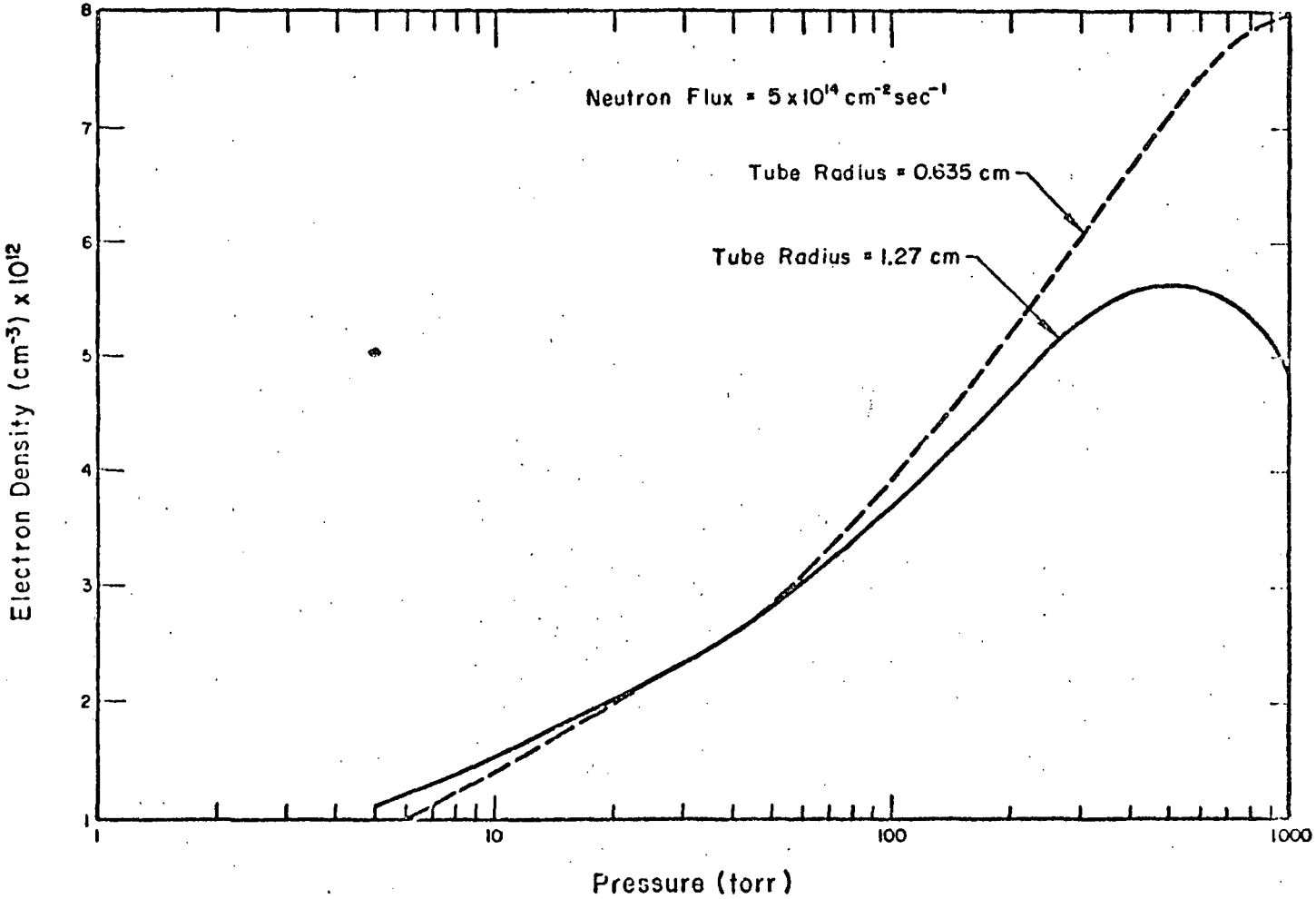

Figure G-5. Electron Density vs. Pressure at the Center of Tube for Tube Radii = 0.635, 1.27 cm and a Neutron Flux of 5 x 10^{14} cm^{-2}-sec^{-1}

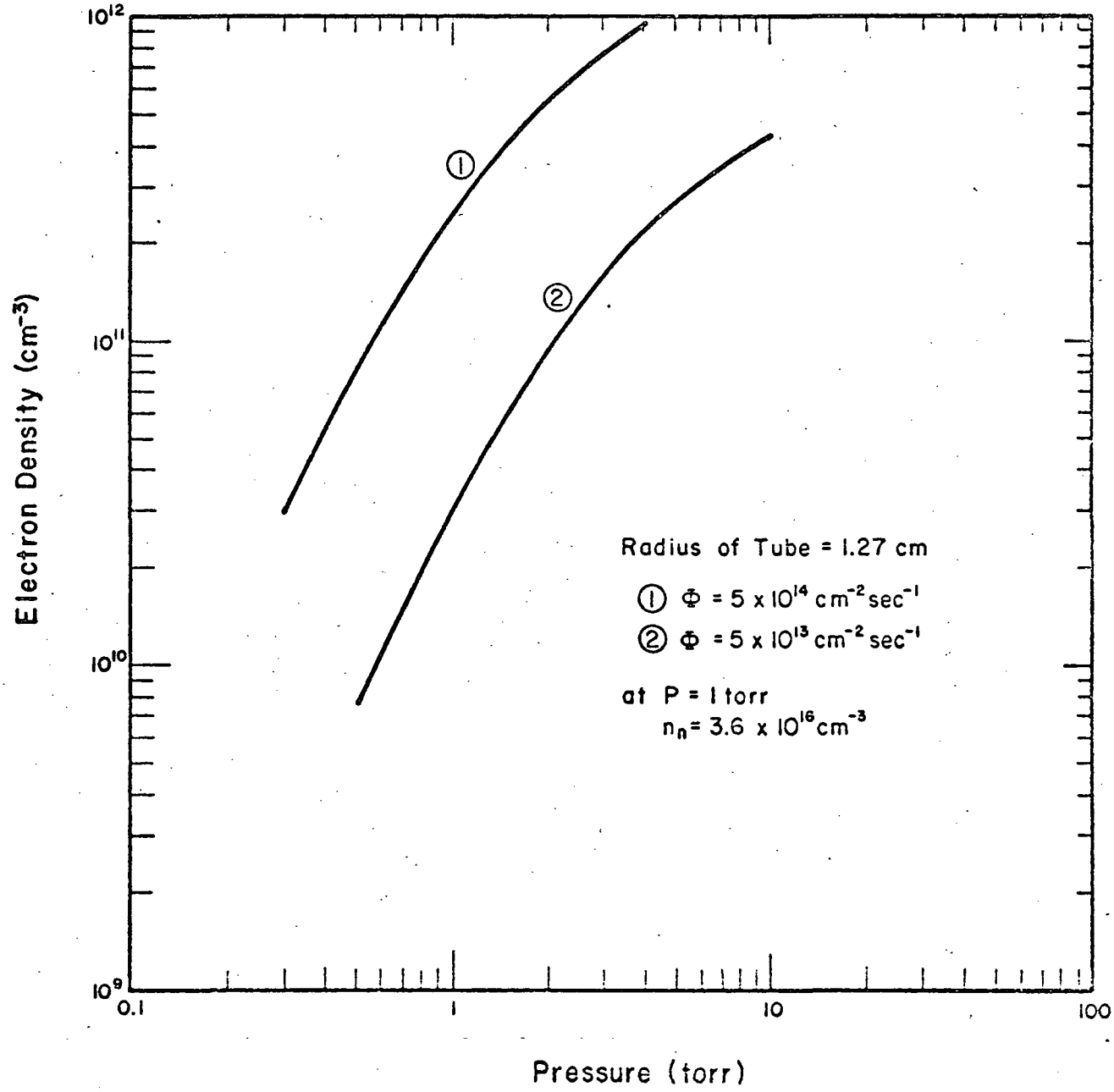

Figure G-6. Comparison of Electron Densities Below 5 Torr for Neutron Fluxes 5 x 10^{13} and 5 x 10^{14} -2 $-sec^{-1}$

Equation (G-6) has been evaluated using the coefficients given in references [49], [50] and [63] and the resulting electron density vs. pressure for several tube sizes and neutron flux densities is illustrated in Figures (G-4) - (G-6). The densities shown are for the centerline of the tube. The cross-over of the curves at about 30 torr is due to the balance between leakage and energy deposition rate. The peak electron density occurs at about 550 torr because higher pressures reduce the number of heavy-charged particles reaching the centerline.

The addition of a distributed primary source S(E) in the low energy region makes equation (III-10) inhomogeneous; namely:

$$-D(E)\nabla^2\psi(E) + \Sigma_r(E)\psi(E) = \tfrac{3}{2}\Sigma_s\left[(2kT-E)\frac{d\psi(E)}{dE} + EkT\frac{d^2\psi(E)}{dE^2}\right] + \frac{S(E)}{M(E)} \qquad \text{(G-7)}$$

A series solution $\Phi(y)$ for equation (III-10) was given earlier in equation (III-15). [A second independent homogeneous solution, $\Phi_2(y)$, given by De Sabre (equation (8) of Ref. 65) was discarded by Horwitz et al.[43] because it gives negative slowing down density at y = 0.] A particular solution to equation (G-7) can be found by the method of variation of parameters from the two homogeneous solutions. This method gives:

$$\Phi_p(y) = \int_0^y \frac{S_1(x)\left[\Phi_1(x)\Phi_2(y) - \Phi_2(x)\Phi_1(y)\right]}{\Phi_1(x)\Phi_2'(x) - \Phi_2(x)\Phi_1'(x)}\,dx \qquad \text{(G-8)}$$

where $S_1(x) = S(x)/\tfrac{3}{2}\Sigma_s EkT$.

Equation (G-8) has been evaluated numerically, the particular solution added to the homogeneous solution, $\Phi_1(y)$, and the entire distribution normalized. Notice that as $y \to 0$, $\Phi_p(y) = 0$ and $\Phi_2(y)$ again has a zero coefficient. Results are presented in figures (G-7) and (G-8) along with a plot of the distribution for the homogeneous case. It is seen that for

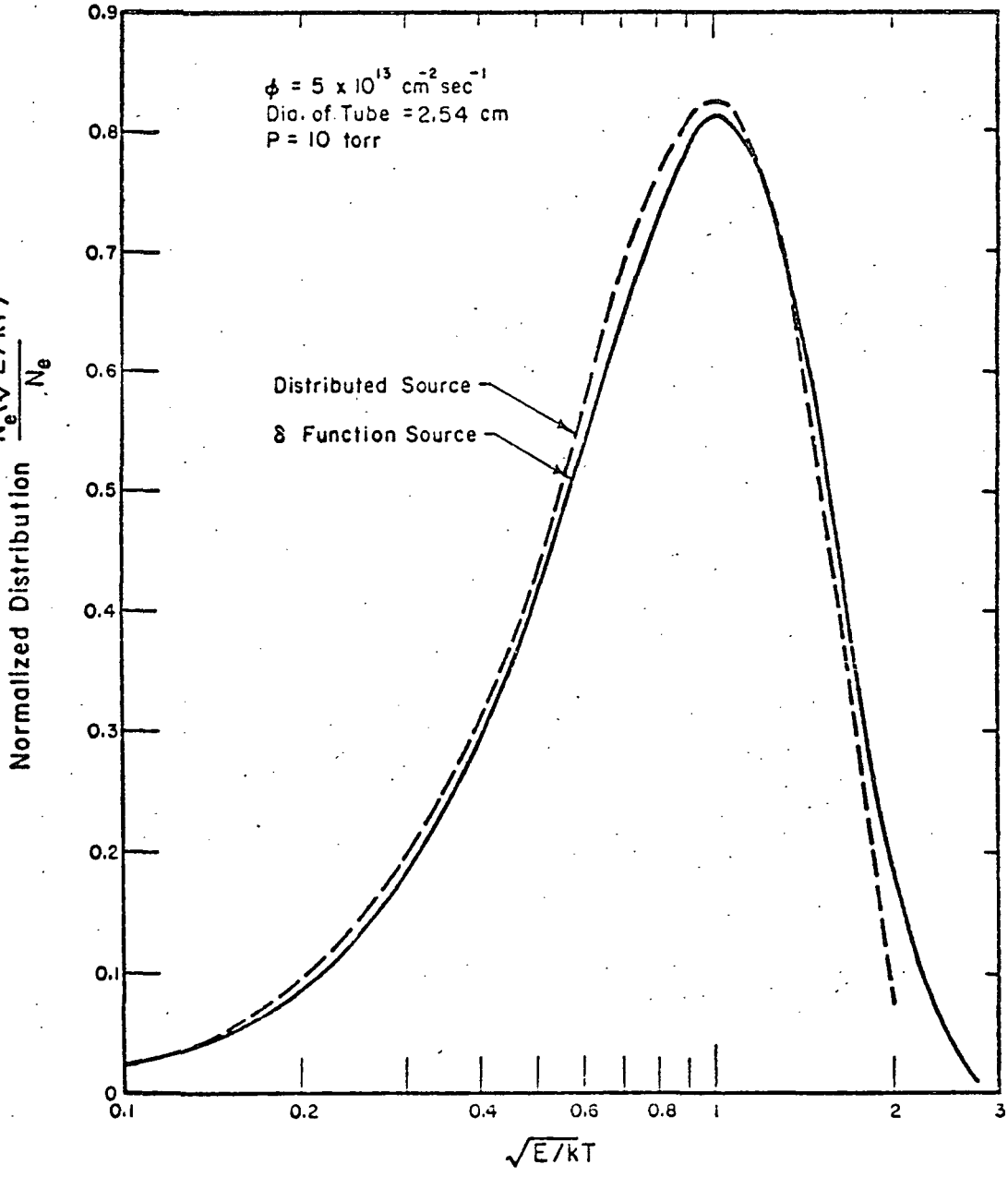

Figure G-7. Comparison of Electron Distributions for a δ-function Source and a Distributed Source

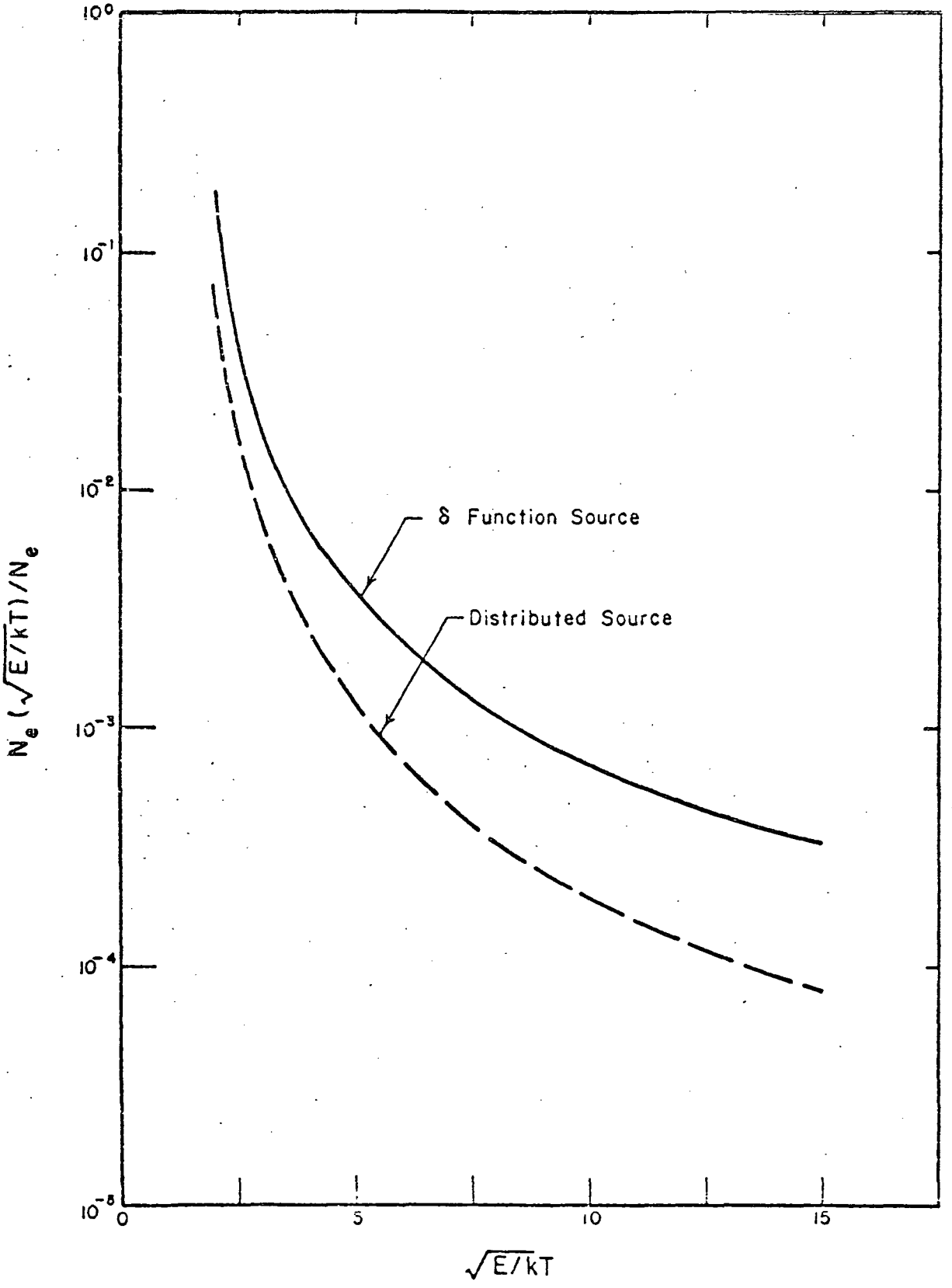

Figure G-8. Comparison of Electron Distributions for a δ-function Source and a Distributed Source

low energies where the electron population is high, the deviation is insignificant. For higher energies, where the population is already small, the difference is about a factor of three.

APPENDIX H

Series Solution of the Thermalization Equation With Recombination and Leakage

With the notation of Chapter III, the thermalization equation, including the second moment of $\overline{\Delta E}$, becomes:

$$-D(E)\nabla^2\psi(E) + \Sigma_r(E)\psi(E) = \tfrac{1}{3}\Sigma_s(E)\left[(2kT-E)\frac{d}{dE}\psi(E) + EkT\frac{d^2}{dE^2}\psi(E)\right] \tag{H-1}$$

with $\Phi(E) = \psi(E)M(E)$,

$$\frac{d\psi(E)}{dE} = \frac{\Phi(E)}{M(E)}\left[\frac{1}{kT} - \frac{1}{E}\right] + \frac{1}{M(E)}\frac{d}{dE}\Phi(E) \tag{H-2}$$

$$\frac{d^2\psi(E)}{dE^2} = \frac{1}{E^2}\frac{\Phi(E)}{M(E)} + \left(\frac{1}{kT} - \frac{1}{E}\right)\left[\frac{2}{M(E)}\frac{d\Phi(E)}{dE} + \left(\frac{1}{kT} - \frac{1}{E}\right)\frac{\Phi(E)}{M(E)}\right] + \frac{1}{M(E)}\frac{d^2}{dE^2}\Phi(E) \tag{H-3}$$

From equations (H-1), (H-2) and (H-3), we obtain

$$-D(E)\nabla^2\Phi(E) + \Sigma_r(E)\Phi(E) = \tfrac{1}{3}\Sigma_s(E)\left[\Phi(E) + E\frac{d}{dE}\Phi(E) + EkT\frac{d^2}{dE^2}\Phi(E)\right] \tag{H-4}$$

To change this result into the variable y, where $y = \sqrt{E/kT}$, we note that:

$$\frac{d}{dE} = \frac{1}{2kT}\frac{1}{y}\frac{d}{dy} \quad , \text{ and } \quad \frac{d^2}{dE^2} = \left(\frac{1}{2kT}\right)^2\frac{1}{y^2}\frac{d^2}{dy^2} - \left(\frac{1}{2kT}\right)^2\frac{1}{y^3}\frac{d}{dy} \, , \tag{H-5}$$

and with these relations, equation (H-4) may be written as:

$$y\frac{d^2\Phi(y)}{dy^2} - [1-2y^2]\frac{d}{dy}\Phi(y) + [4y - gy - \Delta]\Phi(y) = 0 \tag{H-6}$$

where g and Δ are defined in the text. The solution for the special case of

no leakage or recombination, with the boundary condition $\Phi(y) = 0$ at $y = 0$ is c $y^2e^{-y^2}$; i.e. a Maxwellian distribution. We can use this to find a correction factor S(y) applicable to the general case. If one lets $\Phi(y) = y^2e^{-y^2}S(y)$, the differentials of $\Phi(y)$ with respect to y are:

$$\Phi'(y) = e^{-y^2}\left[2yS(y) - 2y^3S(y) + y^2S'(y)\right] \tag{H-7}$$

$$\Phi''(y) = e^{-y^2}\left[S(y)(2 - 10y^2 + 4y^4) + S'(y)(4y - 4y^3) + S''(y)y^2\right] \tag{H-8}$$

The differential equation for the series S(y) from equations (H-6) to (H-8) is:

$$yS''(y) + [3 - 2y^2]S'(y) - S(y)[4 + 9y] = 0 \tag{H-9}$$

Writing out equation (H-9) in terms of the series $S(y) = \sum_{n=0}^{\infty} A_n y^n$ we obtain:

$$\sum_{l=2}^{\infty} A_l\, l(l-1)\, y^{l-1} + 3\sum_{j=1}^{\infty} A_j\, j\, y^{j-1} - 2\sum_{j=1}^{\infty} A_j\, j\, y^{j+1} = -4\sum_{n=0}^{\infty} A_n y^n - 9\sum_{n=0}^{\infty} A_n y^{n+1} = 0 \tag{H-10}$$

The coefficients of (H-10) are seen to be:

$$A_l = \frac{1}{l(l+2)}\left[2(l - 2 + 9/2)\, A_{l-2} + \Delta A_{l-1}\right] \tag{H-11}$$

With the normalization such that $\int_0^{\infty} \Phi(y)\, dy = 1$, the first five coefficients of A_l are:

$$A_0 = 4/\sqrt{\pi}\ , \quad A_1 = \frac{\Delta}{3}A_0\ , \quad A_2 = \frac{A_0}{8}\left[9 + \frac{\Delta^2}{3}\right]$$

$$A_3 = \frac{A_0}{15}\left[2\left(1 + \frac{9}{2}\right)\Delta/3 + 9\Delta/8 + \Delta^3/3\right]\ ,$$

and

$$A_4 = \frac{A_0}{24}\left[(4+9)\tfrac{1}{8}\left(9 + \tfrac{\Delta^2}{3}\right) + \tfrac{2}{15}\left(1 + \tfrac{9}{2}\right)\tfrac{\Delta^2}{2} + \tfrac{9\Delta^2}{8} + \tfrac{\Delta^4}{3}\right] \tag{H-12}$$

Collecting terms of order 1, Δ, g, Δ^2, g^2 and Δg; for Δ, $g \ll 1$; we can write S(y) as:

$$S(y) = A_0 [1 + g\eta_1(y) + g^2 \eta_2(y) + \Delta\mu_1(y) + \Delta^2\mu_2(y) + \Delta g \chi(y)] \quad \text{(H-13)}$$

The series with first order in g appears only with even powers of y;

$$\eta_1(y) = \sum_{n=1}^{\infty} b_{2n} y^{2n} \quad , \quad b_{2n} = b_{2(n-1)} \frac{n-1}{n(n+1)} \quad , \quad b_2 = 1/8$$

i.e.

$$\eta_1(y) = \frac{1}{8} y^2 + \frac{1}{6\cdot 8} y^4 + \frac{1}{6\cdot 6\cdot 8} y^6 + \frac{1}{4\cdot 6\cdot 8\cdot 10} y^8 + \cdots \quad \text{(H-13)}$$

The series with second order in g appears only after y^4 and appears only in even powers of y:

$$\eta_2(y) = \sum_{n=1}^{\infty} d_{2(n+1)} y^{2(n+1)} \quad \text{(H-14)}$$

where $$d_{2(n+1)} = \frac{1}{(2n+2)(2n+4)} [2(2n) d_{2n} + b_{2n}]$$

and $$d_4 = 1/4\cdot 6\cdot 8$$

This gives $$d_6 = 1/6\cdot 8 [8/4\cdot 6\cdot 8 + 1/6\cdot 8] \quad , \quad d_8 = 1/6\cdot 8 [1/6\cdot 8 (\tfrac{1}{4\cdot 6} + \tfrac{1}{6\cdot 8})]$$

The series with first and second order in Δ have been developed by Cohen [66] and they are given as:

$$\mu_1(y) = \sum_{n=0}^{\infty} \frac{y^{2n+1}}{(2n+1)\,\Gamma(n+5/2)} \quad \text{(H-15)}$$

and

$$\mu_2(y) = \frac{1}{4} \sum_{n=1}^{\infty} \frac{y^{2n}}{n(n+1)!} \left[\sum_{k=0}^{n-1} \frac{(k+1)!}{(2k+1)\,\Gamma(k+5/2)} \right] \quad \text{(H-16)}$$

The series with terms in order of Δg starts with y^3 and appears only for odd powers of y. The coefficients of this series are:

$$\chi(y) = \frac{1}{2} \left(\frac{1}{3} - \frac{1}{8}\right) \sum_{n=1}^{\infty} e_{2n+1} y^{2n+1}$$

where $$e_{2n+1} = e_{2n-1} \left[\frac{2(2n-1)}{(2n+1)(2n+3)} \right] \quad , \quad e_1 = 1. \quad \text{(H-17)}$$

The first few terms of e_{2n+1} are; $e_3 = \frac{1}{2}\left(\frac{1}{3}+\frac{1}{8}\right)\left(\frac{2}{3\cdot5}\right)$

$$e_5 = \frac{1}{2}\left(\frac{1}{3}+\frac{1}{8}\right)\left(\frac{2}{3\cdot5}\right)\left(\frac{2\cdot3}{5\cdot7}\right), \quad e_7 = \frac{1}{2}\left(\frac{1}{3}+\frac{1}{8}\right)\left(\frac{2}{3\cdot5}\right)\left(\frac{2\cdot3}{5\cdot7}\right)\left(\frac{2\cdot5}{7\cdot9}\right)$$

These series converge rather rapidly for $y \leq 5$. For larger values of y, the series is given as an inverse power polynomial of y. As it converges rapidly for large y, the series need not be broken into orders of g and Δ. De Sabrino et al[63] give two independent asymptotic series for large y:

$$\Psi_1(y) = y^{-9/2} \sum_{n=0}^{\infty} C_n y^{-n}$$

with

$$C_0 = \Delta/2 \quad , \quad C_1 = (\Delta/2)^2$$

$$C_n = \frac{\Delta C_{n-1}}{2n} - \frac{(9/2 + n - 2)(9/2 + n - 4)}{2n} C_{n-2} \qquad \text{(H-18)}$$

and

$$\Psi_2(y) = y^{-9/2-4}\, e^{y^2} \sum_{n=0}^{\infty} d_n y^{-n}$$

with

$$d_0 = \Delta/2 \quad , \quad d_1 = -(\Delta/2)^2$$

$$d_n = -\frac{\Delta d_{n-1}}{2} + \frac{(n+2-9/2)(n-9/2)}{2n} d_{n-2} \qquad \text{(H-19)}$$

The series $\psi_1(y)$ is damped by the Maxwellian factor; $\Phi(y) = y^2 e^{-y^2} \psi_1(y)$ and it becomes negligibly small because of the exponential factor. The asymptotic solution for equation (H-6) is, therefore:

$$\Phi(y) = y^{-2+9/2} \sum_{n=0}^{\infty} d_n y^{-n} \qquad \text{(H-20)}$$

APPENDIX I

Effect of Electric Field on High Energy Electrons During Slowing Down

Consider an electron above the ionization energy of helium in an electric field E eV/cm. The drift velocity u_e, due to the field is (pg. 122 of ref.[51])

$$m_e \frac{d}{dt} v_e = eE \qquad \text{or} \qquad v_e \simeq \frac{eE}{m_e}\tau \tag{I-1}$$

where τ is the mean collision time. The electrons drift distance in the direction of the field in this time is $\frac{eE\tau^2}{m_e}$, and they acquire an energy ΔT given by:

$$\Delta T = \frac{eE^2\tau^2}{m_e} = \frac{eE^2}{m_e c^2 \Sigma_i^2} \tag{I-2}$$

where Σ_i is the macroscopic inelastic cross-section and c the random speed of the electron. Consider two extreme cases of 1 Kev and 30 eV electrons in helium at 1 Torr with an electric field of 10 V-cm^{-1}. For 1 Kev, $\Sigma \simeq 0.5$ cm^{-1} (pg. 63 of ref.[51]) and $\Delta T \simeq 0.2$ eV. For a 30 eV electron, $\Sigma \simeq 3$ cm^{-1} and $\Delta T \simeq 0.3$ eV. The loss of energy due to an inelastic collision, however, is larger than 20 eV. For higher pressures, the gain in energy due to the drift in electric field is even less because $\Delta T \sim 1/\Sigma^2 \sim 1/p^2$. After an inelastic collision, the electron emerges in random directions. The drift in the electric field has to be started anew. As illustrated above, the gain in energy from the field between two inelastic collisions, for both of those extreme energies, are less than 1 eV. It is concluded that the energy gain in the field can be neglected compared to the energy losses for electrons with energies above the ionization energy. This, however, is limited to moderate electric fields of 10 V-cm^{-1} or less.

APPENDIX J

Discussion of the Equation for the Distrubtion Function in an Electric Field

Various authors[1],[2],[3] have used different forms of the equations for the two term expansion $f_0(\bar{u})$ and $\bar{f}_1(\bar{u})$ of the distribution function in an electric field. Chapman and Cowling [67] give the coupled equation for f_o and f_1 in velocity space as:

$$\frac{e\vec{E}\cdot\vec{c}}{m_e c}\frac{\partial f_o(c)}{\partial c} = -\frac{e\vec{E}\cdot\vec{c}\, f_1(c)}{m_e\, \ell(c)} - \beta\frac{e\vec{E}}{m_e}\cdot\vec{c}\, f_1(c) \qquad \text{(J-1)}$$

$$\left(\frac{eE}{m_e}\right)^2\left[f_1(c) + \frac{c}{3}\frac{\partial f_o}{\partial c}\right] = \left(\frac{\delta f_o}{\delta t}\right)_c \qquad \text{(J-2)}$$

with

$$f_o(c) = f_o(\vec{c})$$
$$f_1(c) = \vec{f}_1(\vec{c})\cdot\frac{\vec{c}}{c}$$
$$\ell(c) = c/\nu_c(c)$$

where $f_o(\vec{c})$, $\vec{f}_1(\vec{c})$, β and $\nu_c(c)$ are defined in chapter IV and the leakage term has been neglected. Without recombination Equation (J-1) becomes:

$$-\frac{eE}{m_e}\frac{d}{dc}f_o(\vec{c}) = -\nu_c(c)\,\vec{f}_1(c) \qquad \text{(J-3)}$$

and the LHS of equation (J-2) is:

$$\frac{1}{3}\left(\frac{eE}{m_e}\right)^2\left[3c^2 f_1(c) + c^3\frac{d}{dc}f_1(c)\right]$$
$$= \frac{1}{3c^2}\frac{d}{dc}\left[c^2\left(\frac{e\vec{E}}{m_e}\right)\cdot\vec{f}_1(\vec{c})\right] \qquad \text{(J-4)}$$

With $\nu_c(c)$ expressed as $\sum_j N_j c Q_j(c)$ where j denotes the type of molecules, N_j the density and Q_j the momentum transfer cross section; Nigham[3] arrives at a set of coupled equations:

$$-\frac{e\vec{E}}{3mv^2}\cdot\frac{d}{dv}\left(v^2\vec{f}_1(v)\right)=\left(\frac{\delta f_0}{\delta t}\right)_c \tag{J-5}$$

$$-\frac{e\vec{E}}{m}\frac{d}{dv}f_0(v)=-\sum_j N_j Q_{ej}(v)\,v\,\vec{f}_1(v) \tag{J-6}$$

Combining (J-5) and (J-6) and changing the variable u to $w=\frac{mu^2}{2e}$, with $\frac{d}{du}=\frac{um}{e}\frac{d}{dw}$, Nigham obtains the following working equation:

$$-\frac{E^2}{3}\frac{d}{dw}\left[w\frac{d}{dw}f^0(w)\Big/\sum N_j Q_{ej}(w)\right]=\left(\frac{\delta f_0}{\delta t}\right)_c\frac{m}{2e}u \tag{J-7}$$

However, if recombination is included, equation (J-1) becomes

$$f_1(c)=-\left[\frac{\ell(c)}{c^2+\beta c\,\ell(c)}\right]\frac{\partial f_0}{\partial c} \tag{J-8}$$

and equation (J-2) is given by Chapman[67] as:

$$\frac{1}{3}\left(\frac{eE}{m_e}\right)^2 c^3 f_1(c)=\frac{kT}{M\ell(c)}\frac{\partial f_0}{\partial c}+\frac{mc^4}{M\ell(c)}f_0+\int_0^c(\alpha-\beta f_0)c^2\,dc \tag{J-9}$$

where unlike in Nigham's case, ionization sources, recombination and the kT term have now been included. Combining equations (J-8) and (J-9) and assuming $\beta\,\ell(c) \ll c$, we find:

$$-\left[\frac{1}{3}F^2 c\,\ell(c)+\frac{kT}{M\ell(c)}\right]\frac{\partial f_0(c)}{\partial c}-\frac{mc^4}{M\ell(c)}f_0(c)=\int_0^c(\alpha-\beta f_0)c^2\,dc \tag{J-9}$$

Then, after a formal integration, equation (IV-6) of chapter IV is obtained.

LIST OF REFERENCES

1. T. Holstein, "Energy Distribution of Electrons in High Frequency Gas Discharge," Phys. Rev. 70, 367 (1949).

2. M. J. Druyvestyen and F. M. Penning, "The Mechanism of Electrical Discharges in Gases of Low Pressure," Rev. Mod. Phys., 12, 87, (1940).

3. W. L. Nighan, "Electron Energy Distributions and Collision Rates in Electrically Excited N_2, CO and CO_2," Phys. Rev., 2A, 1989, (1970).

4. V. Fano, "Degradation and Range Staggling of High-En rgy Radiation," Phys. Rev. 92, 328,(1953).

5. R. T. McGinnies, "Energy Spectrum Resulting From Electron Slowing Down," Cir. 597, National Bureau of Standards, Washington, D.C., (1959).

6. G. R. Russell, "Feasibility of a Nuclear Laser Excited by Fission Fragments Produced in a Pulsed Nuclear Reactor," Trans. Symposium on Res. on Uranium Plasmas and Their Tech. Appl., University of Florida, Gainesville, (1970).

7. D. R. Rees, C. B. Leffert and D. J. Rose, "Electron Density in Mixed Gas Plasmas Created by Fission Fragments," J. Appl. Phys., 40, 1884, (1969).

8. K. Thom and R. Schneider, "Nuclear Pumped Lasers," AIAA, 10, 400, (1972). Also J. C. Guyot, G. H. Miley, J. T. Verdeyen, and T. Ganley, "On Gas Pumping via Nuclear Radiations," in Research on Uranium Plasmas and Their Technological Applications, NASA SP-236, NASA, Washington, D.C., (1970).

9. N. Krascella, "Analytical Study of the Spectral Radiant Flux Emitted From the Fuel Region of a Nuclear Light Bulb Engine," U.A.R.L. Report J-910904-1, (1970).

10. E. P. Muntz, "The Electron Beam Fluorescence Technique," NATO Report, AD-692-860, (1968).

11. J. T. Ganley, J. Verdeyen and G. Miley, "Enhancement of Co_2 Laser Power and Efficiency by Neutron Irradiation," App. Phys. Lett., 18, 568, (1971).

12. J. C. Guyot, G. Miley and J. Verdeyen, "Metastable Densities in Noble-Gas Plasmas Created by Nuclear Radiations," J. App. Phys., 42, 5379, (1971).

13. J. C. Guyot, "Measurements of Atomic Metastable Densities in Noble Gas Plasmas Created by Nuclear Irradiations," Ph.D. Thesis, University of Illinois, (1970).

14. B. Wang, G. Miley, "Monte Carlo Simulation of Radiation-Induced Plasmas", Trans. Am. Nucl. Soc. 15, No. 2, (1972).

15. B. Wang, "Monte Carlo Simulation of Non-linear Radiation Induced Plasma," Ph.D. Thesis, Dept. of Computer Science, Univ. of Illinois, Urbana, Illinois, (1972).

16. L. V. Spencer and V. Fano, "Energy Spectrum Resulting From Electron Slowing Down," Phys. Rev. 93, 1172 (1954).

17. L. F. Miller, R. E. Faw, "Effects of Radiation Quality on the Radiolysis of Water," Sp. Report #66, Kansas State Univ., Manhattan, Kansas, (1966).

18. C. Möller, "Über den Stoss zweier Teilchen unter Berücksichtigung der Retardation der Krafte," Zeit F. Phys. 70, 786, (1931).

19. L. Vriens, "Binary-Encounter Electron-Atom Collision Theory," Phys. Rev. 141, 88, (1966).

20. L. Vriens, "Electron Exchange in Binary Encounter Collision Theory," Proc. Phys. Soc. 89, 13, (1966).

21. Von F. Lenz, "Zur Streuung mittelschneller Elektronen in kleinste Winkel," Z. Naturforschung 9A, 185, (1954).

22. M. Gryzinski, "Classical Theory of Electronic and Ionic Inelastic Collision," Phys. Rev. 115, 374,(1959).

23. M. Gryzinski, "Two Particle Collisions. I-General Relations for Collisions in the Laboratory System. II-Coulomb Collisions in the Laboratory System of Coordinates," Phys. Rev. 138, A305-335, (1965). Also, "Classical Theory of Atomic Collisions. I-Theory of Inelastic Collisions," Phys. Rev. 138, A336-358, (1965).

24. E. Gerjouy, "Cross-Section for Energy Transfer Between Two Moving Particles," Phys. Rev. 148, 54,(1966).

25. R. C. Stabler, "Classical Impulse Approximation for Inelastic Electron-Atom Collisions," Phys. Rev. 133, A1268, (1964).

26. V. I. Ochkur and A. M. Petrunkim, "The Classical Calculation of the Probabilities of Excitation and Ionization of Atom by Electron Impact," Opt. Spectry. (USSR) 14, 245, (1963).

27. A. Burgess, Proceeding of the Third International Conference on Electronic and Atomic Collisions, North-Holland Publishing Co., Amsterdam, p. 237, (1964).

28. C. B. Opal, W. K. Peterson and E. C. Beaty, "Measurements of Secondary-Electron Spectra Produced by Electron Impact Ionization of a Number of Simple Gases," J. of Chem. Phys. 55, 4100, (1971).

29. D. Rapp, P. Englander-Golden, "Total Cross Sections for Ionization and Attachment in Gases by Electron Impact. I.Positive Ionization," J. Chem. Phys., 43, 1464, (1965).

30. Y. Kim and M. Inokuti, "Total Cross-Section for Inelastic Scattering of Charged Particles by Atoms and Molecules. V Evaluation to the Next Order Beyond the Bethe Asymptote," Phys. Rev. 3, 3, (1971).

31. Y. Kim and M. Inokuti, "Generalized Oscillator Strengths of the Helium Atom. I," Phys. Rev. 175, 176,(1968).

32. L. Vriens, J. A. Simpson and S. R. Mielszarck, Test of Born Approximation: Differential and Total 2^3S, 2^1P and 2^1S Cross Sections for Excitation of He by 100 to 400 eV Electrons," Phys. Rev. 165, 7, (1968).

33. R. St. John, F. L. Miller, and C. C. Lin, "Absolute Electron Excitation Cross-Sections of He," Phys. Rev. 134, 888, (1964).

34. H. S. W. Massey and B. L. Moiseiwitsch, "The Application of Variations Methods to Atomic Scattering Problems, IV. The Excitation of the 2^1S and 2^3S States of Helium by Electron Impact," Proc. Roy. Soc. A227, 38, (1955).

35. H. Maier-Leibnitz, "Ausbeutemessuhgen beim Stoss langamer Elektronen mit Edelgasatomen," Zeit. f. Physik, 95, 499, (1935).

36. T. Itoh and T. Musha, "Monte Carlo Calculations of Motion of Electrons in Helium," J. Phys. Soc. of Japan, 15, 1675, (1960).

37. W. Jesse and J. Sadanskis, "Ionization in Pure Gas and the Average Energy to Make an Ion Pair for Alpha and Beta Particles," Phys. Rev. 97, 1665, (1955).

38. L. R. Peterson and A.E.S. Green, "The Relation Between Ionization Yields, Cross Sections and Loss Functions," Proc. Phys. Soc. 1, 1131, (1968).

39. N. Mott and H.S.W. Massey, The Theory of Atomic Collisions, 3rd ed., Oxford U. Press, London, pg. 455, (1965).

40. R. Labahm, and J. Callaway, "Distortion Effects in the Elastic Scattering of 100-400-eV Electrons From Helium," Phys. Rev. 180, 91, (1969). Also L. Vriens, C. Kuyatt and S. Mielczarek, "Test of Born Approximation; Differential and Total Cross Sections for Elastic Scattering of 100- to 400-eV Electrons by Helium," Phys. Rev. 170, 163, (1968).

41. D. Golden and H. Bandel, "Absolute Total Electron-Helium Scattering Cross-Sections for Low Electron Energies," Phys. Rev. 138, 14, (1965).

42. C. Normand, "The Absorption Coefficient for Slow Electrons in Gases," Phys. Rev. 35, 1217, (1936).

43. H. Hurwitz, M. S. Nelkin and G. J. Habetler, "Neutron Thermalization, I. Heavy Gas Modulator," Nucl. Sci. Eng. 1, 280, (1956).

44. K. Beckurts and K. Wirtz, Neutron Physics, Springer=Verlag Press, New York, pg. 88, (1964).

45. T. F. O'Malley, "Extrapolation of Electron-Rare Gas Atom Cross Section to Zero Energy," Phys. Rev. 130, 1020, (1968).

46. D. Rose and M. Clark, Jr., Plasmas and Controlled Fusion, The MIT Press, Cambridge, Mass., pg 165ff, (1961).

47. L. Spitzer, Jr., Physics of Fully Ionized Gases, Interscience Publ., New York, 2nd ed., pg 127ff, (1964).

48. E. H. Holt and R. E. Haskell, Plasma Dynamics, The Macmillan Co., New York, pg 269ff, (1965).

49. H. J. Oskam and V. R. Mittelstadt, "Recombination Coefficient of Molecular Rare-Gas Ions," Phys. Rev. 132, 1445, (1963).

50. A. V. Phelps and S. C. Brown, "Positive Ions in the Aterglow of a Low Pressure Helium Discharge," Phys. Rev. 86, 102, (1952).

51. A. von Engel, Ionized Gases, Oxford Press, 2nd ed., pg 164, (1965).

52. A. E. Heyen and T. J. Lewis, "Electron Energy Distribution Functions and Transport Coefficients for Rare Gases," Proc. Roy. Soc. 271, A531, (1963).

53. W. P. Allis, Handbuch der Physik, Vol. XXI, 304, Springer, Berlin, (1956).

54. von J. A. Smit, "Berechnung der Geschwindigkeits-Verteilung der Elektronen bei Gasentladungen in Helium," Physica 3, 543, (1936).

55. Domenick Barbiere, "Energy Distribution, Drift Velocity and Temperature of Slow Electrons in Helium and Argon," Phys. Rev. 84, 653, (1950).

56. M. H. Hughes, "Electron Energy Distribution and Transport Coefficients in Helium and Neon," J. Phys. B: Atom. Molec. Phys. 3, 1544, (1970).

57. J. T. Ganley, "Effect of a Heavy Particle External Ionization Source on Carbon Dioxide Laser Discharges," Ph.D. Thesis, Dept. of Electrical Engr., Univ. of Illinois, Urbana, Ill., (1972).

58. H. J. Oskam, "Microwave Investigation of Disintegrating Gaseous Discharge Plasmas," Philips Res. Report, 13, 432, (1958).

59. A. K. Bhattacharya, Microwave Investigation of Plasmas Produced in a Nuclear Reactor, Ph.D. Thesis, Nuclear Engineering Program, Univ. of Illinois, Urbana, Ill., (1966).

60. N. Mott, "The Collision Between Two Electrons," Proc. Roy. Soc. A-126, 259 (1930).

61. E. A. Hylleraas, "Neue Bercchnung der Energie des Heliums im Grundzustande, sowie des tiefsten Terms von Ortho-Helium," Zeit f. Phy. 54, 347, (1929).

62. G. Bell and S. Glasstone, Nuclear Reactor Theory, Van Nostrand Reinhold Press, New York, pg 144, (1970).

63. J. C. Guyot, G. Miley and J. T. Verdeyen, "Application of a Two-Region Heavy-Charged Particle Transport Model to Noble-Gas Plasmas Induced by Nuclear Radiations," Nucl. Sci. & Engr. 48, 373, (1972).

64. G. H. Miley, Direct Energy Conversion of Nuclear Energy, Am. Nuc. Soc., Hinsdale, Ill., pg 113ff, (1971).

65. Luis De Sobrino and M. Clark, Jr., "A Study of Wilkins Equations," Nuc. Sci. Eng., 10, 388, (1961).

66. E. R. Cohen,"The Neutron Velocity Spectrum in a Heavy Modulator," Nuc.Sci. Eng., 2, 227, (1957).

67. S. Chapman and T. Cowling, The Mathmetical Theory of Non-Uniform Gases, 2nd. ed., Cambridge University Press, London, pp.356, (1960).

VITA

Ronnie Hung-Kie Lo was born in [redacted], on [redacted]. He received the B.S. degree in Applied Mathematics and Engineering Physics with honor from the University of Wisconsin in 1966. He received the M.S. degree in Nuclear Engineering from the University of Wisconsin in 1968. He joined the Picker Corporation and served as a R. & D. engineer for one and a half years.

In September 1969, he came to the University of Illinois to study for a Ph.D. degree in the Nuclear Engineering Program.

As an undergraduate, Mr. Lo was awarded the Non-resident Scholarship from 1963-66. In graduate school he was awarded the University Fellowship and Research Assistantships. Mr. Lo has co-authored with Professor Miley an article in the Transaction of the American Nuclear Society, 18th Annual Meeting, June, 1972, and a paper accepted for presentation in the 25th Annual Gaseous Electronics Conference, University of Western Ontario, London, Ont., October, 1972.